THE IMPACT OF STREAMBED SEDIMENT SIZE ON HYPORHEIC TEMPERATURE PROFILES IN A LOW GRADIENT THIRD-ORDER AGRICULTURAL STREAM

Vanessa Beach

128 Pages August 2008

This study assesses the impact of sediment size on thermal profiles and transport within the hyporheic zone of a low gradient stream in central Illinois.

APPROVED:

Date Eric Peterson, Chair

Date Stephen Van der Hoven

Date Heather Conley

THE IMPACT OF STREAMBED SEDIMENT SIZE ON HYPORHEIC TEMPERATURE PROFILES IN A LOW GRADIENT THIRD-ORDER AGRICULTURAL STREAM

Vanessa Beach

128 Pages August 2008

The impacts of temperature on stream and hyporheic environments are manifold, and an understanding of the factors controlling temperature changes within both environments can be central to the comprehension of their respective ecosystems. This study aims to assess the impact of sediment size on thermal profiles and processes within the hyporheic zone of a low gradient stream in central Illinois.

Both chloride and temperature data were collected at two sites featuring different sediment sizes. Streambed chloride levels were graphically compared to stream chloride levels, indicating little change in streambed chloride concentrations with depth or through time, suggesting a constant groundwater component. Statistical methods involved general summary statistics and time-series cross-correlation. Lateral and longitudinal temperature profiles were compared and found to differ based on factors influencing thermal transport, such as the presence of preferential flow paths. Additionally, advection was hypothesized to be a major controlling factor of diurnal temperature signal penetration depth. Finally, a modeling approach using the 2-D heat

transport model VS2DH simulated observed streambed temperatures of both lateral and longitudinal profiles over a four-day period. Thermal transport following the direction of stream flow dominated both site thermal profiles, causing the failure of lateral 2-D models. Based on longitudinal models, increased sediment size led to higher hydraulic conductivities and lower porosities, impacting advection. Additionally, the degree of sediment sorting impacted thermal transport. Poorly sorted gravels showed distinct preferential flow paths, greater variation in vertical versus horizontal specific discharge, and greater variability in the dominant thermal transport mechanism. In contrast, moderately sorted sands showed homogenization of vertical and horizontal specific discharge, as well as a uniform dominance of advection as the dominant thermal transport mechanism. Ultimately, the results suggest that physical heterogeneities such as a greater range in sediment size are reflected as thermal heterogeneities in the subsurface.

APPROVED:

Date Eric Peterson, Chair

Date Stephen Van der Hoven

Date Heather Conley

THE IMPACT OF STREAMBED SEDIMENT SIZE ON HYPORHEIC TEMPERATURE PROFILES IN A LOW GRADIENT THIRD-ORDER AGRICULTURAL STREAM

VANESSA BEACH

Thesis Submitted in Partial
Fulfillment of the Requirements
for the Degree of

MASTER OF SCIENCE

Department of Geography-Geology

ILLINOIS STATE UNIVERSITY

2008

THESIS APPROVED:

Date	Eric Peterson, Chair
Date	Stephen Van der Hoven
Date	Heather Conley

ACKNOWLEDGEMENTS

First and foremost I would like to thank my thesis adviser Dr. Eric Peterson, for his infinite amounts of much needed encouragement and support. Without his help this project would not have been possible, and timely completion would have looked more like a far off dream than an attainable reality.

I would also like to thank my other thesis committee members, Dr. Stephen Van der Hoven and Dr. Heather Conley, for their constant willingness to assist and reassure. Both chemical and statistical realms became much less daunting thanks to your help.

Further, I would like to thank the faculty of the Geology-Hydrogeology department, as well as the greater Illinois State University educational community for their support through the years, and specific help with this project.

For funding of this project I would like to thank both the Geological Society of America and Grant-In-Aid of Research from Sigma Xi, The Scientific Research Society.

I would also like to give a huge thanks to all my friends, who helped me maintain acceptable levels of sanity throughout the past 2 years. Thanks for the laughter. It meant a lot to me.

Lastly I would like to thank my family for both their emotional and financial support, and my husband, Adam, for his patience and love. Thanks for understanding all the days and nights when work had to come first, and for always being the first to believe in me. V. B.

CONTENTS

		Page
ACKNOWLEDGEMENTS		i
CONTENTS		ii
TABLES		iv
CHAPTER		
I.	GENERAL INTRODUCTION AND OVERVIEW	1
	Introduction	2
	Hypotheses and Objectives	6
	Site Description	7
II.	SITE DESIGN AND WATER CHEMISTRY METHODS	16
III.	WATER CHEMISTRY RESULTS AND DISCUSSION	19
IV.	THE IMPACT OF STREAMBED SEDIMENT SIZE ON HYPORHEIC TEMPERATURE PROFILES IN A LOW GRADIENT THIRD ORDER AGRICULTURAL STREAM – A STATISTICAL APPROACH	32
	Abstract	33
	Introduction	34
	Study Site	37
	Methodology	40
	Temperature Measurements	40
	Statistical Methods	42
	Data	44
	Results	46
	Summary Statistics	46
	Seasonal Cross-correlation	51
	Diurnal Cross-correlation	61

Discussion 69
Conclusion 74
References 77

V. THE IMPACT OF STREAMBED SEDIMENT SIZE ON HYPORHEIC TEMPERATURE PROFILES IN A LOW GRADIENT THIRD ORDER AGRICULTURAL STREAM – A MODELING APPROACH 79

Abstract 80
Introduction 81
Study Site 83
Methodology 88

Temperature Measurements 88
Model Setup 90

Results and Discussion 94

Time Series Data 94
Model 102
Sensitivity Analysis 114
Thermal Transport 117

Conclusion 119
References 121

VI. SUMMARY OF CONCLUSIONS 123

REFERENCES 126

TABLES

Table		Page
III-1.	Chloride concentration data for Sites 1 and 2, collected over a roughly 3 month period.	21
V-1.	Physical and thermal properties for the calibrated models.	117

FIGURES

Figure		Page
I-1.	Schematic illustration of the hyporheic zone below a stream.	4
I-2.	Theoretical depiction of temperature variation with depth in both gaining and losing reaches of a stream.	5
I-3.	Site location within the U.S. and Illinois, as well as a detailed overview of the immediate site region.	8
I-4.	Figure showing an aerial map of the Randolph well field study area with cross section line locations, as well as cross sections along lines A-Al and B-Bl.	11
I-5.	Water table contour map of the RWF. Contours are based on elevations in meters above mean sea level.	13
I-6.	Piper plot of water chemistry by well at the RWF. Only key wells are labeled for reference.	15
II-1.	Birds-eye view of well setup in the stream channel. Capital letters indicate respective well names used at each site.	17
II-2.	Detailed view of individual well design.	18
III-1.	Aerial map of Randolph well field showing location of Sites 1 and 2, as well as the location of the Peterson and Sickbert (2006) study site.	24
III-2.	Chloride concentration (mg/L) of LKC stream water through time.	25
III-3.	Stream stage measured as elevation above mean sea level. The gray vertical line indicates the date 10/2/2007.	26
III-4.	Stream and HZ chloride concentrations for Site 1. Some isolated data points are represented only by their respective symbols and are not connected by a line to further data points due to missing values.	28
III-5.	Stream and HZ chloride concentrations for Site 2. Some isolated data points are represented only by their respective symbols and are not connected by a line to further data points due to missing values.	29

IV-1. Site location within the U.S. and Illinois. 38

IV-2. Grain size analysis for upstream (Site 1) and downstream (Site 2) sections of LKC. 39

IV-3. Birds-eye view of well setup in the stream channel. 41

IV-4. Detailed view of individual well design. 41

IV-5. Air and stream (Site 1 and Site 2) temperature 15-minute incrementing time series for entire data collection period. 45

IV-6. Site 1 summer (June 21, 2007 to September 23, 2007) box plots with reference lines at 20 ºC and separating wells. 47

IV-7. Site 1 autumn (September 24, 2007 to December 22, 2007) box plots with reference lines at 20 ºC and separating wells. 48

IV-8. Site 2 summer (June 21, 2007 to September 23, 2007) box plots with reference lines at 20 ºC and separating wells. 49

IV-9. Site 2 autumn (September 24, 2007 to December 22, 2007) box plots with reference lines at 20 ºC and separating wells. 50

IV-10. Comparison of unfiltered hourly time series (a and c) and filtered hourly time series (b and d) of wells E and J, respectively. 52

IV-11. Site 1 cross-correlograms per well (indicated by Letters A through E), showing correlation between hourly, filtered (24 hr averaging filter and first order differencing) time series of surface stream temperatures and depths 30, 60, 90 and 140 cm within the HZ. 54

IV-12. Site 2 cross-correlograms per well (indicated by Letters F through J), showing correlation between hourly filtered (24 hr averaging filter and first order differencing) time series of surface stream temperatures and depths 30, 60, 90 and 140 cm within the HZ. 55

IV-13. Site 1 cross-correlograms at 30 cm (a), 60 cm (b) and 140 cm (c), showing correlation between hourly filtered (24 hr averaging filter and first order differencing) time series between wells along longitudinal (black lines) and lateral (gray lines) profiles. 57

IV-14. Site 2 cross-correlograms at 30 cm (a), 60 cm (b) and 140 cm (c), showing correlation between hourly filtered (24 hr averaging filter and first order differencing) time series between wells along longitudinal (black lines) and lateral (gray lines) profiles. 58

IV-15. Site comparison cross-correlogram, showing correlation between hourly filtered (24 hr averaging filter and first order differencing) time series gradients (the difference between respective stream and 140 cm depth temperatures) of Site 1 wells to Site 2 wells at corresponding positions within LKC. 61

IV-16. Site 1 cross-correlograms per well (indicated by letters A through E), showing correlation between hourly transformed (first order differencing) time series of surface stream temperatures and depths 30, 60, 90 and 140 cm within the HZ. 63

IV-17. Site 2 cross-correlograms per well (indicated by letters F through J), showing correlation between hourly transformed (first order differencing) time series of surface stream temperatures and depths 30, 60, 90 and 140 cm within the HZ. 64

IV-18. Site 1 cross-correlograms at 30 cm (a), 60 cm (b) and 140 cm (c), showing correlation between hourly transformed (first order differencing) time series between wells along longitudinal (black lines) and lateral (gray lines) profiles. 66

IV-19. Site 2 cross-correlograms at 30 cm (a), 60 cm (b) and 140 cm (c), showing correlation between hourly transformed (first order differencing) time series between wells along longitudinal (black lines) and lateral (gray lines) profiles. 67

IV-20. Site comparison cross-correlogram, showing correlation between hourly transformed (first order differencing) time series gradients (the difference between respective stream and 140 cm depth temperatures) of Site 1 wells to Site 2 wells at corresponding positions within LKC. All lines overlay each other exactly. 68

V-1. Site map and site location within the US and Illinois. Site 1 is upstream and represents a gravel dominated streambed. Site 2 is downstream, representing a sand dominated streambed. 84

V-2. Grain size analysis for upstream (Site 1) and downstream (Site 2) sections of LKC. 85

V-3. Conceptual model of Randolph well field and Sites 1 and 2 with respect to meander flow-through paths. 87

V-4. Plan view of well setup in the stream channel. 89

V-5. Detailed view of individual well design. 89

V-6.Final longitudinal model setups for Sites 1 and 2. Temperatures for negative fluxes were not required and are represented by n/a. 93

V-7.Air and stream (Site 1 and Site 2) temperature 15-minute incrementing time series for entire data collection period. 95

V-8.Site 1 surface stream temperature and well temperatures at depths 30, 60, 90, and 140 cm within the streambed. 96

V-9.Site 2 surface stream temperature and well temperatures at depths 30, 60, 90, and 140 cm below streambed. 99

V-10. Temperatures recorded in wells B and H at 4 depths, surface stream temperature, and stream stage. 102

V-11. Temperature profiles at the start of the modeling period (June 13, 2007). Contours show temperature in ºC. Diamonds represent logger locations, while gray dashed lines represent hypothesized HZ flow paths. 105

V-12. Comparison of observed versus simulated temperatures per depth at Site 1. 106

V-13. Site 1 final calibrated model output temperature contour patterns at 60, 72, 84, and 96 hours since time 0. All temperatures are given in ºC. Left sides of model domains are upstream, while right model domain sides are downstream. 107

V-14. Site 2 final calibrated model output temperature contour patterns at 60, 72, 84, and 96 hours since time 0. All temperatures are given in ºC. Left sides of model domains are upstream, while right model domain sides are downstream. 108

V-15. Comparison of observed versus simulated temperatures per depth at Site 2. 110

V-16. Contours of model output values for total head, and dashed lines indicating flow directions 112

V-17. Sensitivity analysis results, showing percent change versus mean absolute error for all adjustable physical and thermal model properties. 115

CHAPTER I

GENERAL INTRODUCTION AND OVERVIEW

Introduction

The development of various research methods has allowed water temperature to play an important role in hydrogeology. Fundamentally, the heat-flow theory was important in developing the science of groundwater hydrology (Anderson, 2005). More specifically, temperature profiles below streams can be used to quantify groundwater/stream interactions (Stonestrom and Constantz, 2003). Streambed temperatures can be used to delineate flows in the hyporheic zone (HZ) (Conant, 2004). Flow velocity of groundwater can be determined from groundwater temperature measurements, while a combination of groundwater temperature and hydraulic head measurements allows estimations of groundwater recharge/discharge rates and flow through fractures (Anderson, 2005). Despite all of these uses of water and hyporheic temperatures, the volume of literature discussing temperature as a tracer remains light (Anderson, 2005), and HZ studies are mostly performed on low order, high-gradient streams (Bencala, 2005).

Temperature's significance reaches beyond hydrogeologic calculations and theories. It is most importantly an environmental variable that affects biology on a daily basis (Sinokrot and Stefan, 1993). In streams, base flow, which is groundwater inflow to a stream, helps maintain constant water temperatures, impacting both the chemistry and biology of surface streams (Jones and Holmes, 1996). These more stable temperatures allow benthic and hyporheic aquatic life to survive the different seasonal as well as diurnal water temperature variations that stagnant surface water experiences (Hayashi and Rosenberry, 2002; Silliman and Booth, 1993). Ultimately many benthic organisms seek

refuge in the HZ during chemical and/or temperature based stress times (Hayashi and Rosenberry, 2002).

The HZ is defined as a zone below the stream channel where surface and groundwater mix (Conant, 2004; Hayashi and Rosenberry, 2002). Hyporheic ecological importance became well-established in the early 1980s (Bencala, 1993) and the HZ is now recognized as a distinct biogeochemical environment. The HZ can be viewed as a subsurface flowpath, along which water flowing in from a stream channel mixes with subsurface water, and then returns to the stream (Bencala, 2000; Cardenas et al., 2004; Bencala, 2005) (Figure I-1). Effectively, HZs function as continual connection sites between the transport of water and solutes in the stream channel and the stream's catchment (Bencala, 1993). The hydrological exchanges that occur between stream and hyporheic ecotones supply hyperheos (hyporheic biota) with nutrients, organic matter, and dissolved oxygen (Boulton and Scarsbrook, 1997); they also control the distribution of solutes and colloids from bed form to watershed scales (Cardenas et al., 2004). The degree to which the HZ contributes to stream ecosystem functioning is directly related to the rate of subsurface biogeochemical processes, and the proportion of stream discharge flowing through the hyporheic sediments (Jones and Holmes, 1996).

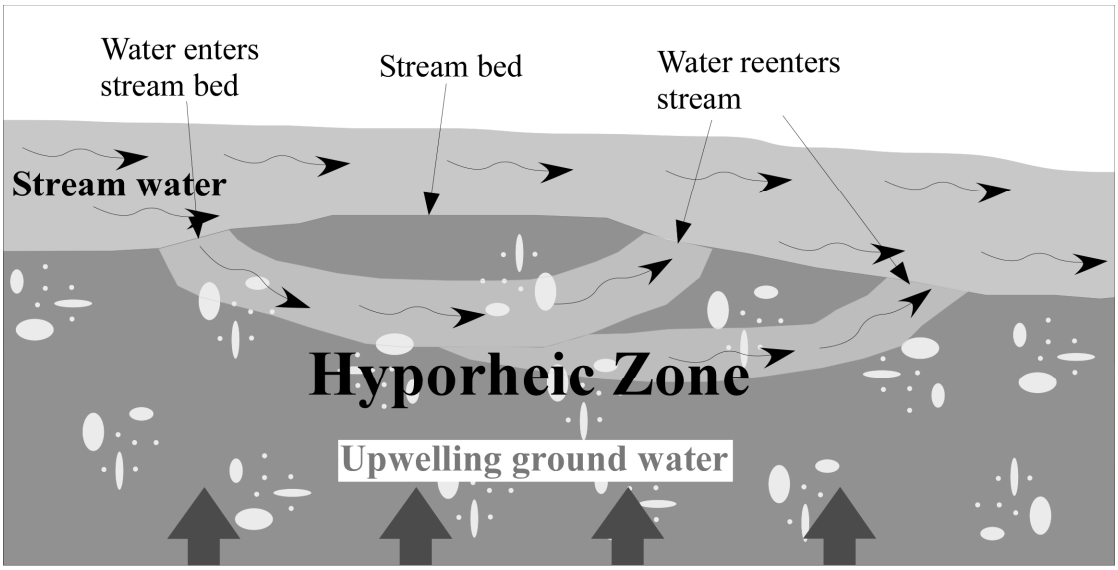

Figure I-1: Schematic illustration of the hyporheic zone below a stream.

Hyporheic temperatures are controlled by the mixing of groundwater and surface water, where groundwater temperatures generally vary one to two degrees from mean annual air temperatures, disregarding geothermal influences, and surface water temperatures show both diel and seasonal fluctuations (Brunke and Gonser, 1997). Dogwiler and Wicks (2006) show that upper HZ temperatures are primarily a function of air temperature in a karst environment, though the temperature range of the substrate is suppressed relative to the air temperature range. With increasing depth or distance from infiltration sites the diel and seasonal fluctuations become attenuated and lagged, while the annual air temperature cycle persists (Figure I-2). These patterns can be a valuable tool in defining HZ depth and extent (Crowther and Pitty, 1982; White et al., 1987). However, delineations of HZ extent are not constant through time, as shown by Fraser and Williams (1998) who attempt to identify seasonal boundary dynamics of the hyporheic/groundwater boundary. Their main findings include: 1) seasonal discharge

extremes coincided with boundary fluctuations, and 2) boundary fluctuations were regulated by the relative strength of upward baseflow force and downward advecting surface water force. Effectively these results suggest that the extent of the HZ varies both seasonally as well as with event-based fluctuations.

In addition to using HZ temperatures to delineate HZ extent, Silliman and Booth (1993) successfully used HZ temperatures to identify losing and gaining portions of a stream in Indiana featuring diffuse inflow. Areas with relatively constant HZ temperatures through time were identified as gaining reaches, where HZ temperatures were held constant by an influx of groundwater. If HZ temperatures varied with diurnal surface stream temperature variations, reaches were identified as losing reaches, where stream water infiltrates into streambed sediment (Figure I-2).

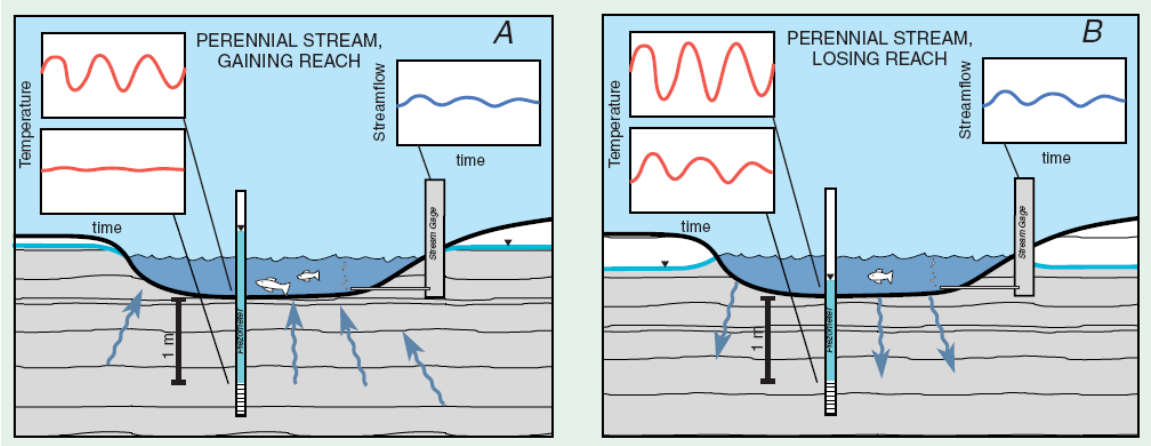

Figure I-2: Theoretical depiction of temperature variation with depth in both gaining and losing reaches of a stream (Stonestrom and Constantz, 2003).

While HZ temperatures are dominantly controlled by advective processes, conductive processes may also play an important role (Evans et al., 1995). The influence

of both advective and conductive processes on hyporheic water temperatures suggests that sediment size can influence the effectiveness of both by 1) partially characterizing the hydraulic conductivity of the stratum, effectively limiting advection, and 2) controlling the connectivity of the sediment, there by limiting conduction. Vaux (1968) and Cooper (1965) suggest that larger objects in or on the streambed surface alter the flow paths of hyporheic and stream waters. With respect to finer sediments, Ringler and Hall (1975) showed that the largest gradients between stream and hyporheic water temperatures occur at heavily silted sites, where slow inter-gravel flows persist. Additionally, variations in hydraulic conductivity of the streambed may result in uneven discharge and flow geometry (Becker et al., 2004).

The use of temperature as a tracer is attractive for several reasons: 1) its presence in a groundwater-surface water system is natural, 2) temperature is a very robust environmental variable to continuously monitor (Constantz et al., 2003) and 3) it can be monitored and recorded with inexpensive and simple equipment (Keery et al., 2007). Yet thermal energy can quickly dissipate into surrounding sediments, thereby greatly weakening its signal and traceability (Constantz et al., 2003). This can be counteracted by limiting the spatial scale of the investigation with respect to the temperature cycle length of interest. In the case of this study, the spatial scale is restricted to a 2 m × 2 m × 1.4 m volume, as the shortest temperature cycle anticipated is diurnal.

Hypotheses and Objectives

Ultimately this study focuses on determining the effect of streambed sediment grain size on temperature profiles of the HZ, with the hope of furthering existing

knowledge of water temperature in the environment. This overall goal has been broken into several more specific ambitions that this study addresses:

1. To compare temperature profiles of two sites featuring different sediment sizes, identifying and explaining similarities and differences between the two.
2. To compare lateral and longitudinal temperature profiles, identifying and explaining similarities and differences between the two.
3. To assess the prevalence of advection verses conduction as thermal transport mechanisms in sites featuring different sediment sizes.
4. To define the lower boundary of the HZ of a low gradient stream using available temperature data.

Site Description

Field investigations focused on two sites along a stretch of the Little Kickapoo Creek (LKC) running through the Illinois University Randolph Well Field (RWF) (Figure I-3), located in McLean County, central Illinois, USA. LKC is a low gradient third-order perennial stream, which meanders (sinuosity of 1.8) through Wisconsinan glacial plains and originates in an urban area approximately 11 km north of the study site (Peterson and Sickbert, 2006). Regionally LKC is a gaining stream, with a gradient of 0.002. Locally, by the meander along which the two (2) study sites are located, a gradient of 0.003 exists (Peterson and Sickbert, 2006). The stretch under investigation is unmodified and meanders through an approximately 300 m wide alluvial valley. Terrain bordering the

stream is used predominantly as agricultural farm land, alternating corn and soy bean production.

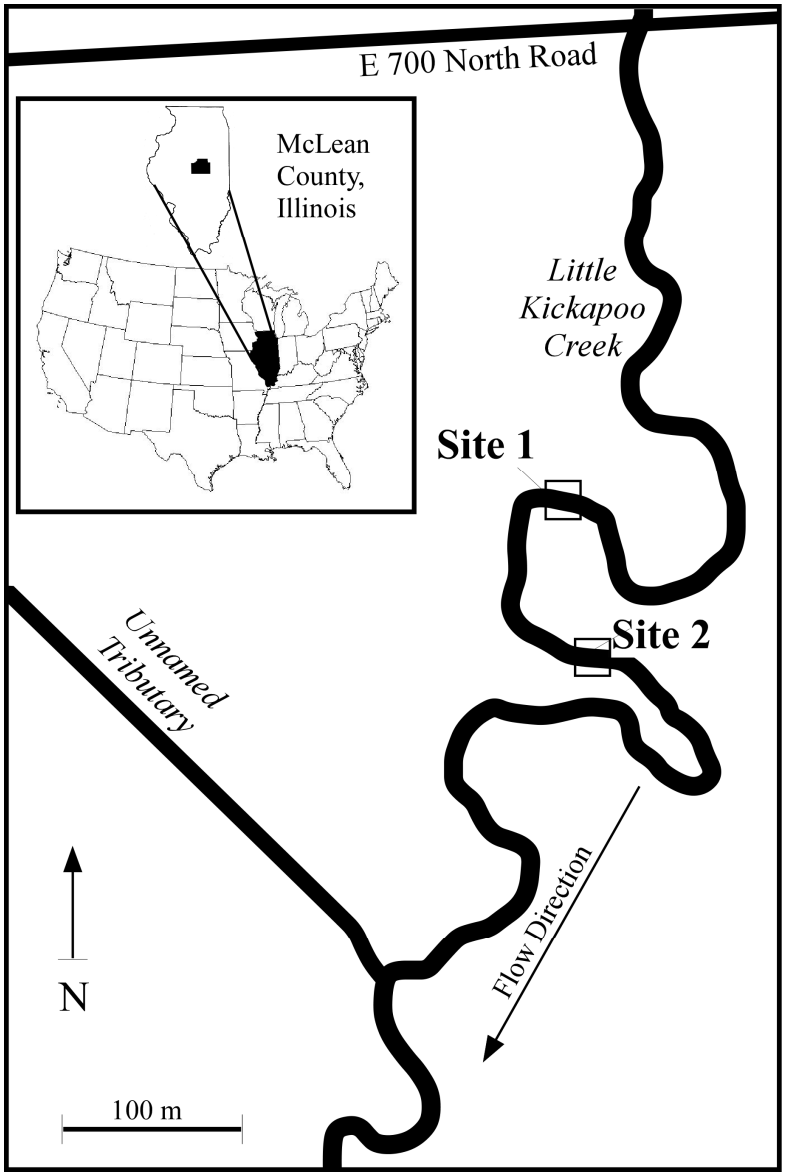

Figure I-3: Site location within the U.S. and Illinois, as well as a detailed overview of the immediate site region.

Three geologic units comprise the alluvial valley through which LKC meanders: the Wedron Formation (WF), the Henry Formation (HF), and the Cahokia Formation (CF) (listed from oldest to youngest).

The WF acts as a lower confining unit to the HF, being a clay-rich low-permeability till with some interstitial sand and gravel which was deposited by past glacial activity. It is typically grey in color due to reducing conditions, and very dense. The maximum thickness at this site has yet to be determined.

The HF functions as an aquifer due to its poorly sorted gravels and sands, and has an average hydraulic conductivity of 10m/day (Peterson and Sickbert, 2006), and an average thickness of 5-7 m in the outwash valley. The HF was formed by melt water streams draining out of the Bloomington Moraine during glacial standstill and retreat, and appears to pinch out at the edges of the outwash channel. Only a low clay component is present in this unit, appearing "clean" when sampled, and non-cohesive. Specific yield (Sy) and storativity (S) have been determined at approximately 0.127 (12.7 % of bulk volume) and 1.14×10^{-3} respectively.

Above the HF lies the CF, consisting of silts and clays, with some interstitial sand lenses. The CF was deposited by repeated flooding of LKC, and has an average thickness of approximately 2 meters across the outwash valley. Macro-porosity is prevalent, and varying degrees of soil formation exist, depending on the frequency of depositional and erosional events. Recent sediment deposition sites show less mature soils than areas that have remained unchanged for some time. Varying stages of oxidation can also be observed, and redoxomorphic features are frequent at depth. Some cut and fill features can be found in proximity to LKC. Due to abundant macroporosity, and evidence of a high degree of connectivity between LKC and the HF, the CF is not considered a confining unit.

The LKC channel is inset in the CF, occasionally cutting into the top of the HF (Figure I-4). The channel sediments are primarily gravel and coarse sand, with interstitial silt, where surface sediments vary with distance along the channel. For this study two locations along LKC featuring different streambed sediment sizes were used; site 1 consisting predominantly of coarse sand and gravel, while site 2 is composed of fine sands and silt.

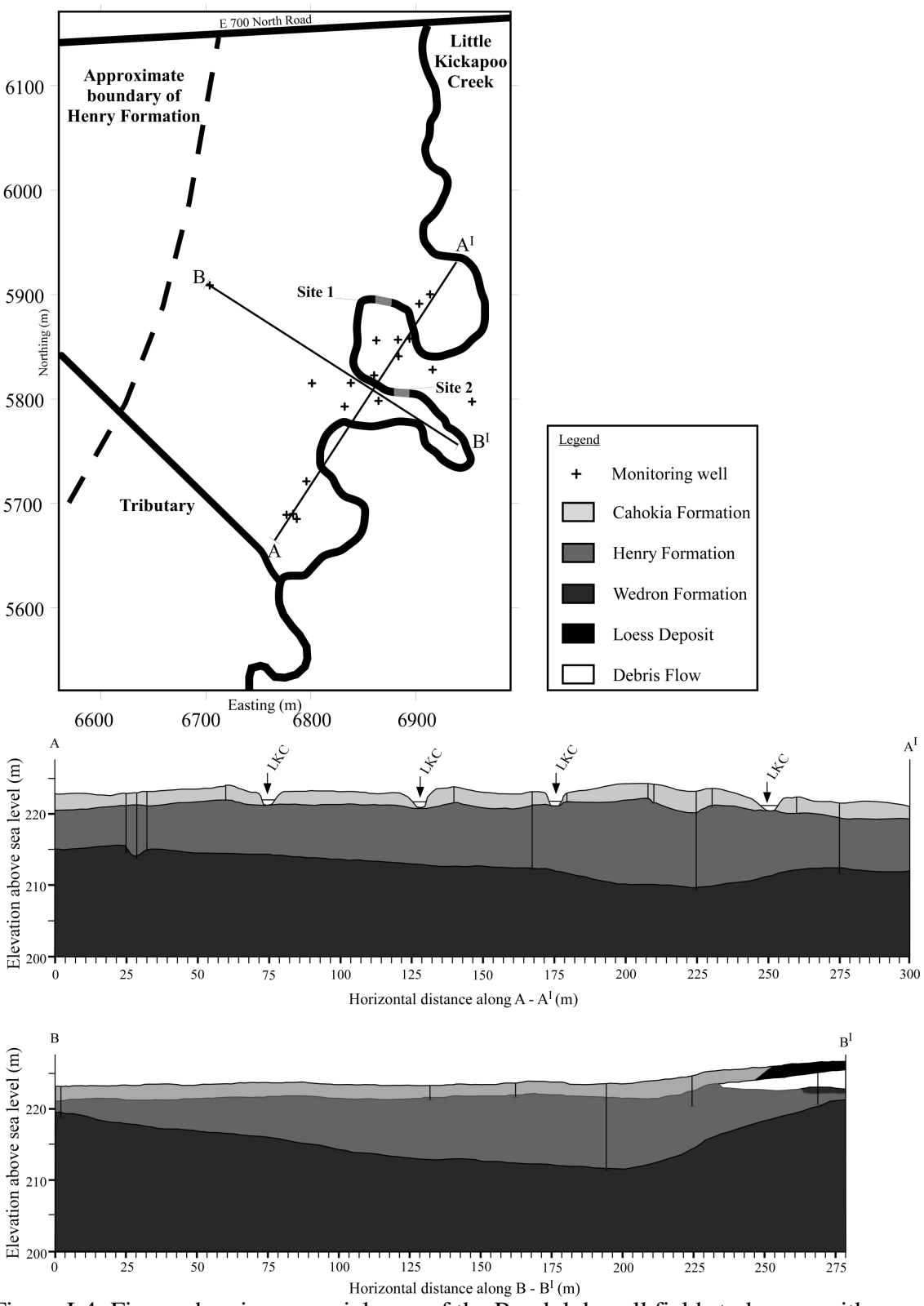

Figure I-4: Figure showing an aerial map of the Randolph well field study area with cross section line locations, as well as cross sections along lines A-Al and B-Bl.

A water table contour map (Figure I-5) utilizing water table elevation data from 6/6/2007 was created to allow interpretation of groundwater flow patterns at the RWF. Only wells screened near the water table were used. The map reveals two major groundwater flow patterns.

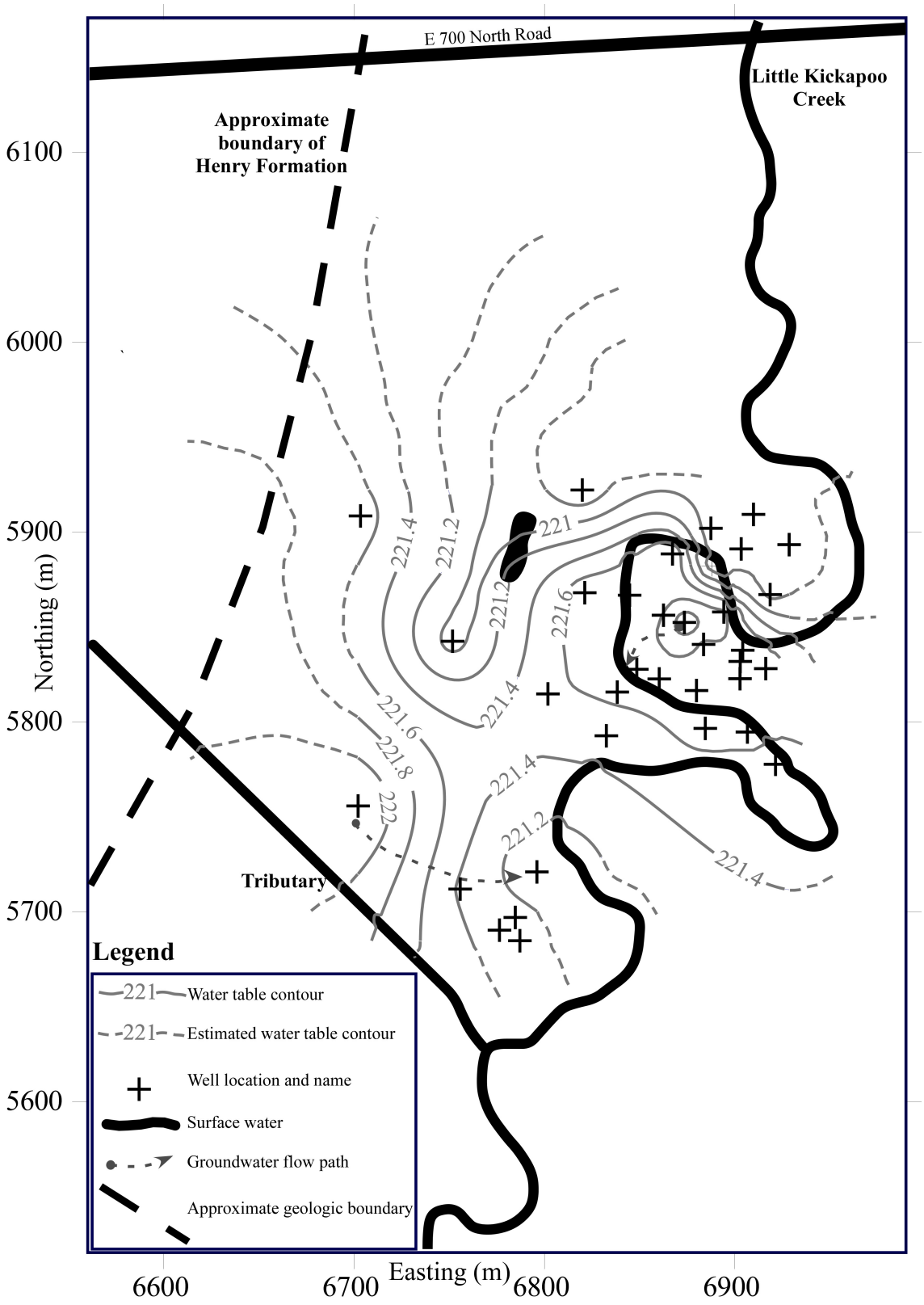

Figure I-5: Water table contour map of the RWF. Contours are based on elevations in meters above mean sea level.

The first set of flow paths parallel the stream, showing groundwater flow roughly from north to south/south east, revealing a tendency for surface water to leave and reenter the stream by flowing beneath meanders. This suggests the presence of an extensive hyporheic zone. A second set of flow paths show groundwater flowing from west to east, eventually discharging into LKC. Regionally LKC is considered a gaining stream (Peterson and Sickbert, 2006), which these flow paths support.

Evaluation of the water types present at the RWF shows base calcium-magnesium bicarbonate water chemistry (Figure I-6), with a trend of increasing total dissolved solids (TDS) to calcium-sodium bicarbonate. The increase in TDS can be linked to increasing levels of chloride (Cl^-) and sodium (Na^+) due to road salting in the headwaters of LKC.

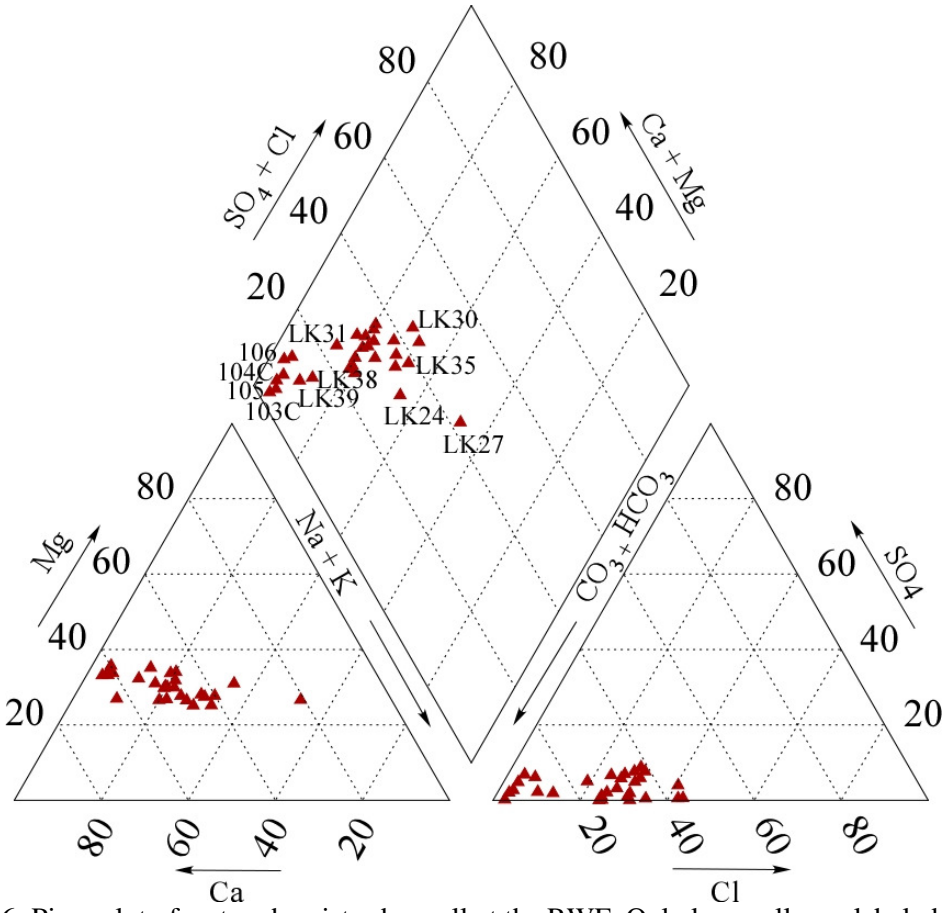

Figure I-6: Piper plot of water chemistry by well at the RWF. Only key wells are labeled for reference.

The water chemistry and temperature data collected during this study are used to quantitatively define the HZ, while also calibrating a predictive model using VS2DH (Healy and Ronan, 1996). The results are presented in Chapters 3, 4, and 5 where Chapter 3 will outline chemistry findings, Chapter 4 will focus on a statistical approach, and Chapter 5 will focus on a modeling approach.

CHAPTER II

SITE DESIGN AND WATER CHEMISTRY METHODS

Two identical sampling well grids were set up along riffles within the designated LKC sites 1 and 2, using a drive-point installation method. Each grid consisted of five wells creating both lateral and longitudinal profile lines across the channel. The two profile lines intersected roughly in the stream's thalweg, where one well provided data for both profiles (Figure II-1). Within each 6.35 cm PVC well, sampling tubes were positioned at depths of 30 cm, 60 cm, 90 cm, and 140 cm (Figure II-2). The 140 cm depth was set as a result of advancement refusal during the installation process. Foam sealant was used to partition off different depths to reduce vertical mixing, while holes drilled into the walls at each depth provided connection to the matrix.

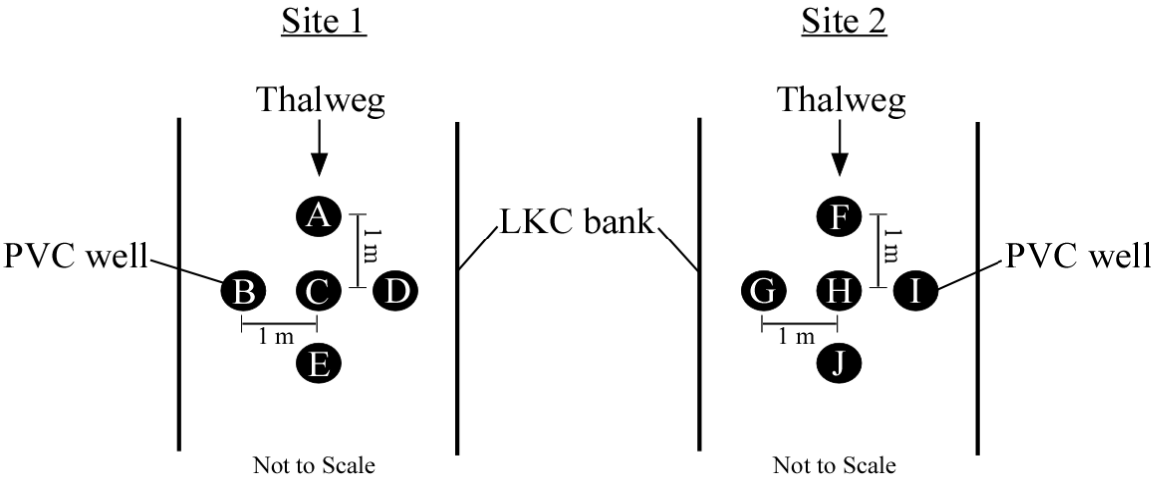

Figure II-1: Birds-eye view of well setup in the stream channel. Capital letters indicate respective well names used at each site.

Weather permitting, water samples were drawn from all sampling tubes on a weekly basis, using a peristaltic pump and very low flow pumping conditions to minimize mixing. Prior to sampling, approximately three sampling tube volumes were

purged to remove stagnant water. Samples were stored in a cooler during field collection, and were transferred to a refrigerator until analyzed. Samples were analyzed for major anion chemistry using a Dionex DX 120 ion chromatograph within 48 hours of sample collection.

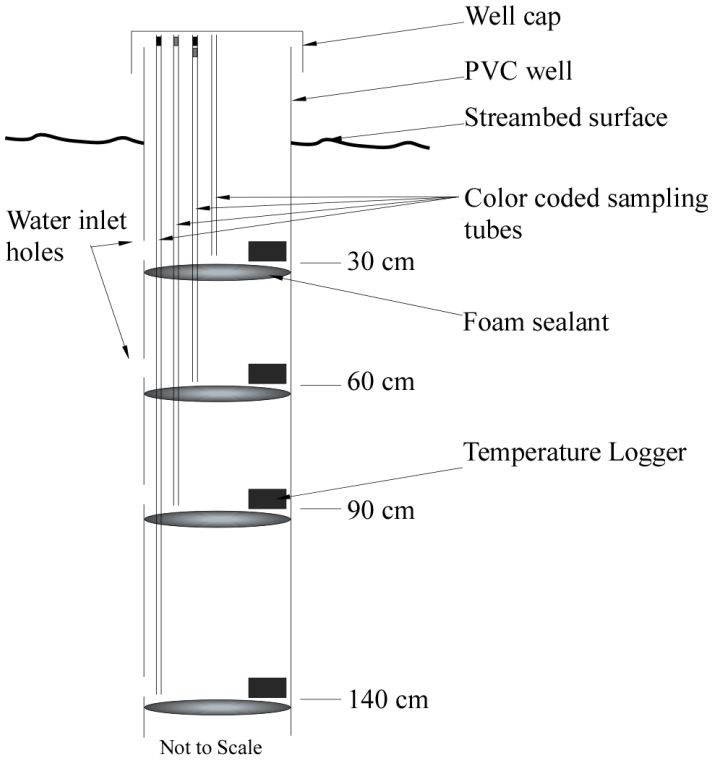

Figure II-2: Detailed view of individual well design.

CHAPTER III

WATER CHEMISTRY RESULTS AND DISCUSSION

Chloride concentrations for samples collected are displayed in Table III-1. It is thought that sediment clogging caused the sporadic working or complete failing of sampling tubes, resulting in somewhat patchy data.

As seen by Buyck (2005), it was expected that chloride concentrations in the hyporheic zone (HZ) predominantly reflect the mixing of chloride signatures from both stream water and groundwater. The equation used by Buyck (2005) to calculate the percent surface water in a sample is as follows:

$$\left(\frac{Cl_h - Cl_g}{Cl_s - Cl_g} \right) x100 = \%SW \qquad (1)$$

where Cl_h, Cl_g and Cl_s are the chloride concentrations within the HZ, of groundwater, and of surface water respectively, where all concentrations are given in mg/L. $\%SW$ is the percent surface water at the point of calculation. Stream chloride levels were measured directly (Table III-1), while groundwater concentrations were not. Fromm (2005) established a high degree of variability in groundwater chloride concentrations within the meander to the north of Site 2. Therefore, averaging chloride concentrations for use in equation 1 would give unreliable results. Groundwater chloride concentrations in wells in the meander up-gradient of Site 1 ranged from 62 mg/L to 108 mg/L in 2005 (Van der Hoven, 2008). In contrast to this, chloride concentrations in the meander to the north of Site 2 ranged from 50 to 350 mg/L (Van der Hoven et al., 2008), while mostly maintaining concentrations between 100 mg/L to 300 mg/L.

Table III-1: Chloride concentration data for Sites 1 and 2, collected over a roughly 3 month period.

Site	Depth (cm)	Well	Chloride (mg/L)								
			7/12/2007	7/23/2007	8/1/2007	8/28/2007	9/11/2007	9/18/2007	9/25/2007	10/2/2007	10/17/2007
1	30	A	72.8	68.8	80.8	71.6	93.1	74.3	65.4	56.4	53.2
		B	66.0	81.5	81.2	74.8	100.2	70.4	72.6	64.5	19.9
		C	66.3	55.2	73.9	72.7	94.3	75.7	68.1	55.2	25.8
		D	85.3	82.3	81.5	80.0	102.9	76.7	66.4	75.7	53.4
		E	70.0	74.3	75.8	73.0	97.7	69.8	66.7	63.8	63.3
	60	A	82.8	81.5	80.6	82.8	95.1	73.7	67.4	61.6	67.7
		B	68.0	72.9	76.7	72.7	76.5	68.2	69.4	62.0	28.8
		C	-	77.9	80.6	78.1	-	-	69.7	61.1	46.1
		D	79.8	86.1	83.1	80.3	101.2	77.1	66.9	74.5	54.5
	90	A	87.0	85.5	83.1	76.7	96.1	73.7	69.4	61.2	70.3
		B	74.4	83.3	79.8	74.7	77.5	70.3	72.1	64.9	24.9
		D	86.7	86.6	81.0	81.5	93.0	87.4	85.7	51.7	77.7
	140	A	-	86.5	84.8	78.4	82.7	74.7	69.6	61.9	67.9
		B	-	73.7	-	-	-	-	-	-	-
		D	84.2	84.7	82.4	81.7	86.1	86.2	88.4	82.4	93.1
2	30	F	109.5	119.9	117.4	123.5	68.1	41.2	47.2	39.8	53.4
		G	57.1	-	104.5	70.5	39.6	42.4	42.5	45.2	35.7
		H	110.8	126.2	117.7	117.4	39.3	48.7	-	-	-
		I	89.7	-	-	-	142.7	129.2	131.2	-	-
		J	147.4	130.5	124.4	117.8	46.7		64.6	57.3	68.2
	60	G	117.7	139.1	144.1	122.4	38.5	45.2	55.6	51.3	-
		H	-	-	-	121.3	-	-	-	-	-
		I	-	87.2	-	-	109.2	-	132.3	-	-

21

Table III-1 cont.: Chloride concentration data for Sites 1 and 2, collected over a roughly 3 month period.

Site	Depth (cm)	Well	Chloride (mg/L)								
			7/12/2007	7/23/2007	8/1/2007	8/28/2007	9/11/2007	9/18/2007	9/25/2007	10/2/2007	10/17/2007
2	90	F	151.1	145.6	140.7	122.9	-	-	-	-	-
		G	-	136.4	131.4	118.7	55.8	69.4	83.7	69.9	57.8
		H	115.9	115.8	109.9	106.2	40.3	49.5	49.9	59.8	62.0
		I	152.0	147.0	142.6	-	131.4	119.8	125.9	105.1	-
		J	147.3	132.1	123.6	111.6	54.8	-	104.6	86.4	83.9
	140	F	-	-	-	96.2	-	-	-	-	-
		G	-	-	116.0	-	100.4	-	-	91.2	88.9
		I	-	104.7	102.7	-	-	-	92.9	91.9	-
stream	N/A	N/A	-	46.8	40.1	29.0	82.4	33.8	65.8	258.4	22.8

* The symbol "-" indicates no sample was collected.

With the uncertainty of actual groundwater chloride concentrations, the use of equation 1 is effectively invalidated in this instance. Additionally, when actual concentrations are examined closely, streambed values are not always bracketed by stream and variable groundwater concentrations. Similar difficulties were encountered by Buyck (2005) only in two samplers, although to a much lesser degree.

A portion of the groundwater component discharging at Sites 1 and 2 is thought to originate from within the meanders upstream of each site, based on research conducted by Van der Hoven et.al. (2008), and Peterson and Sickbert (2006). The study by Peterson and Sickbert (2006) establishes a flow of stream water specifically through the meander neck separating Sites 1 and 2 of this study (Figure III-1). The study by Van der Hoven et al. (2008) furthers the delineation of meander flow paths by quantifying nitrogen cycling beneath the meander. Ultimately, the presence of stream water within meander flow paths implies that meander groundwater chloride concentrations may be dictated largely by stream chloride concentrations, as also suggested by Fromm (2005).

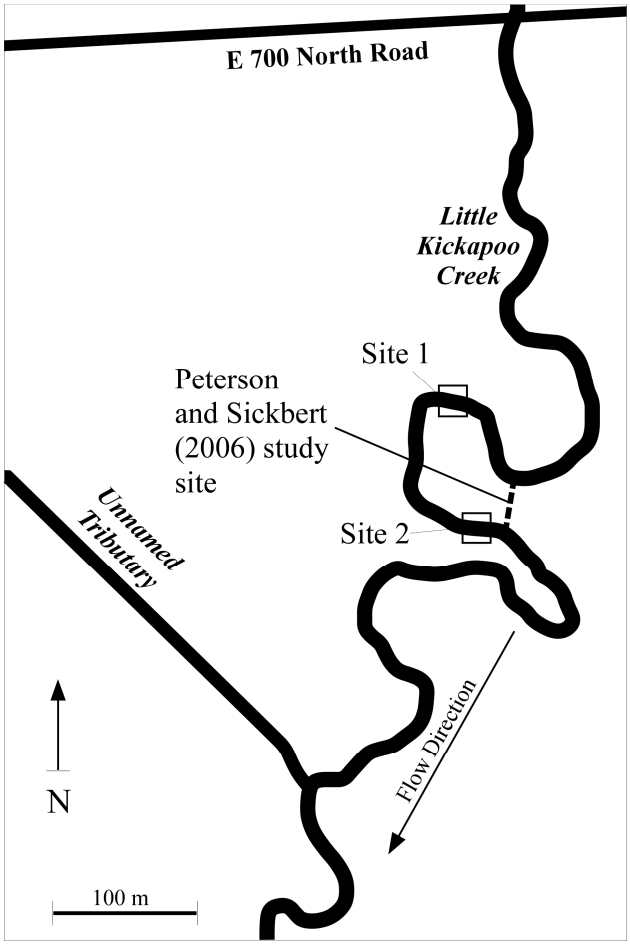

Figure III-1: Aerial map of Randolph well field showing location of Sites 1 and 2, as well as the location of the Peterson and Sickbert (2006) study site.

Long term monitoring of Little Kickapoo Creek (LKC) chloride concentrations shows a high degree of variability through time (Figure III-2). In general, stream chloride concentrations tend to be highest in the winter, due to the application of road salts, with periods of lower and less variable concentrations throughout the rest of the year. Given that groundwater chloride concentrations beneath the meanders are likely dictated by stream chloride concentrations, this reinforces the variability of meander groundwater chloride concentrations detected by Fromm (2005). Additionally, a study by Lax and Peterson (*in review*) establishes that groundwater serves as a reservoir for road salts. This

reservoir is often flushed during storm events, resulting in higher stream chloride concentrations. A potential example of this can be seen in the stream chloride concentration of 258.4 mg/L on 2 October, 2007 (Table III-1), following a period of higher stream stage suggestive of a storm event (Figure III-3).

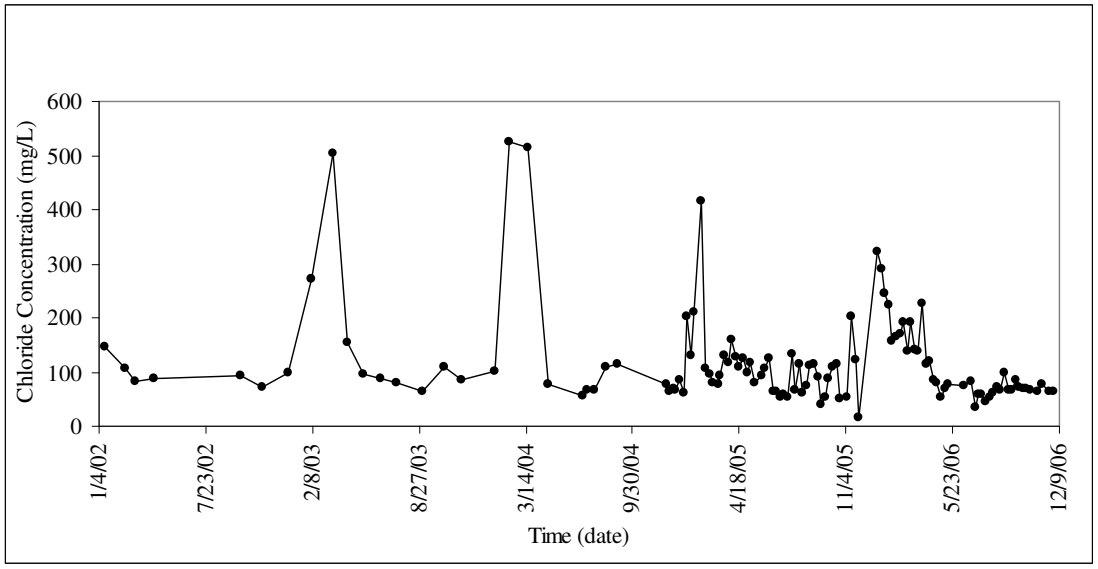

Figure III-2: Chloride concentration (mg/L) of LKC stream water through time (Van der Hoven, 2008).

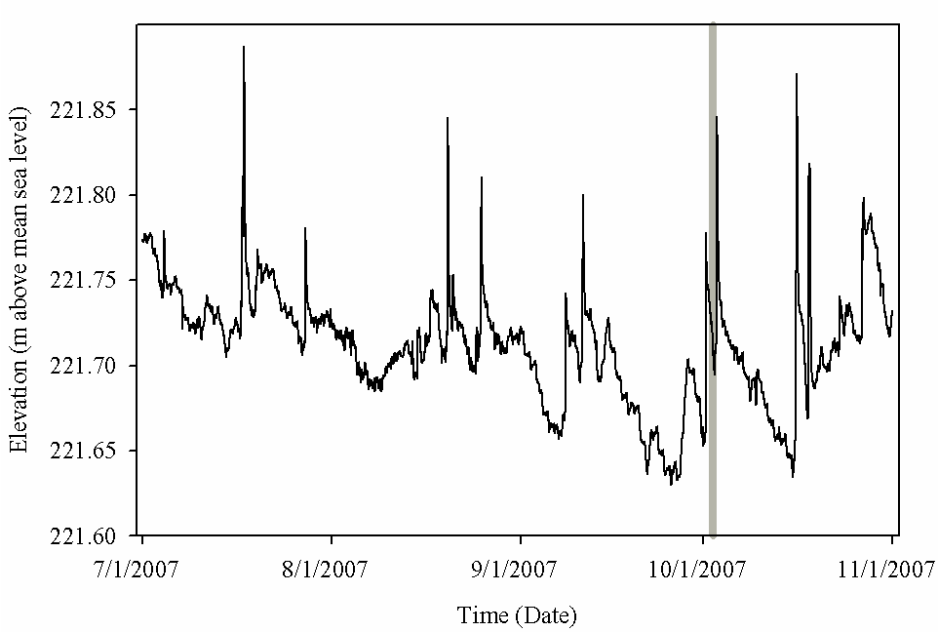

Figure III-3: Stream stage measured as elevation above mean sea level. The gray vertical line indicates the date 10/2/2007.

Finally, the meander flow through time along the most direct route through the meander neck calculated by Peterson and Sickbert (2006) was 107 days (~3.5 months). Longer flow paths are possible through wider sections of the meander, as shown by Van der Hoven et al. (2008), with estimates of 200 to 250 days for the longer meander flow paths. It is therefore hypothesized that a lag in the chloride concentrations of groundwater associated with meander flow through exists, invalidating the use of average groundwater chloride concentrations. With respect to the concentrations witnessed in the data in Table III-1, it is projected that the remnants of winter chloride concentrations are still seen to varying degrees in discharging groundwater. Due to a lack of background data, no plausible groundwater chloride concentration estimates can be formed at this time.

Despite inherent difficulties, several general interpretations can be made. Since stream chloride concentrations are known, similarities between streambed and stream

chloride concentrations can be identified; this would suggest the influence of a significant stream water component on HZ chloride concentrations.

At Site 1 average hyporheic chloride concentrations fluctuate around 75 mg/L (Figure III-4), though some well- and depth-specific variations exist. Concentrations at 30 cm depth typically seem to best mimic stream concentrations. This is as expected, based on the close proximity of 30 cm depth to the surface of the streambed. However, even at 30 cm within the HZ there already appears to be a large groundwater component present, since no concentrations follow stream chloride concentrations very closely.

Site 2 chloride concentrations are much higher than at Site 1 (Figure III-5), which is attributed to the difference in groundwater chloride concentrations in different meanders, as previously discussed. More data are missing than for Site 1, further restricting interpretations. From what can be seen of chloride concentrations at 30 cm, concentrations patterns appear to follow those of other depths more than stream concentration patterns. This suggests the impact of infiltrating stream water on streambed chloride concentrations is minimal at Site 2, possibly due to the extremely high groundwater chloride concentrations. Additionally, chloride concentrations in nearly all wells and at all depths is fairly constant and consistent, suggesting a strong steady flux of chloride from the meander.

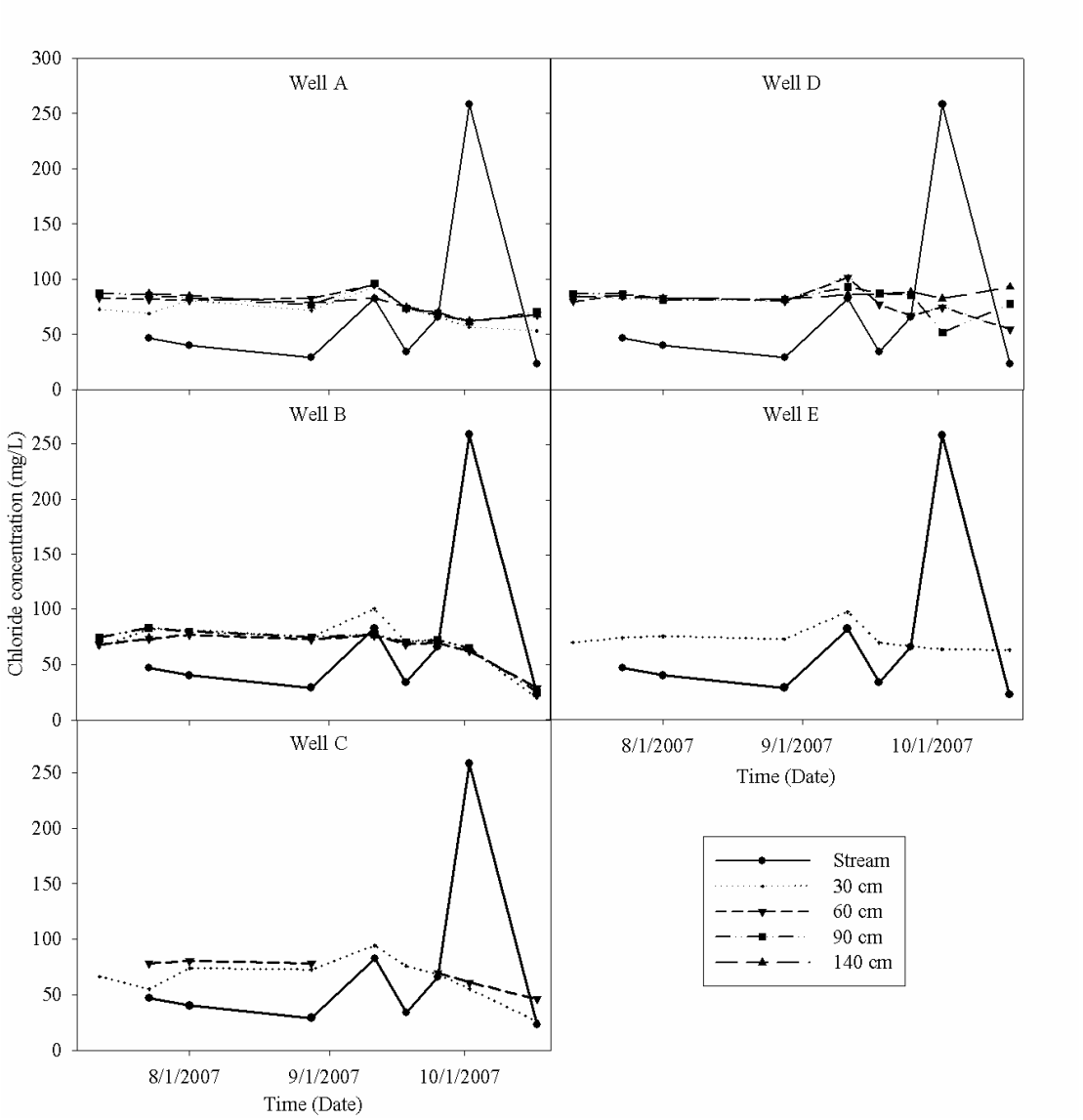

Figure III-4: Stream and streambed chloride concentrations for Site 1. Some isolated data points are represented only by their respective symbols and are not connected by a line to further data points due to missing values.

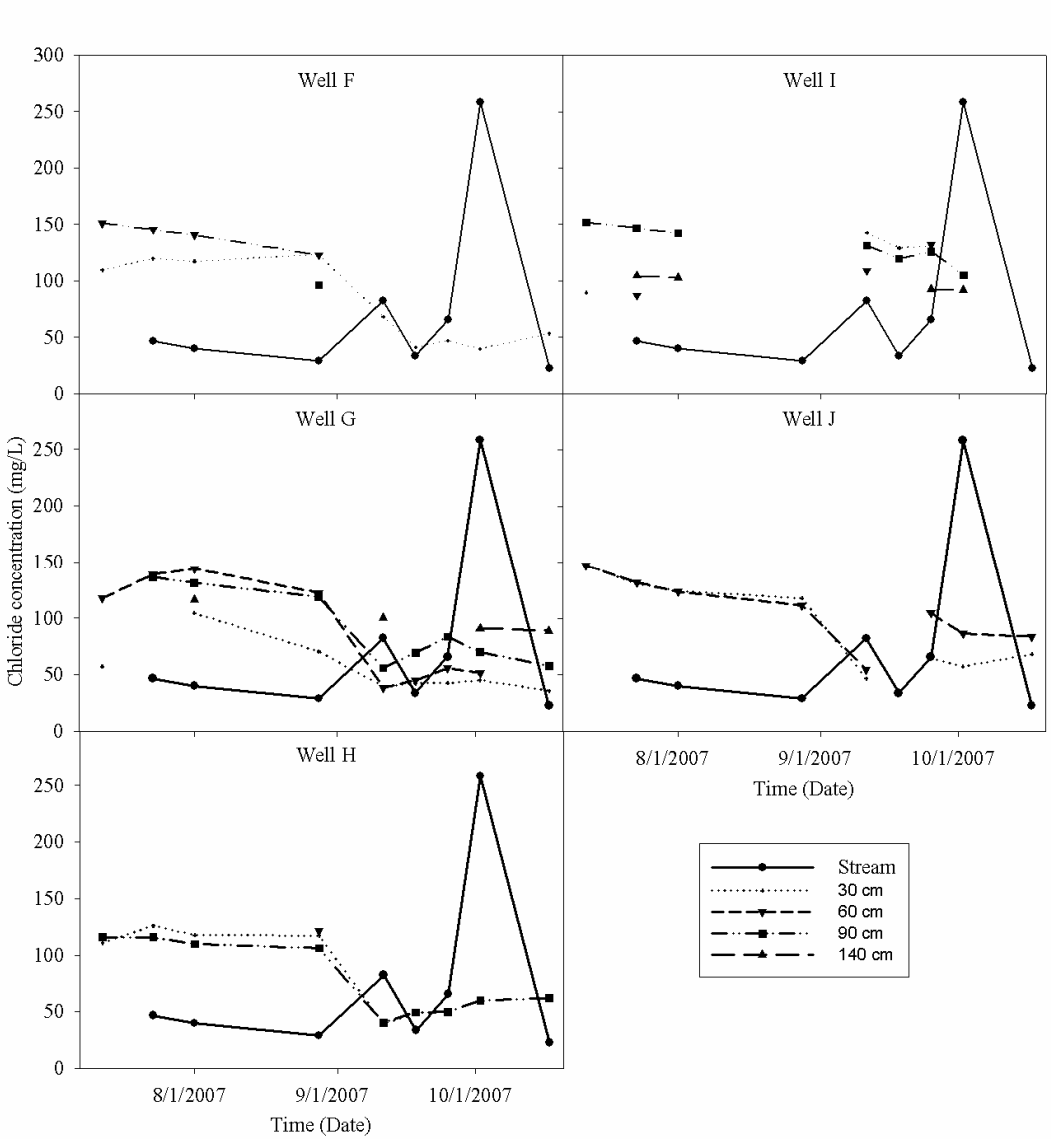

Figure III-5: Stream and streambed chloride concentrations for Site 2. Some isolated data points are represented only by their respective symbols and are not connected by a line to further data points due to missing values.

Overall, HZ chloride concentrations vary little temporally and with depth, and when they do vary they do not appear to follow stream chloride concentration patterns. This suggests the influence of a more constant groundwater source rather than a varying stream source. This is in conflict with findings by Buyck (2005), who found that HZ

chloride concentrations mimic stream chloride concentrations closely, even at depths of 90 cm below the streambed surface. Several possible explanations exist, as summarized below.

Due to the dynamic nature of both stream and HZ environments, as recognized by Fraser and Williams (1998), it is very likely that exchange conditions between LKC and its HZ have changed since 2005. Fraser and Williams (1998) noticed fluctuations in HZ extent in response to both seasonal discharge extremes, as well as to the changes in the relative strengths of down and upwelling waters. Low flow conditions persisted for most of the sampling period of this study, potentially giving groundwater a greater influence within the HZ, while Buyck (2005) sampled during a variety of conditions, most of which were higher flow. Additionally, during the majority of this study's sampling period, LKC at Sites 1 and 2 was under dammed conditions, due to the construction of a beaver dam upstream of Site 1. This also contributed to decreased surface flow in LKC.

Another possibility is that groundwater chloride concentrations during the Buyck study were lower than the hypothesized ranges for this study, effectively reducing the signal strength of groundwater, while allowing stream chloride concentrations to appear as though overwhelming HZ concentrations. This is supported by the high variability of LKC chloride concentrations through time (Figure III-2) and the established flow paths through meanders at both sites which cause respective groundwater bodies to have similar variable signatures. However, since the Buyck study looked at chloride concentrations over an extended period of time, the possibility of an overall lower groundwater chloride concentration seems implausible.

Additionally, though the presence of meander flow paths was recognized by Buyck (2005) as a potential third mixing component, a change in their prevalence or efficiency at discharging waters into respective HZ's may have changed through time or in response to dammed conditions or other changes in stream morphology.

Finally, different sampling methods and site setups were employed by Buyck (2005), which may have had minor influences on results.

CHAPTER IV

THE IMPACT OF STREAMBED SEDIMENT SIZE ON HYPORHEIC TEMPERATURE PROFILES IN A LOW GRADIENT THIRD-ORDER AGRICULTURAL STREAM – A STATISTICAL APPROACH

Abstract

To develop an understanding of the impact of sediment size on temperature profiles within the hyporheic zone of a third order agricultural stream, a statistical approach was used. Field data were collected by two temperature probe grids along two riffles, one featuring predominantly gravel (d_{50} = 3.9 mm) and the other predominantly sand (d_{50} = 0.94 mm). Temperature loggers were positioned upon installation uniformly at 30, 60, 90, and 140 cm below the streambed surface, recording at 15-minute intervals over a 6 month period. Surface water and air temperature were recorded also.

Statistical methods involved general summary statistics, and time series cross-correlation.

Distinct differences in thermal profiles were identified. Site 1, featuring poorly sorted gravels, showed a high degree of thermal heterogeneity in the form of a localized downwelling zone within a gaining stream environment. Site 2, characterized by moderately sorted sand, showed a more vertically and horizontally homogenized thermal environment regulated by the constant mixing of upwelling groundwater and downwelling surface water. Additionally, either significant groundwater discharge, or an increased amount of finer sediments at Site 2 was deemed accountable for a noticeable temperature disparity between surface water and shallow hyporheic zone temperatures.

Advection is assessed to be a major controlling factor to diurnal temperature signal penetration depth, where diurnal trends are generally limited to the upper 30 cm of the streambed. Surface seasonal trends were detected at much greater depths, leading to

the conclusion that they are transmitted initially by advection into the HZ, and by conduction to areas beyond the extent of the HZ.

Lateral and longitudinal temperature profiles were found to differ based on factors influencing thermal transport, such as the presence of preferential flow paths. In general, progressive transmission of temperature signals was more apparent in longitudinal profiles, following the direction of stream flow, with minor local abnormalities detected at Site 1.

Key words: hyporheic zone, temperature, time series analysis, cross-correlation

Introduction

Water temperature has had significant impacts on the field of hydrogeology, and the development of various research methods has allowed water temperature to play an integral role in many studies. More specifically, evaluation of streambed temperature profiles can be used to quantify groundwater/stream interactions (Stonestrom and Constantz, 2003), delineate flow paths in the hyporheic zone (HZ) (Conant, 2004), and assist in the evaluation of factors that generate change within thermal profiles (Malard, et al., 2001). Despite many established uses of water and hyporheic temperatures, the volume of literature discussing temperature as a tracer remains light (Anderson, 2005), and HZ studies are mostly performed on low order, high-gradient streams (Bencala, 2005).

The HZ is defined as a zone below the stream channel where surface and groundwater mix (Conant, 2004; Hayashi and Rosenberry, 2002). Hyporheic ecological importance became well-established in the early 1980s (Bencala, 1993) and the HZ is

now recognized as a distinct biogeochemical environment. The HZ can be viewed as a subsurface flowpath, along which water flowing in from a stream channel mixes with subsurface water, and then returns to the stream (Bencala, 2000; Cardenas et al., 2004; Bencala, 2005). More recently, HZ's in low gradient streams have been found to extend beneath meanders, as increased hydraulic gradients across meanders drive portions of stream water out of the stream channel and through meander flow paths instead (Peterson and Sickbert, 2006; and Van der Hoven et al., 2008).

Hyporheic temperatures are controlled by the mixing of groundwater and surface water, where groundwater temperatures generally vary two to three degrees from mean annual air temperatures, disregarding geothermal influences, and surface water temperatures show both diel and seasonal fluctuations (Brunke and Gonser, 1997; Peterson and Sickbert, 2006). Dogwiler and Wicks (2006) show that with increasing depth and/or distance from infiltration sites the diel and seasonal fluctuations of surface water become attenuated and lagged, while the annual air temperature cycle persists. These patterns can be a valuable tool in defining HZ depth and extent (White et al., 1987). However, delineations of HZ extent are not constant through time, as shown by Fraser and Williams (1998) whose results suggest that the extent of the HZ varies both seasonally as well as with event-based fluctuations.

In addition to HZ extent delineation, the identification of losing and gaining reaches has become possible through realization of their unique thermal patterns (Silliman and Booth, 1993; and Stonestrom and Constantz, 2003). Areas with relatively constant HZ temperatures through time were identified as gaining reaches, while reaches

where HZ temperatures varied with diurnal surface stream temperature variations were identified as losing reaches.

While HZ temperatures are dominantly controlled by advective processes, conductive processes may also play an important role (Evans et al., 1995). The influence of both advective and conductive processes on hyporheic water temperatures suggests that sediment size can impact the effectiveness of both by 1) partially defining the hydraulic conductivity of the stratum, effectively limiting advection, and 2) controlling the connectivity of the sediment, there by limiting conduction. Vaux (1968) and Cooper (1965) suggest that larger objects in or on the streambed surface respectively, alter the flow paths of hyporheic and stream waters. With respect to finer sediments, Ringler and Hall (1975) showed that the largest gradients between stream and hyporheic water temperatures occur at heavily silted sites, where slow inter-gravel flows persist. Additionally, variations in hydraulic conductivity of the streambed may result in uneven discharge and flow geometry (Becker et al., 2004).

Ultimately this study focuses on determining the effect of streambed sediment grain size on temperature profiles of the HZ, with the hope of furthering existing knowledge of water temperature in the environment. The use of time-series analysis allows the identification of data trends otherwise concealed. A similar statistical based approach taken by Malard et al. (2001) successfully assessed temperature patterns within a glacial floodplain system.

The primary hypothesis addressed is that streambed sediment size affects HZ temperatures. Specific interests lie in transmission of both seasonal and diurnal surface temperature signals into the subsurface, the comparison of lateral and longitudinal

temperature profiles, and the possibility of quantitatively delineating the HZ using temperature data.

Study Site

Field investigations focused on two sites along a stretch of the Little Kickapoo Creek (LKC) running through the Illinois University Randolph Well Field (Figure IV-1), located in McLean County, central Illinois, USA. Central Illinois has a temperate climate, with cold, snowy winters and hot, wet summers. Mean annual air temperature for the period from 1950 to 2002 was 11.2 ºC (Peterson and Sickbert, 2006).

LKC is a low gradient third-order perennial stream, which meanders (sinuosity of 1.8) through Wisconsinan glacial plains and originates in an urban area approximately 11 km north of the study site (Peterson and Sickbert, 2006). Regionally LKC is a gaining stream, with a gradient of 0.002. Locally, by the meander along which the two (2) study sites are located, a gradient of 0.003 exists (Peterson and Sickbert, 2006). The stretch under investigation is unmodified and meanders through an approximately 300 m wide alluvial valley. Terrain bordering the stream is used predominantly as agricultural farm land, alternating corn and soy bean production.

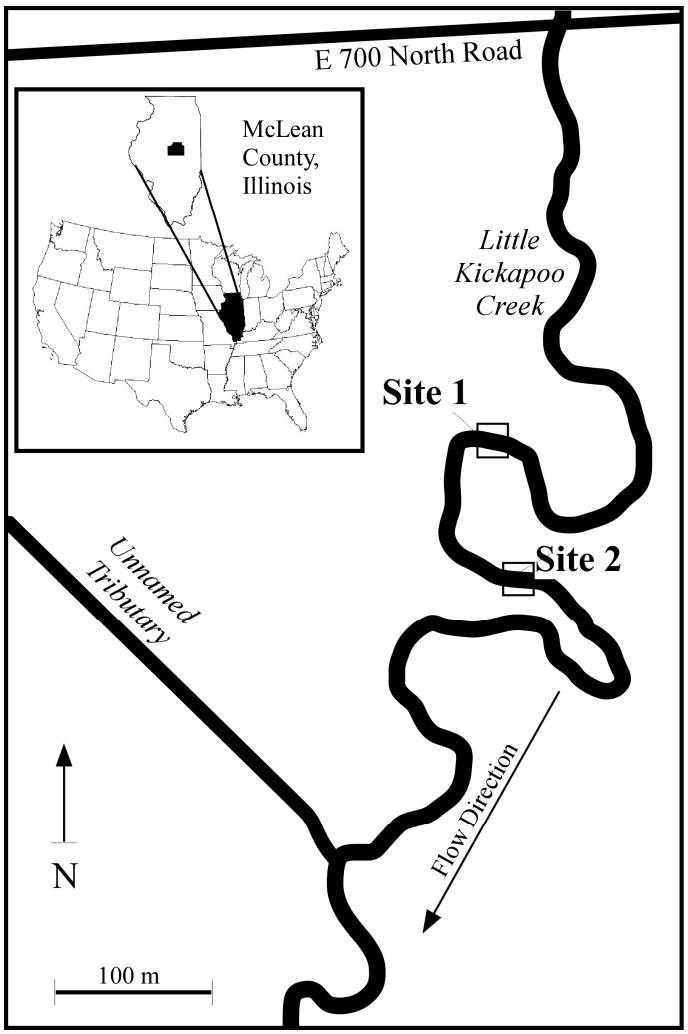

Figure IV-1: Site location within the U.S. and Illinois.

Three geologic units comprise the alluvial valley through which LKC meanders: the Wedron Formation (WF), the Henry Formation (HF), and the Cahokia Formation (CF) (listed from oldest to youngest). The WF acts as a lower confining unit to the HF, being a clay-rich low-permeability till. The HF functions as an aquifer due to its poorly sorted gravels and sands, and has an average hydraulic conductivity of 10 m/day (Peterson and Sickbert, 2006), and an average thickness of 5-7 m in the outwash valley. Above the HF lies the CF, consisting of fine-grained sand and mud, with a thickness of

up to 2 m. LKC channel is inset into the CF, cutting into the top of the HF. LKC streambed sediments are composed of mostly HF materials, consisting primarily of gravel and coarse sand with interstitial silt. Surface sediments vary with distance along the channel.

Both sites are located in riffle sections of the stream channel. Site 1 is the further upstream site, featuring predominantly gravel (d_{50} = 3.9 mm) while Site 2 lies further downstream with predominantly sand size sediments (d_{50} = 0.94 mm) (Peterson, 2008) (Figure IV-2). Sediment samples represent a composite of the top 30 cm of the streambed.

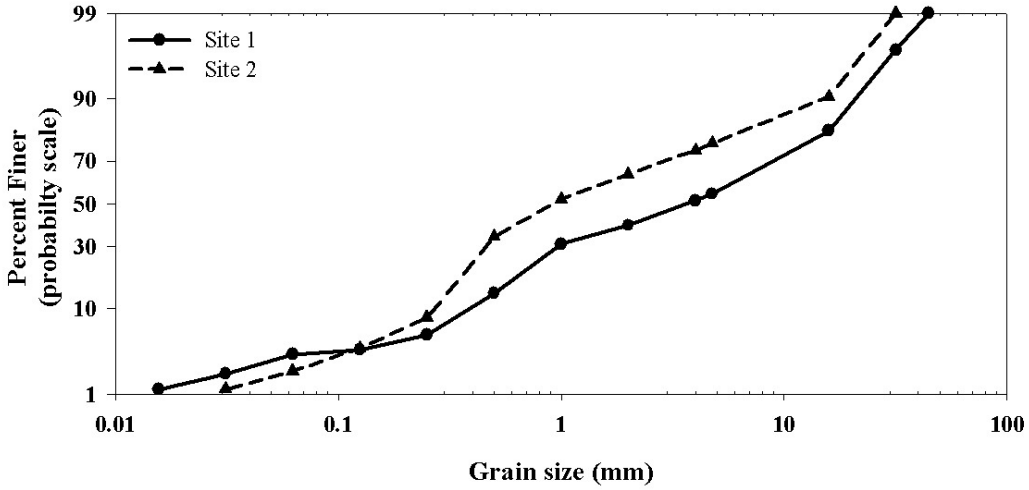

Figure IV-2: Grain size analysis for Site 1 and Site 2 sections of LKC.

Methodology

Temperature Measurements

Two identical temperature probe grids were set up along riffles within LKC sites. Each grid consisted of five vertical logger nests (referred to as wells) creating both lateral and longitudinal profile lines across the channel. The two profile lines intersected roughly in the stream's thalweg, where one nest provided data for both profiles (Figure IV-3). Within each 6.35 cm PVC well, temperature loggers were positioned at depths of 30 cm, 60 cm, 90 cm, and 140 cm (Figure IV-4). Foam sealant was used to partition off different depths to reduce vertical mixing, while holes drilled into the walls at each depth provided connection to the matrix. Two different styles of temperature loggers were used, composed of 10 HOBO® Temperature/Light Data Loggers (at 25 °C, accuracy: ±0.47 °C; resolution: 0.1 °C) and 32 HOBO® Stowaway Tidbit Data Loggers (at 25 °C, accuracy: ±0.4 °C; resolution: 0.3°C). Two additional temperature loggers recorded surface water temperatures. All loggers were programmed to record temperatures at 15-minute intervals. Data collection started on the June 30, 2007 and ended on the January 16, 2008, when all loggers were removed from the substrate. Grid appearance and outer condition were monitored throughout the data collection period.

Additional data collection included stream stage and air temperature. The stream stage was recorded at a permanent stilling well located 20 m upstream of Site 1. Air temperature was obtained from a weather station 220 m away. Both stream stage and air temperature were recorded on a 15-minute interval.

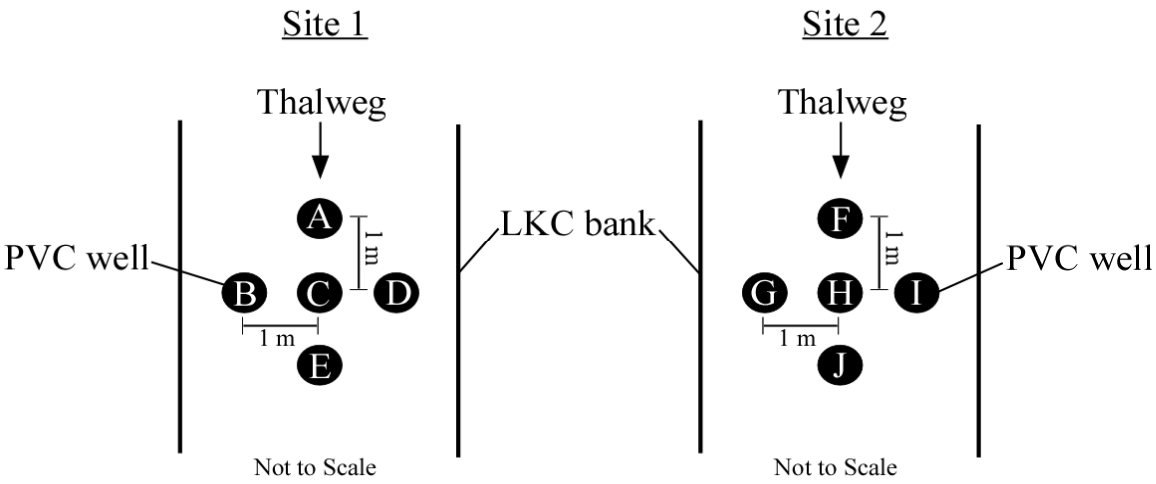

Figure IV-3: Birds-eye view of well setup in the stream channel.

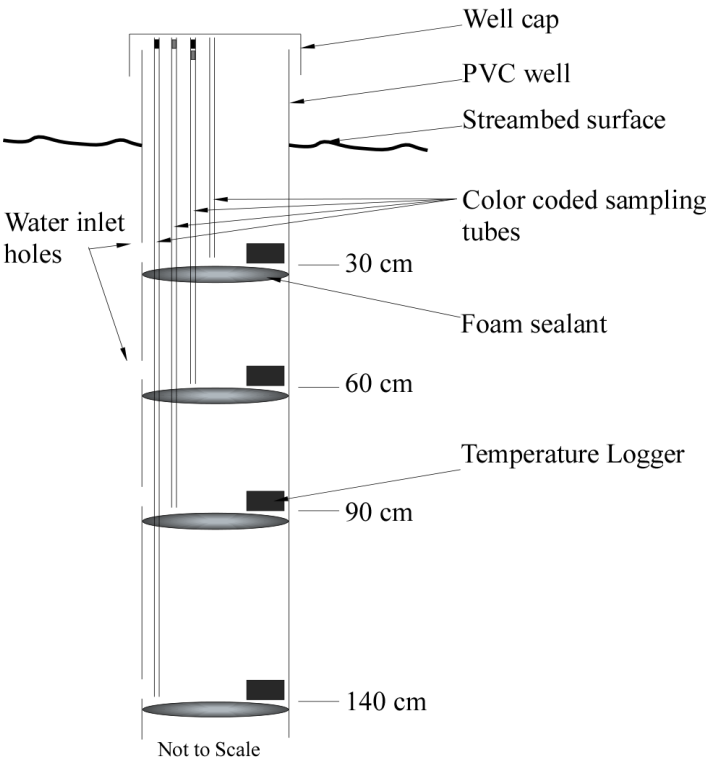

Figure IV-4: Detailed view of individual well design.

Statistical Methods

For all statistical calculations, fifteen minute (n = 15711) or hourly (n = 3904) temperature values from June 30, 2007 to December 10, 2007 were used, due to failure of the upstream temperature logger after this period. Statistics were compiled using SPSS version 16.0 (SPSS Inc., 2007).

Using 15-minute data, box plots were created for both the summer (June 21, 2007 to September 23, 2007) and autumn (September 24, 2007 to December 22, 2007) seasons (defined by the use of equinoxes and solstices), although data for both periods is incomplete. Summer collection started late on June 30, 2007 while autumn collection ended early on December 10, 2007 due to a stream logger failure. The temperature reversal (an isothermal period during which temperatures change from warm to cool) occurring in autumn, requires the separation into seasons for unbiased summary statistics, and though neither season is fully complete, the separation into seasons gives a more accurate overview of temperatures than a grouped approach.

Time series cross-correlation was used to understand the relationship of streambed temperatures both within each site, as well as between sites in more detail. The cross correlation coefficient (r) was obtained using the formula proposed by Jenkins and Watts (1968), as previously done by Malard et al. (2001) to analyze streambed time series temperature data:

$$r_{+k} = \frac{C_{x,y(k)}}{S_x S_y} \text{ with } C_{x,y(k)} = n^{-1} \sum_{i=1}^{n-k} \left(x_i - \bar{x}\right)\left(y_{i+k} - \bar{y}\right)$$

$$r_{-k} = \frac{C_{x,y(k)}}{S_x S_y} \text{ with } C_{x,y(k)} = n^{-1}\sum_{i=1}^{n-k}\left(y_i - \bar{y}\right)\left(x_{i+k} - \bar{x}\right)$$

And with

$x_1, x_2, \ldots, x_n =$ hourly values of surface water temperature or temperatures at shallower depths

$y_1, y_2, \ldots, y_n =$ hourly values of hyporheic water temperature or temperatures at deeper depths

$k = 0,1,2,\ldots,m$ where k is equal to the lag, and m is equal to the maximum number of lags.

$\bar{x} = n^{-1}\sum_{i=1}^{n} x_i$ and $\bar{y} = n^{-1}\sum_{i=1}^{n} y_i$

$S_x^2 = n^{-1}\sum_{i=1}^{n}\left(x_i - \bar{x}\right)^2$ and $S_y^2 = n^{-1}\sum_{i=1}^{n}\left(y_i - \bar{y}\right)^2$ are the standard deviations of the respective x and y series.

For the evaluation of cross-correlation the dataset was reduced to hourly data to remove redundancy. For the comparison of seasonal trends of both surface water and hyporheic water temperatures a 24-hour moving filter was applied to hourly data prior to cross-correlation, removing diel temperature fluctuations. Each filtered temperature at time X equaled the average temperature from 12 hours prior to and 12 hours after time X (including the temperature at time X in the averaging).

For computation of between-site comparisons, gradients (the difference between surface water temperatures and temperatures at 140 cm depth) were used for cross-correlation in substitution of actual recorded temperatures. This eliminated the influence of differing surface stream temperatures, and allowed instead a comparison of the degree of temperature change with depth between sites.

First order differencing was applied to all time series prior to cross-correlation, removing the data's temporal trend component and reducing autocorrelation. The resulting transformed time series are defined by: $\hat{\chi}_{(t)} = (\chi_t - \chi_{t-1})$ where $\hat{\chi}$ = term of the filtered time series, and χ_t = term of the original time series. All cross-correlations were computed using a lag (k) of 1 hr, and a maximum number of lags (m) of 125 determined so that $m * k$ is less than or equal to $n/3$ as recommended in the literature (Mangin, 1984). Though $m \leq 500$ could have been used, $m = 125$ was found sufficient for this study, minimizing excess cross-correlation output data.

For the evaluation of cross-correlation results, correlation coefficients (r) equal to or greater than 0.2 were treated as statistically significant. This was determined based on the number of observations used, and assuming rejection of the null hypothesis if alpha > 0.01.

During the data collection period several unforeseen problems were encountered. Temperature loggers located at A-90 cm, E-90 cm, G-90 cm, and I-90 cm failed completely. Additionally, the Site 1 stream logger recorded temperatures only until December 12, 2007. Furthermore, due to extensive beaver dam construction upstream of both sites, stream flow intermittently became a trickle from approximately August 2, 2007 to October 1, 2007, resulting in low flow conditions at Site 1, and periods of no

visible surface flow at Site 2. The temperature effects of this can be seen in Figure IV-5. Initially, Site 2 surface stream temperatures closely mimic Site 1 surface stream temperatures. However, near the beginning of August, Site 2 surface stream temperatures show an increase in diurnal amplitude, approximating the variability of daily air temperatures. Additionally, surface stream temperatures at Site 2 are warmer than at Site 1, beginning near October 1, 2007. This temperature difference is likely due to a greater short wave radiation exposure at Site 2 once trees begin to lose their foliage.

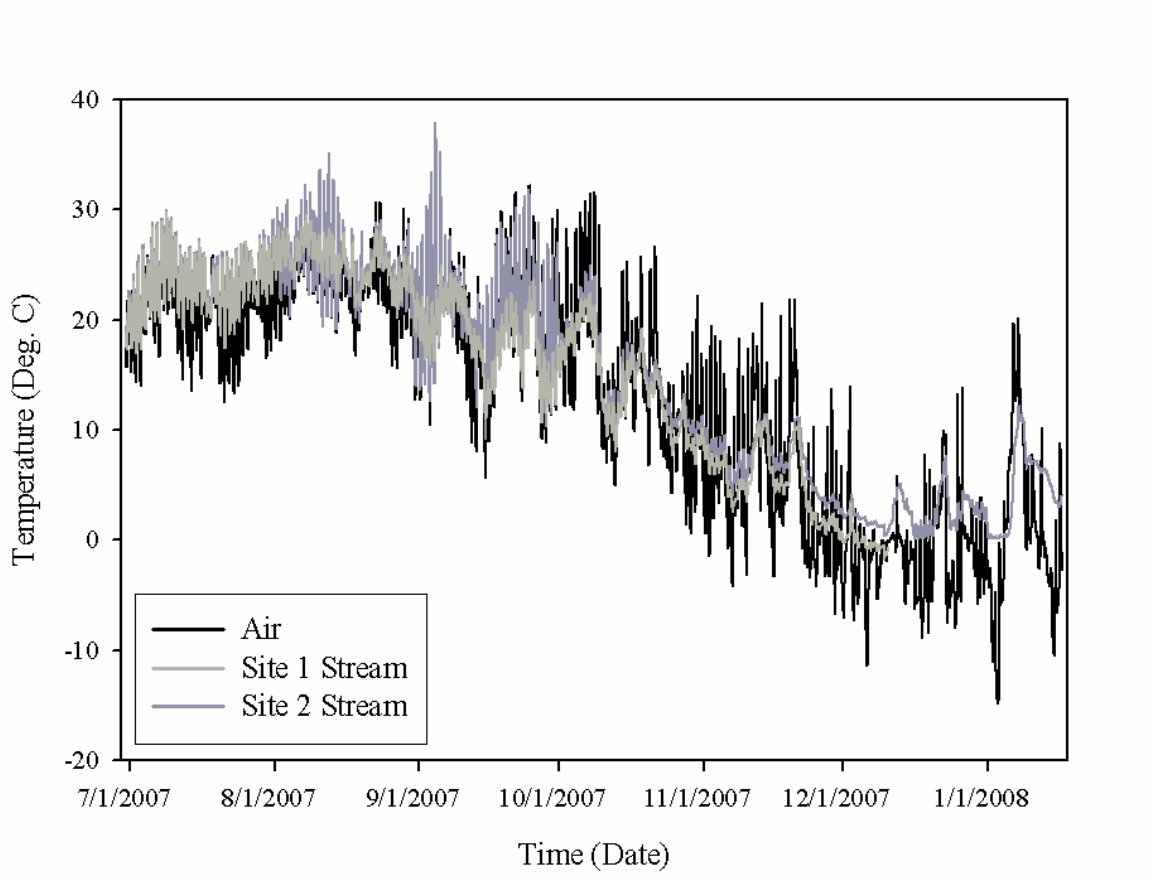

Figure IV-5: Air and stream (Site 1 and Site 2) temperature 15-minute incrementing time series for entire data collection period.

Results

Summary Statistics

Box plots were created to highlight general trends in the temperature data of both sites, and to provide an overview of the temperatures at various depths within each well.

A distinct difference in temperature patterns is seen when comparing summer and autumn results (Figures IV-6, IV-7, IV-8, and IV-9). In summer, mean streambed temperatures fall at or below mean surface stream temperatures, and pronounced cooling is witnessed with depth into the streambed at both sites. Distinct mean temperatures define different depths within the streambed. In autumn, these patterns are reversed, but only by a small margin. In autumn, mean surface stream temperatures are at or below mean streambed temperatures, and a slight warming trend is witnessed in mean streambed temperatures with depth. Additionally, temperatures appear more homogenized top to bottom, where mean temperatures at increasing depths are not distinctly different. It can be projected that the degree of opposition of autumn to summer temperature patterns would increase in winter, and decrease again in spring with the next reversal. Irrespective of the differences observed between summer and autumn temperatures, a decrease in temperature ranges with streambed depth is experienced universally to varying degrees. In general, the observations above show the data from this study to be in line with general patterns witnessed in other HZ temperature studies, such as by Dogwiler and Wicks (2006), in a karst environment featuring similar stream sediments as at Site 1, and by White et al. (1987) in a Michigan river.

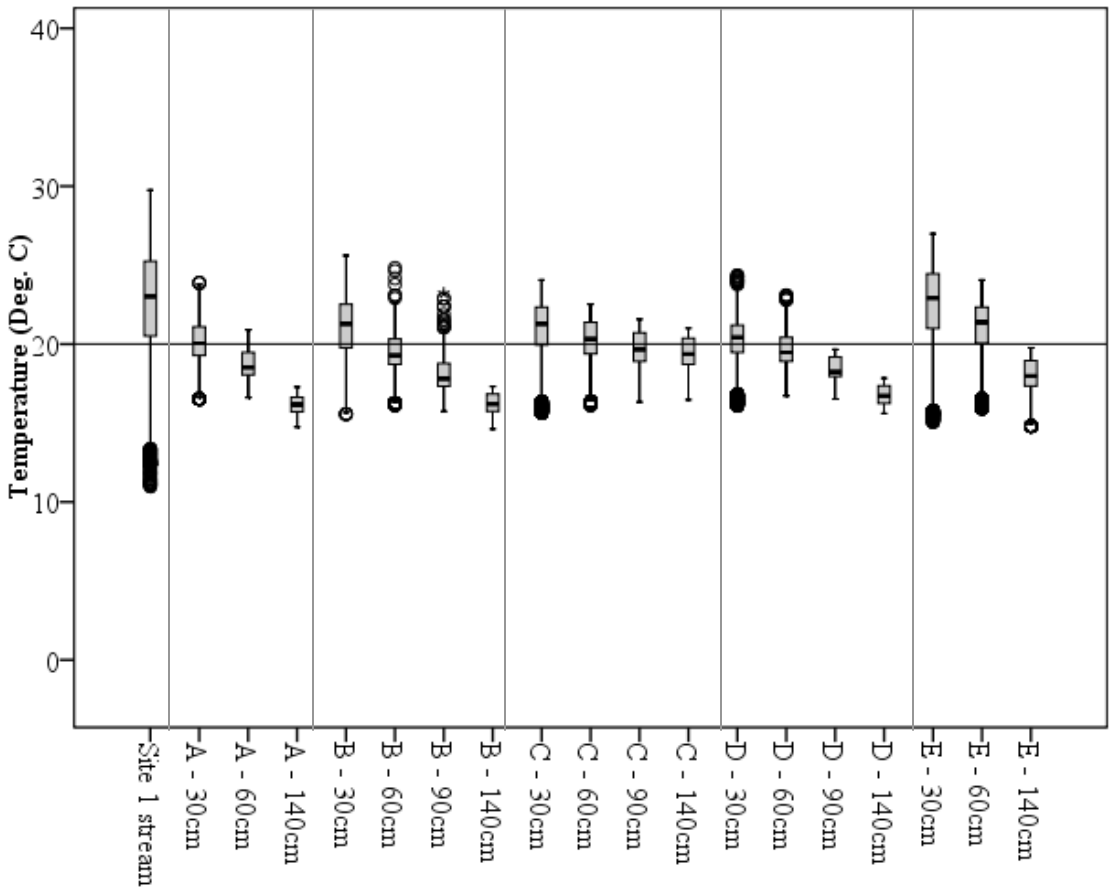

Figure IV-6: Site 1 summer (June 21, 2007 to September 23, 2007) box plots with reference lines at 20 ºC and separating wells.

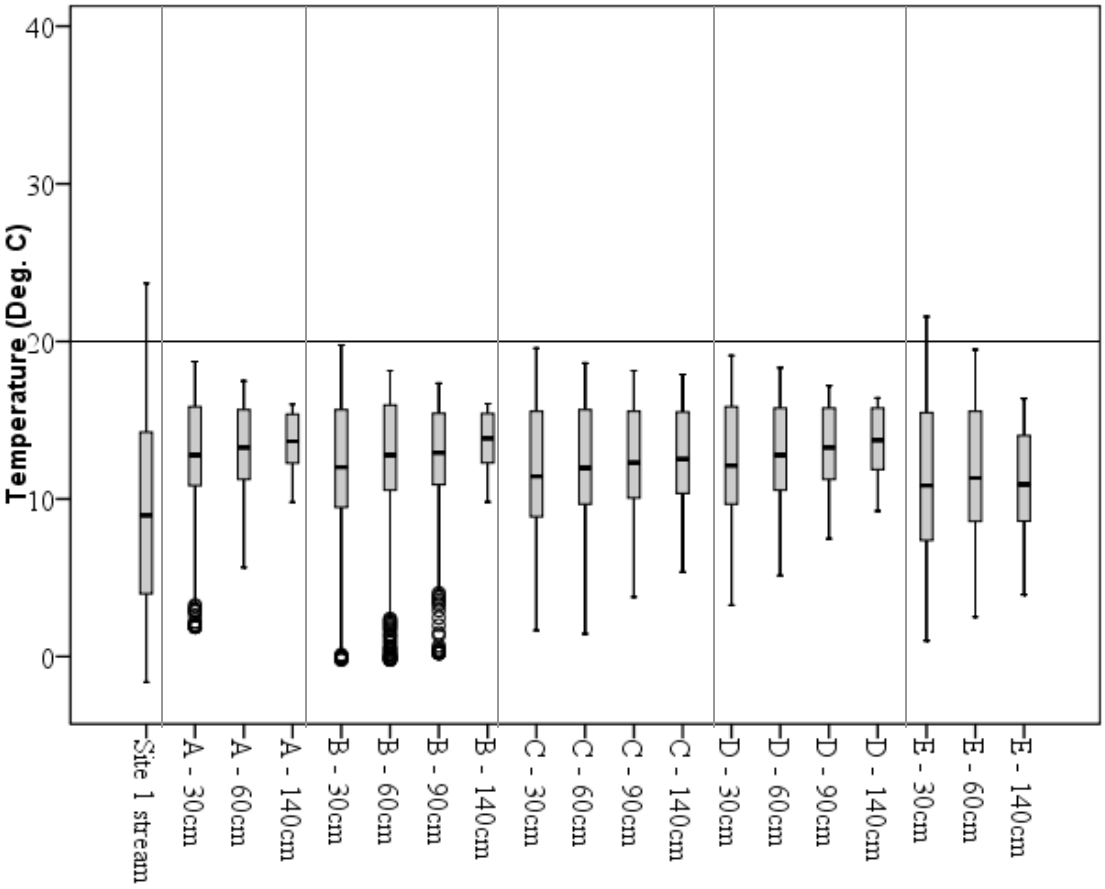

Figure IV-7: Site 1 autumn (September 24, 2007 to December 22, 2007) box plots with reference lines at 20 ºC and separating wells.

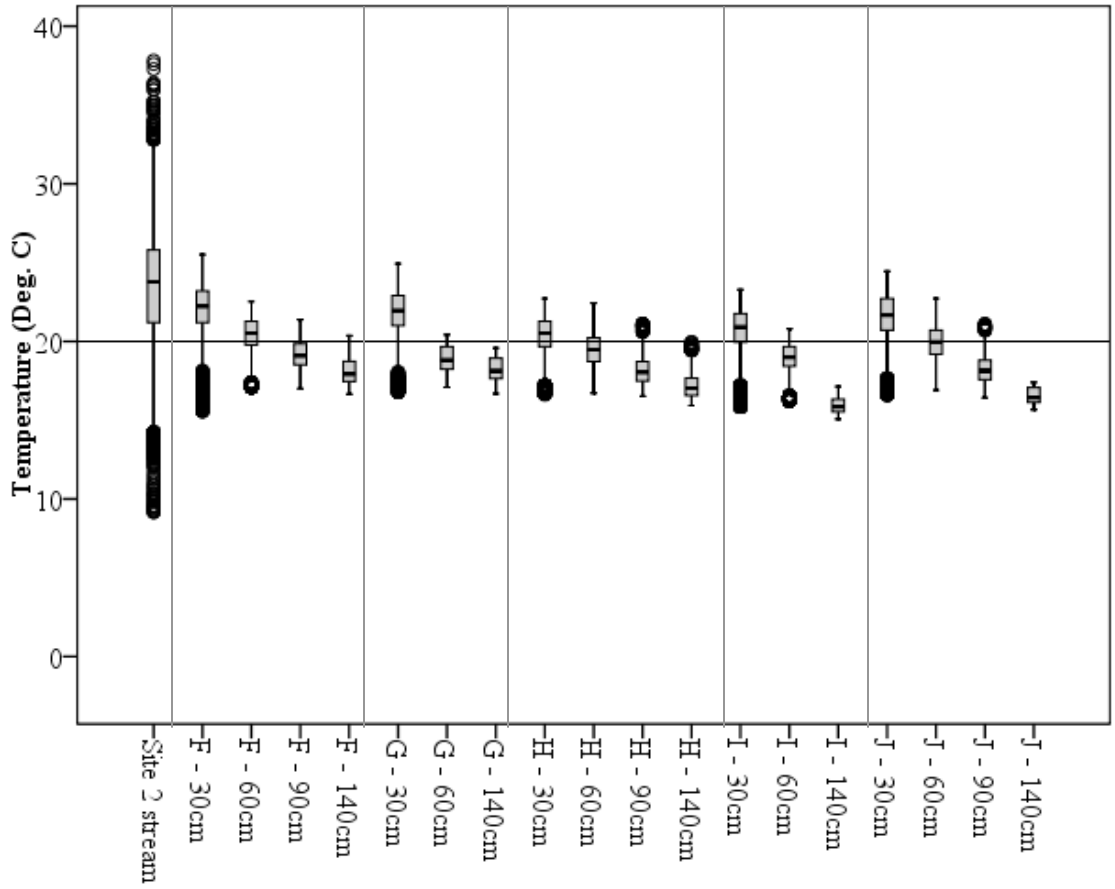

Figure IV-8: Site 2 summer (June 21, 2007 to September 23, 2007) box plots with reference lines at 20 ºC and separating wells.

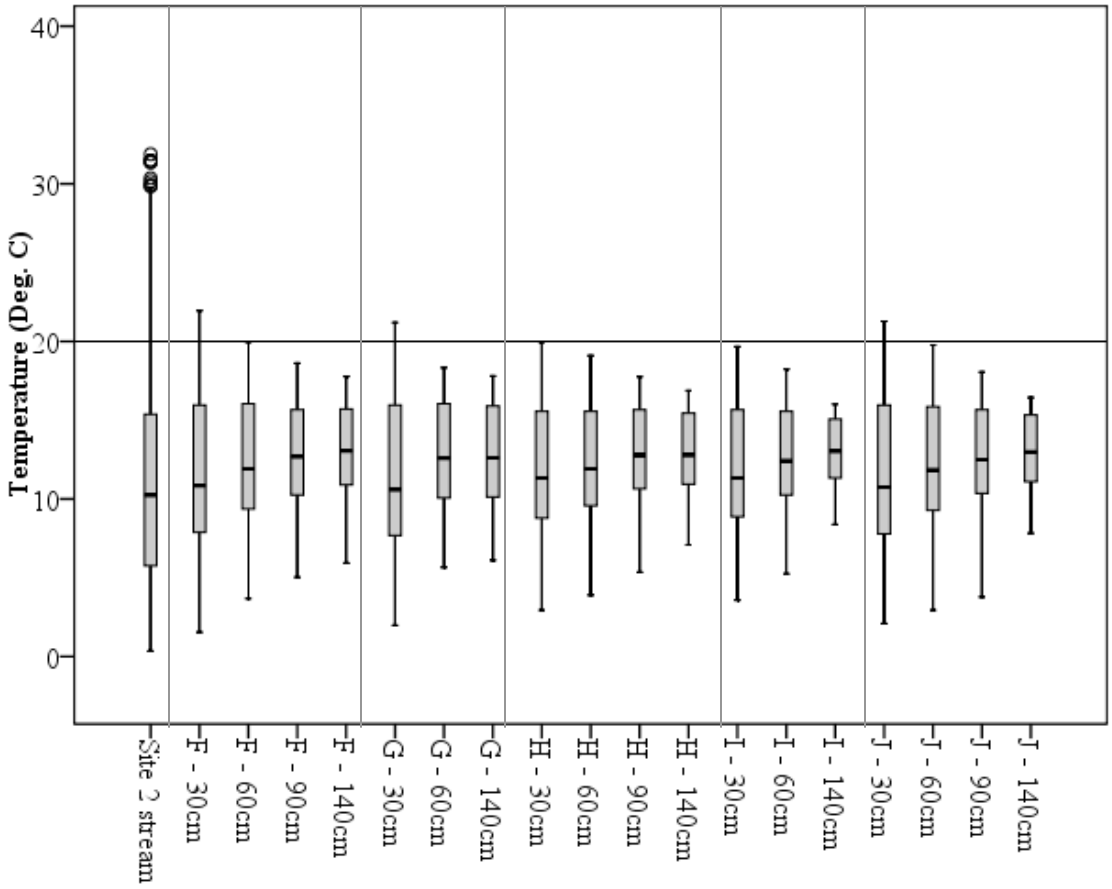

Figure IV-9: Site 2 autumn (September 24, 2007 to December 22, 2007) box plots with reference lines at 20 ºC and separating wells.

A site comparison of summer box plots reveals more uniform temperature decreases with increasing streambed depth in each well at Site 2. At Site 1, wells C and E have greater temperature ranges persisting at depth, suggesting that wells C and E manage to maintain effective temperature transmission at depth. Additionally, Site 2 surface stream temperatures vary over a wider temperature range than at Site 1, experiencing more days when temperatures are warmer, (up to a maximum temperature of 38 ºC), due to the previously mentioned dry period. Interestingly however, Site 2 streambed temperatures do not noticeably reflect this increased temperature range.

A site comparison of autumn box plots reinforces summer box plot observations. Temperatures in wells C and E again maintain larger temperature ranges at depth than do other wells at Site 1. Also, surface stream temperatures at Site 2 again experience warmer temperatures, presumably due to the remainder of the dry period as well as to generally warmer temperatures in late autumn due to increased exposure to short wave radiation. Surprisingly, Site 2 wells experience smaller temperature ranges than do equivalent Site 1 wells, suggesting slower transmission of surface temperatures into the streambed.

Seasonal Cross-correlation

Results of the 24-hour averaging filter applied to well E and J can be seen in Figure IV-10, and are representative of filter applications to all other wells. The greatest impact is on time series featuring a strong diurnal component, such as surface stream temperatures. Temperatures at depth within the streambed were only mildly affected by the filter, due to their already dampened diurnal signals. Both a seasonal trend and short-term thermal fluctuations are observed in the filtered time series, closely matching the findings of Malard et. al (2001).

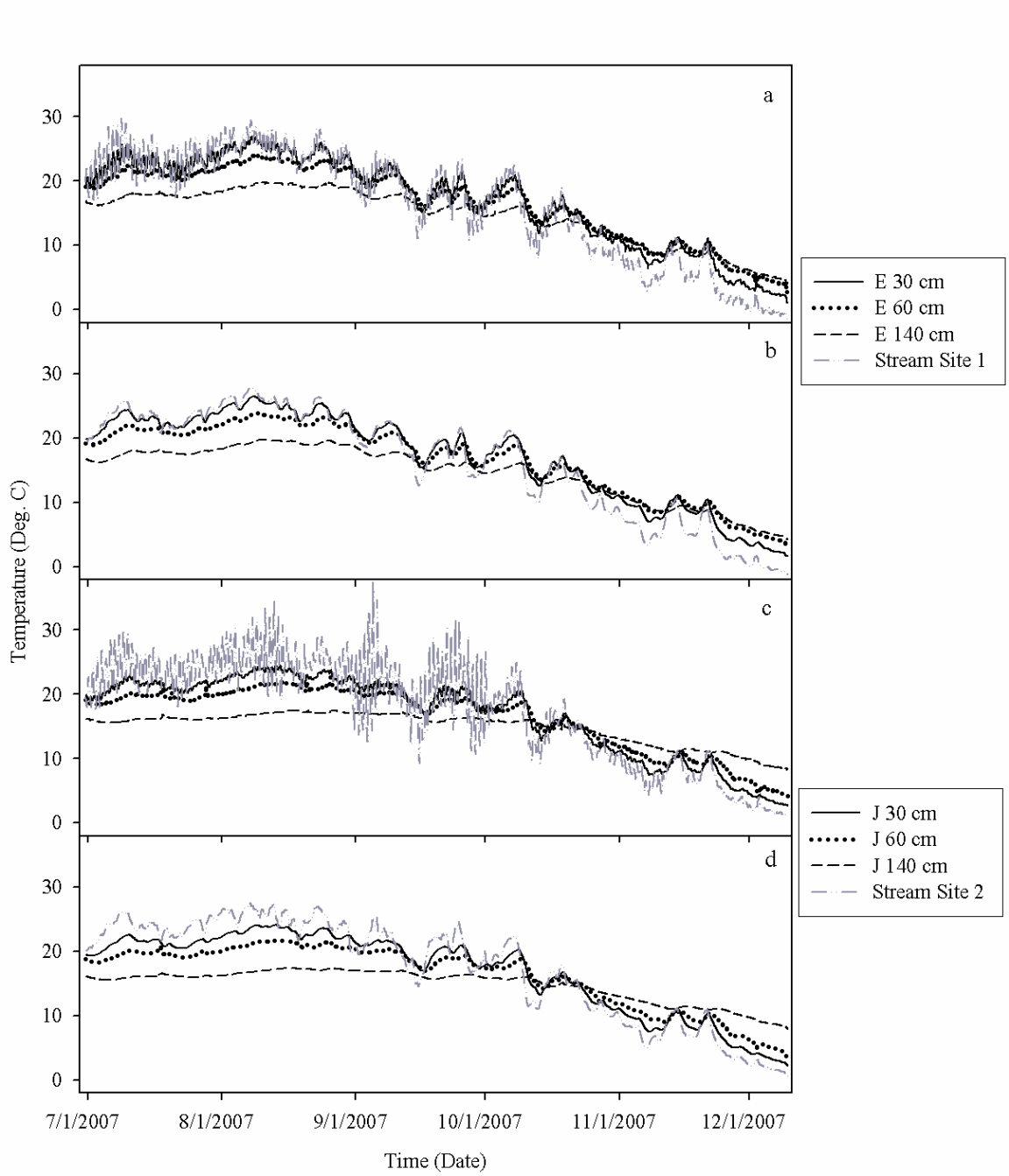

Figure IV-10: Comparison of unfiltered hourly time series (a and c) and filtered hourly time series (b and d) of wells E and J, respectively.

Cross-correlation of seasonal temperature trends between stream water and various depths within separate wells were computed to test the hypothesis that seasonal temperature trends within the streambed originate predominantly from stream water.

All streambed temperatures show significant correlation to seasonal trends in stream water (Figures IV-11 and IV-12). As expected, correlations between temperatures at 30 cm depth and stream water are highest within each well. The correlation coefficient generally decreased with depth into the streambed, as distance from the stream increases, and temperature signals become dampened through the mixing with groundwater. These results are as expected, based on research by Stonestrom and Constantz (2003) amongst others, though not evaluated by cross-correlation.

Correlation coefficients tend to persist for longer periods with increasing depth into the streambed. This is likely due to the greater thermal homogeneity at depth, as illustrated in the filtered data in Figure IV-10. The filtered data at depth 140 cm is relatively insensitive to short-term surface thermal fluctuations, resulting in lower correlation coefficients. However, temperatures remain more constant at 140 cm depth. Thus, a significant yet low correlation value persists for longer periods.

Lag times (the point where the highest correlation coefficient is obtained) of seasonal trends increase with depth to varying degrees, differing between sites as well as among individual wells. Seasonal lag times at 30 cm depth at Site 1 range from 5 hr (r = 0.941) to 23 hr (r = 0.41), and at Site 2 from 8 hr (r = 0.721) to 18 hr (r = 0.575). At 140 cm depth, seasonal lag times at Sites 1 and 2 ranged from 32 hr (r = 0.633) to 109 hr (r = 0.279) and 56 hr (r = 0.29) to 68 hr (r = 0.312) respectively. At 30 cm, relative heterogeneity of lag times is witnessed at both sites. However, at 140 cm depth, lag time

heterogeneity persists only at Site 1, while Site 2 displays relatively uniform seasonal lags.

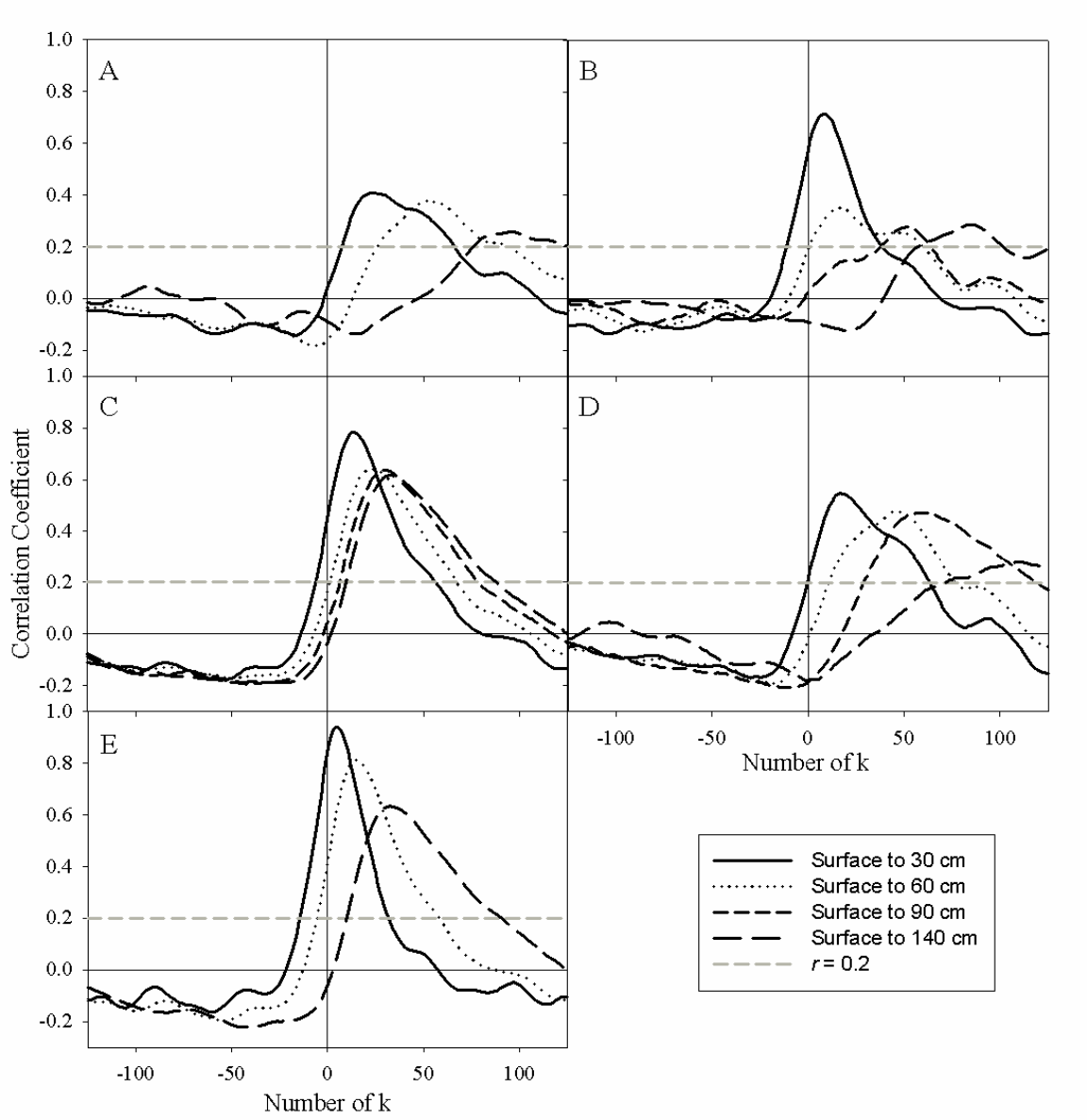

Figure IV-11: Site 1 cross-correlograms per well (indicated by Letters A through E), showing correlation between hourly, filtered (24 hr averaging filter and first order differencing) time series of surface stream temperatures and depths 30, 60, 90 and 140 cm within the streambed.

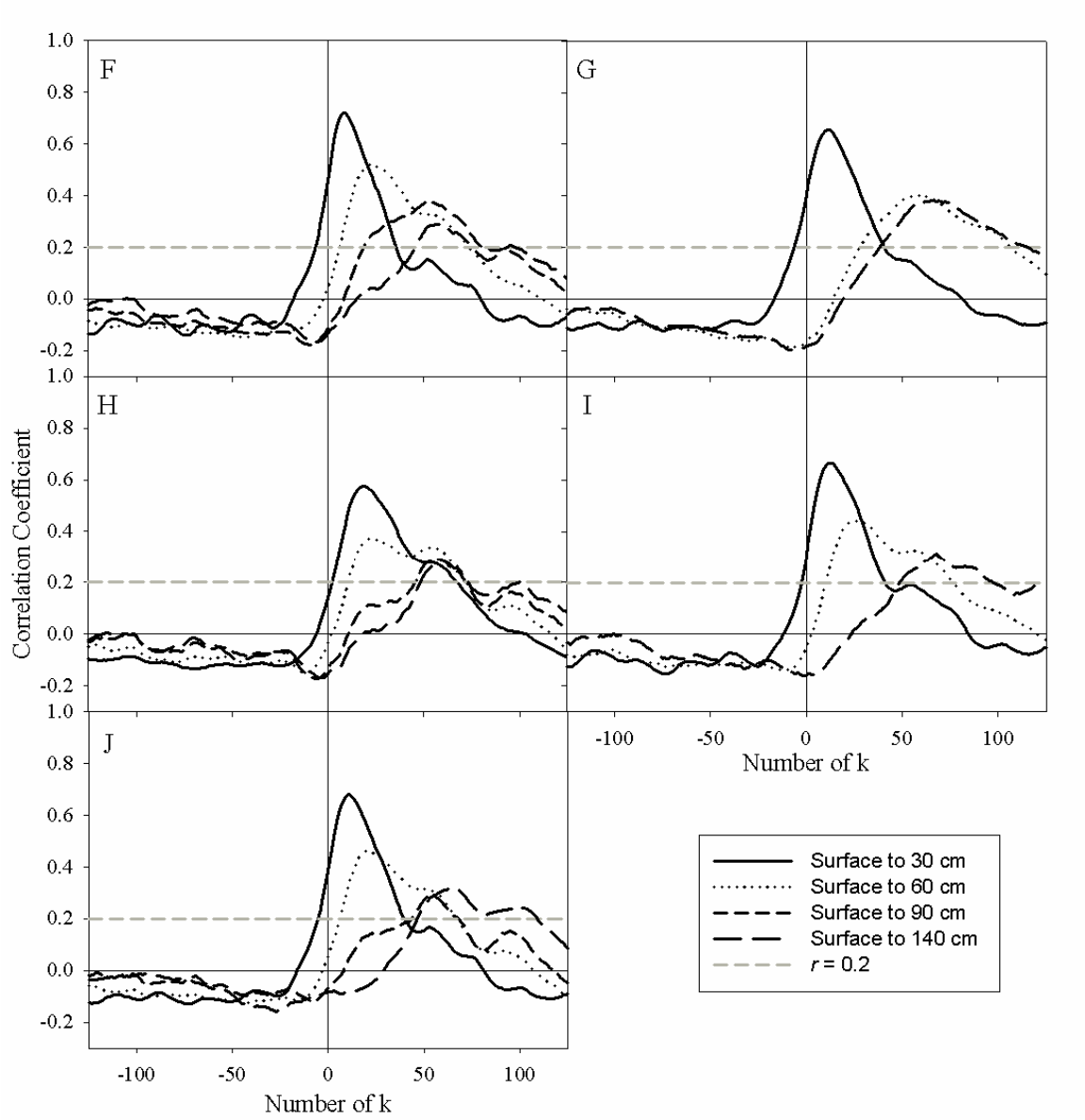

Figure IV-12: Site 2 cross-correlograms per well (indicated by Letters F through J), showing correlation between hourly filtered (24 hr averaging filter and first order differencing) time series of surface stream temperatures and depths 30, 60, 90 and 140 cm within the streambed.

To further the understanding of subsurface connections while also providing a means for lateral and longitudinal profile comparison, seasonal temperature trends were

compared at each site by cross-correlation at equal depths along both profile lines (Figures IV-13 and IV-14).

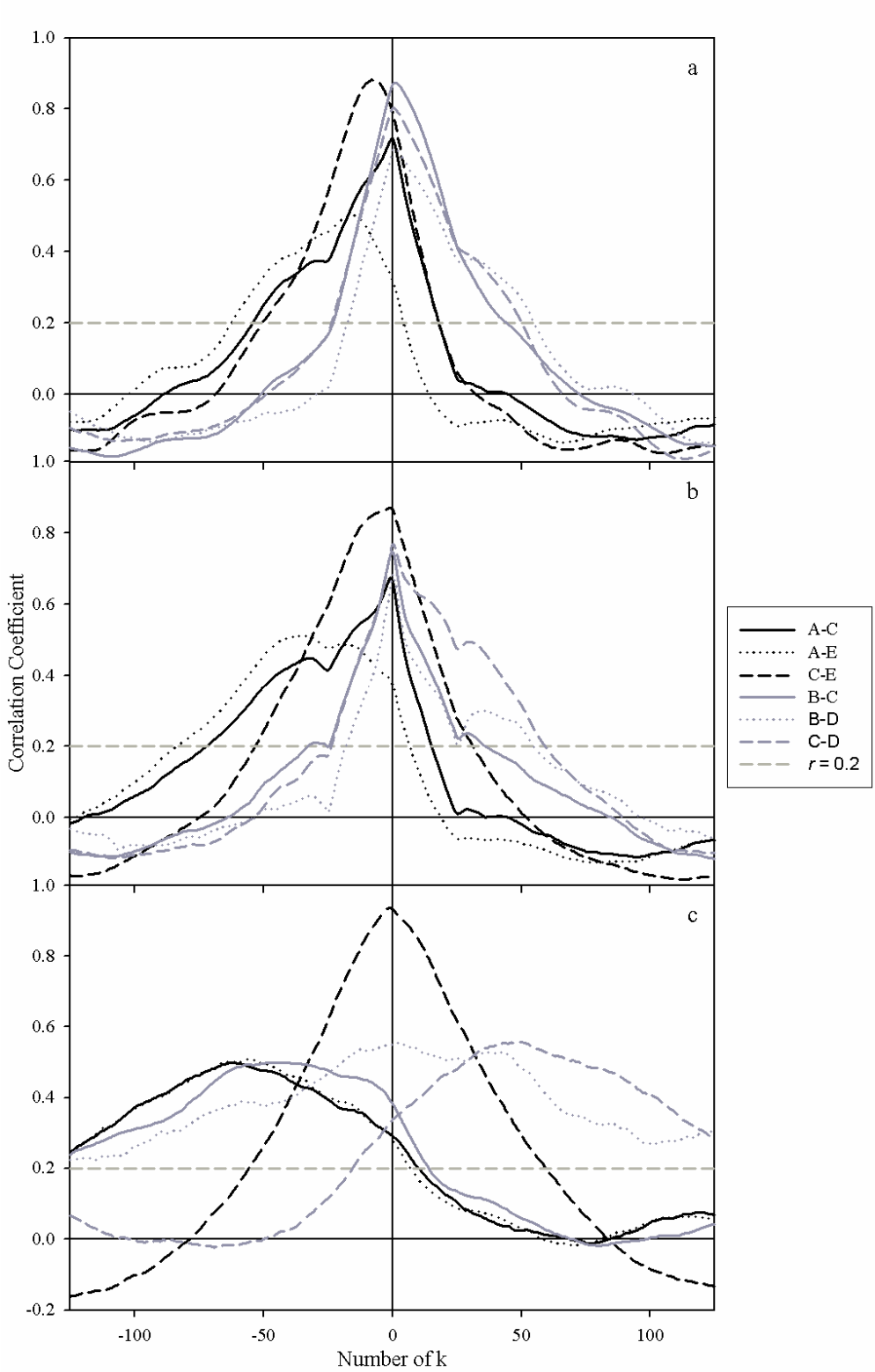

Figure IV-13: Site 1 cross-correlograms at 30 cm (a), 60 cm (b) and 140 cm (c), showing correlation between hourly filtered (24 hr averaging filter and first order differencing) time series between wells along longitudinal (black lines) and lateral (gray lines) profiles.

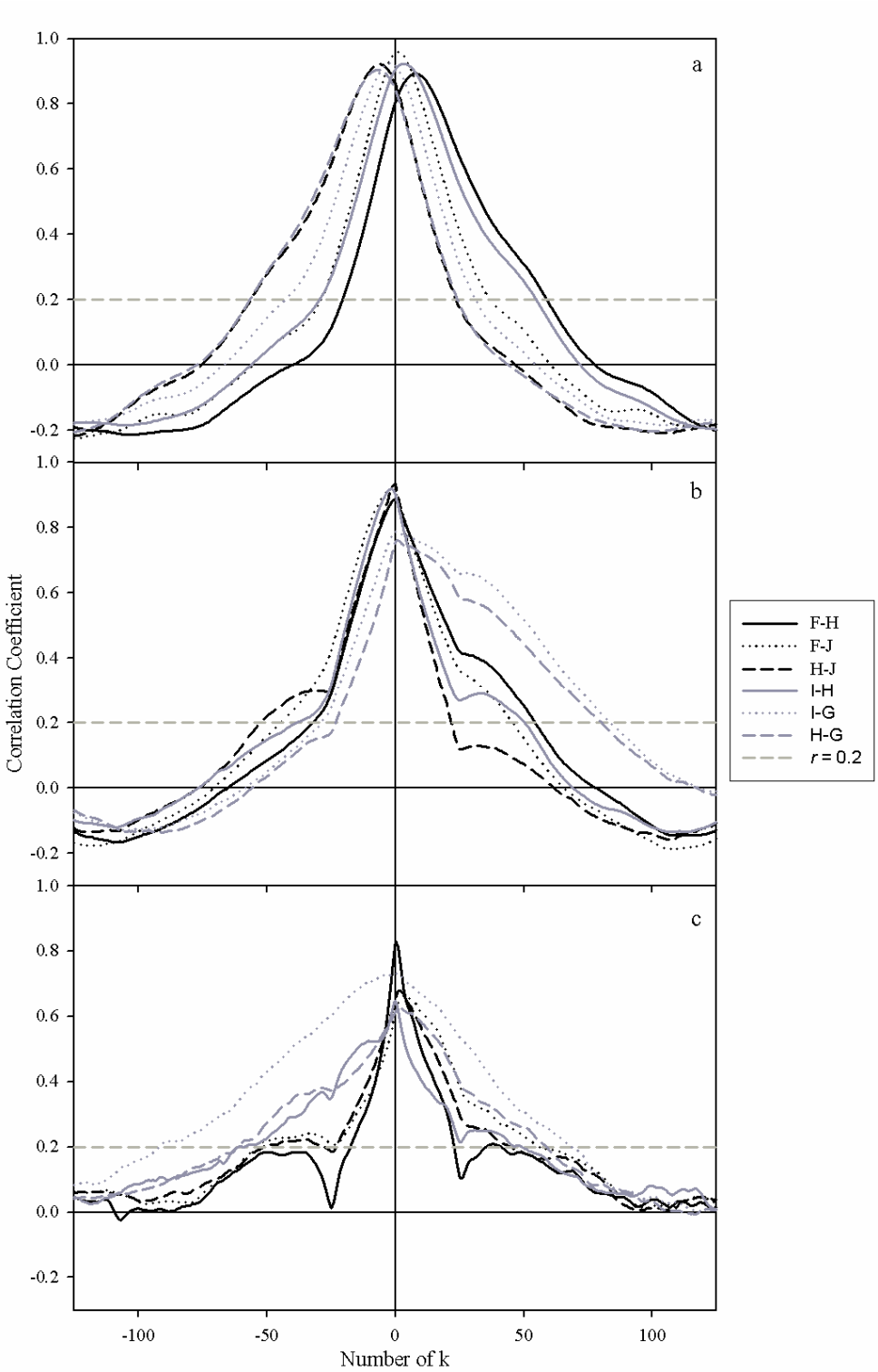

Figure IV-14: Site 2 cross-correlograms at 30 cm (a), 60 cm (b) and 140 cm (c), showing correlation between hourly filtered (24 hr averaging filter and first order differencing) time series between wells along longitudinal (black lines) and lateral (gray lines) profiles.

In general, as depth within the streambed increases (progression from graphs a to b to c in Figures IV-13 and IV-14), the correlation coefficient between temperatures at each depth decreases, regardless of profile type or site. One exception exists, between temperatures at wells C and E. Previously identified as featuring unique temperature patterns, these wells prevail in their uniqueness, which will be discussed later below.

A second generalization can be made when comparing lateral and longitudinal profiles of Sites 1 and 2. Site 1 correlograms show great variation in peak *r* values, both between depths and at the same depth. When referring back to Figures IV-6 and IV-7, both wells C and E showed wider temperature ranges than wells A, B, and D at 140 cm depth, indicating a greater influence of surface water temperatures within the streambed at these locations. Additionally, in well C the 90 cm and 140 cm depths have almost equal mean temperatures throughout the summer season. In contrast, wells A, B, and D show more regularly decreasing temperature ranges and mean temperatures with depth. This is reflected within graph c in of Figure IV-13. Laterally at depth 140 cm, seasonal trends in wells B and D lag behind well C, while longitudinally only seasonal trends in well A lag behind well C. At 140 cm seasonal trends in wells C and E are highly correlated. In contrast, Site 2 correlograms (Figure IV-14) consistently peak at or very near $k = 0$. This is supported by the patterns seen in Figures IV-8 and IV-9, where summer temperature ranges and mean temperature patterns change relatively uniformly across Site 2. Effectively, the differing temperature patterns of lateral and longitudinal profiles at Sites 1 and 2 suggest inherently different physical controls on temperature transmission from the surface stream into the streambed.

As for a comparison between lateral and longitudinal profiles within a single site, no universal patterns were detected. Local variability in streambed flow patterns and materials likely causes observed differences, with a high degree of unpredictability.

A site comparison of seasonal temperature gradients between stream and 140 cm depth was computed to test the hypothesis that both sites feature similar thermal transport mechanisms, despite featuring different sediments. Results support this hypothesis by reveal a high degree of correlation between sites, with r ranging from 0.7720 to 0.7800 and peaking universally at k = -1 (Figure IV-15). Despite local temperature differences and physical and thermal heterogeneities, there is little difference in the gradient of seasonal temperature transmission from stream to 140 cm depth. This confirms that Sites 1 and 2 feature fundamentally the same thermal transport mechanisms, with more than 70% variability accounted for, and are therefore generally comparable.

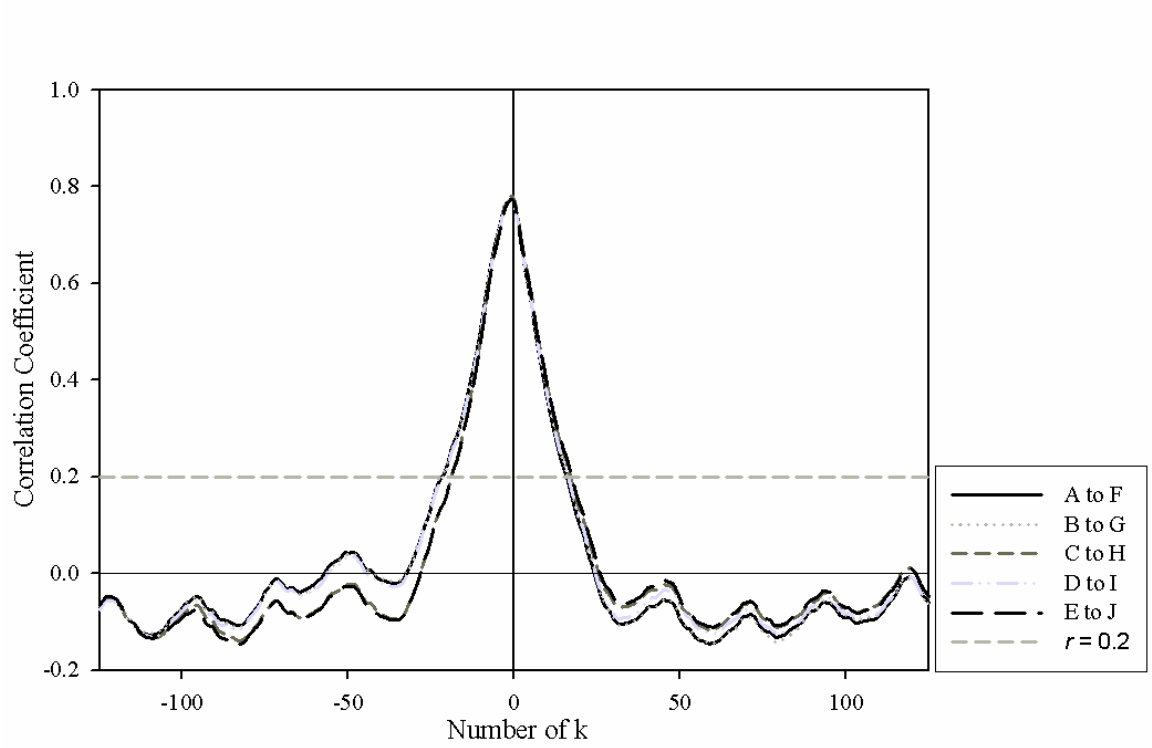

Figure IV-15: Site comparison cross-correlogram, showing correlation between hourly filtered (24 hr averaging filter and first order differencing) time series gradients (the difference between respective stream and 140 cm depth temperatures) of Site 1 wells to Site 2 wells at corresponding positions within LKC.

Diurnal Cross-correlation

Cross-correlation between diurnal temperature trends of surface stream water and streambed water at various depths within wells were computed to test the hypothesis that the advection of stream water into the streambed controls the degree of diurnal temperature changes witnessed within the streambed.

Significant correlation between diurnal stream and streambed temperatures is seen at 2 wells at Site 1, and at 4 wells at Site 2 (Figures IV-16 and IV-17). Additionally, with the exception of well E, significant correlation is seen only between stream and 30 cm depth temperatures. In well E, significant correlation is also seen between stream and 60

cm depth temperatures. Lag times of diurnal temperatures at Sites 1 and 2 range from 3 hr (r = 0.3110) to 9 hr (r = 0.3650) and 6 hr (r = 0.5030) to 8 hr (r = 0.3260) respectively. The trend of greater thermal variability at Site 1 persists in the diurnal temperatures.

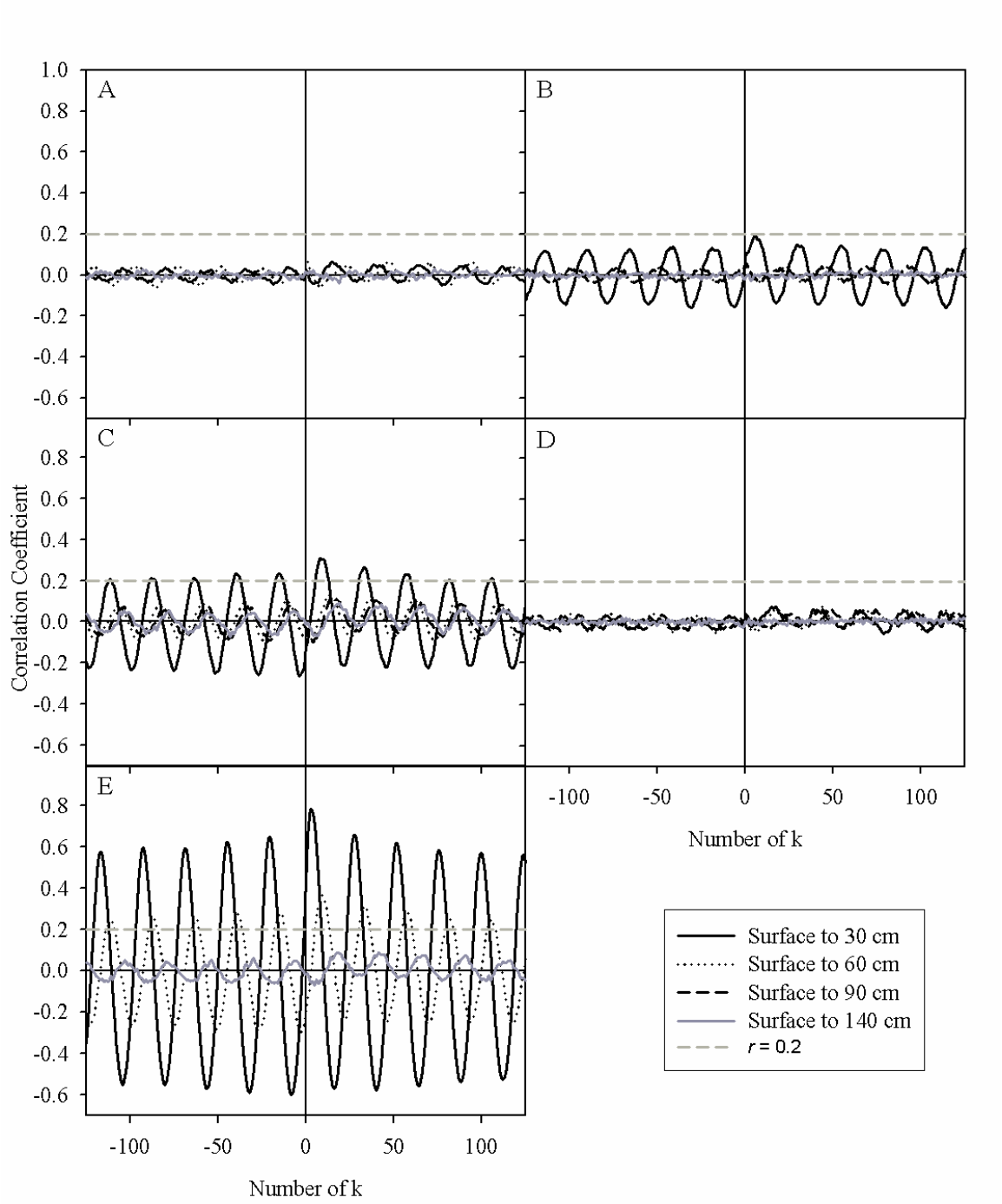

Figure IV-16: Site 1 cross-correlograms per well (indicated by letters A through E), showing correlation between hourly transformed (first order differencing) time series of surface stream temperatures and depths 30, 60, 90 and 140 cm within the streambed.

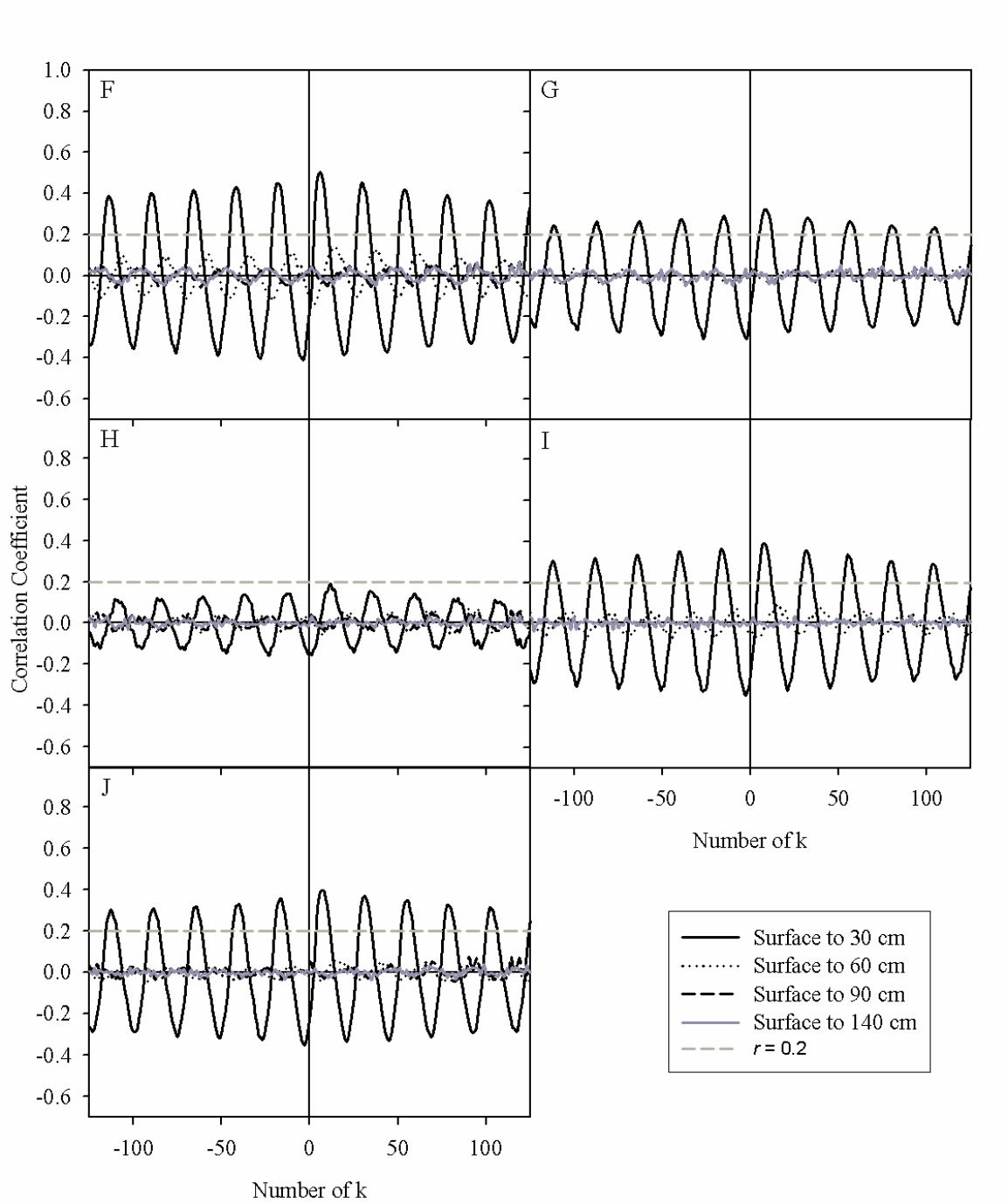

Figure IV-17: Site 2 cross-correlograms per well (indicated by letters F through J), showing correlation between hourly transformed (first order differencing) time series of surface stream temperatures and depths 30, 60, 90 and 140 cm within the streambed.

As with seasonal temperature trends, diurnal temperature trends were analyzed along lateral and longitudinal profile lines across each site (Figures IV-18 and IV-19). At Site 1 significant correlation occurs at both 30 cm and 60 cm depth at $k = 0$. Correlation between wells C and E at 30 cm depth is unique in that it shows significant 24-hour fluctuations. This is likely the effect of their diurnal temperature trends correlating, as seen in Figure IV-15. Interestingly, diurnal patterns in well C lag behind those experienced in well E by 5 hours, despite well C being situated 1 meter upstream of well E. This pattern of temperature change opposing the direction of stream flow could be indicative of preferential flow paths at Site 1.

At Site 2 all wells show significant correlation between diurnal temperature patterns at 30 cm depth, displaying the unique 24-hour cycle. At depths 60 cm and 140 cm however, significant correlation exists only at $k = 0$.

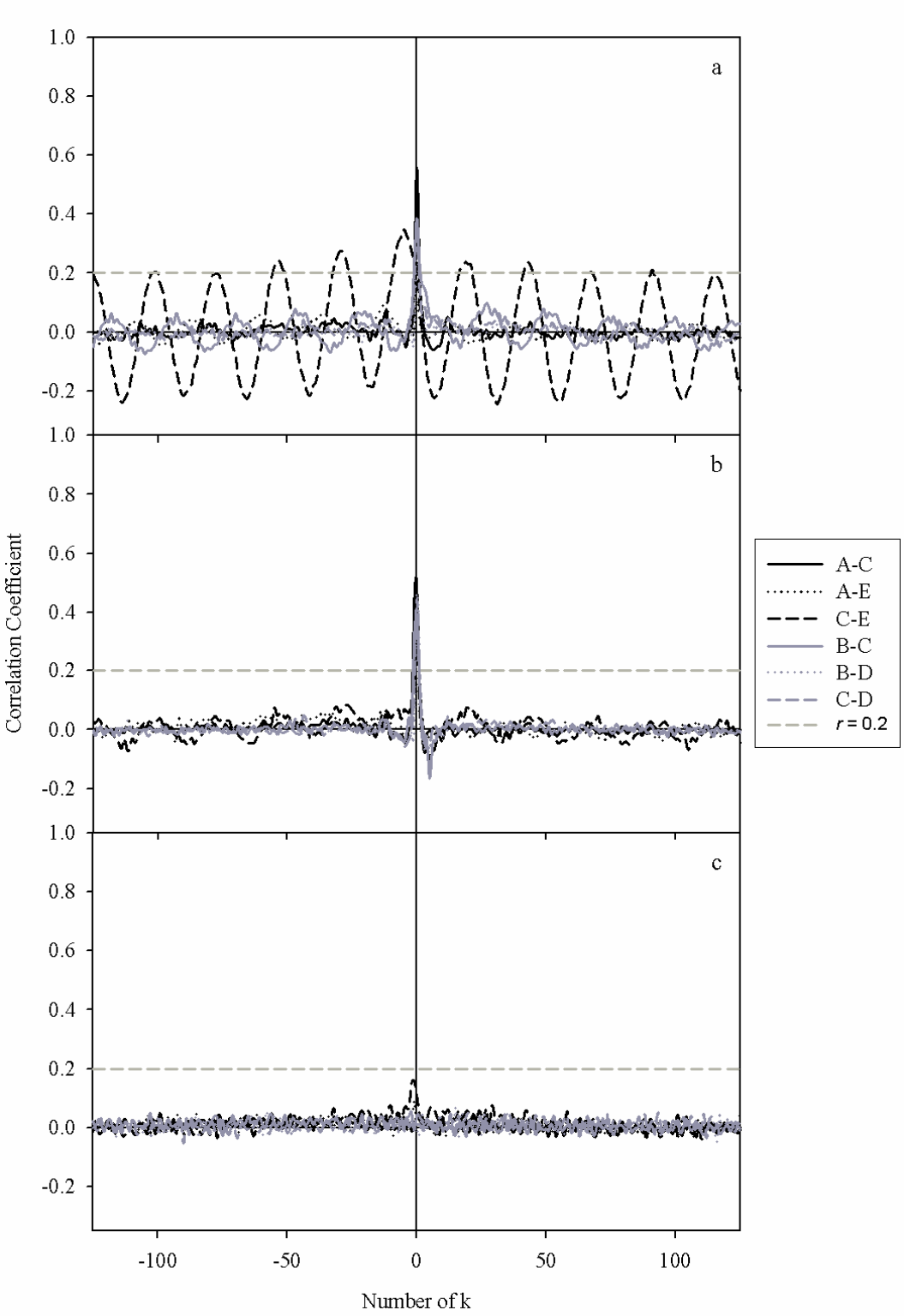

Figure IV-18: Site 1 cross-correlograms at 30 cm (a), 60 cm (b) and 140 cm (c), showing correlation between hourly transformed (first order differencing) time series between wells along longitudinal (black lines) and lateral (gray lines) profiles.

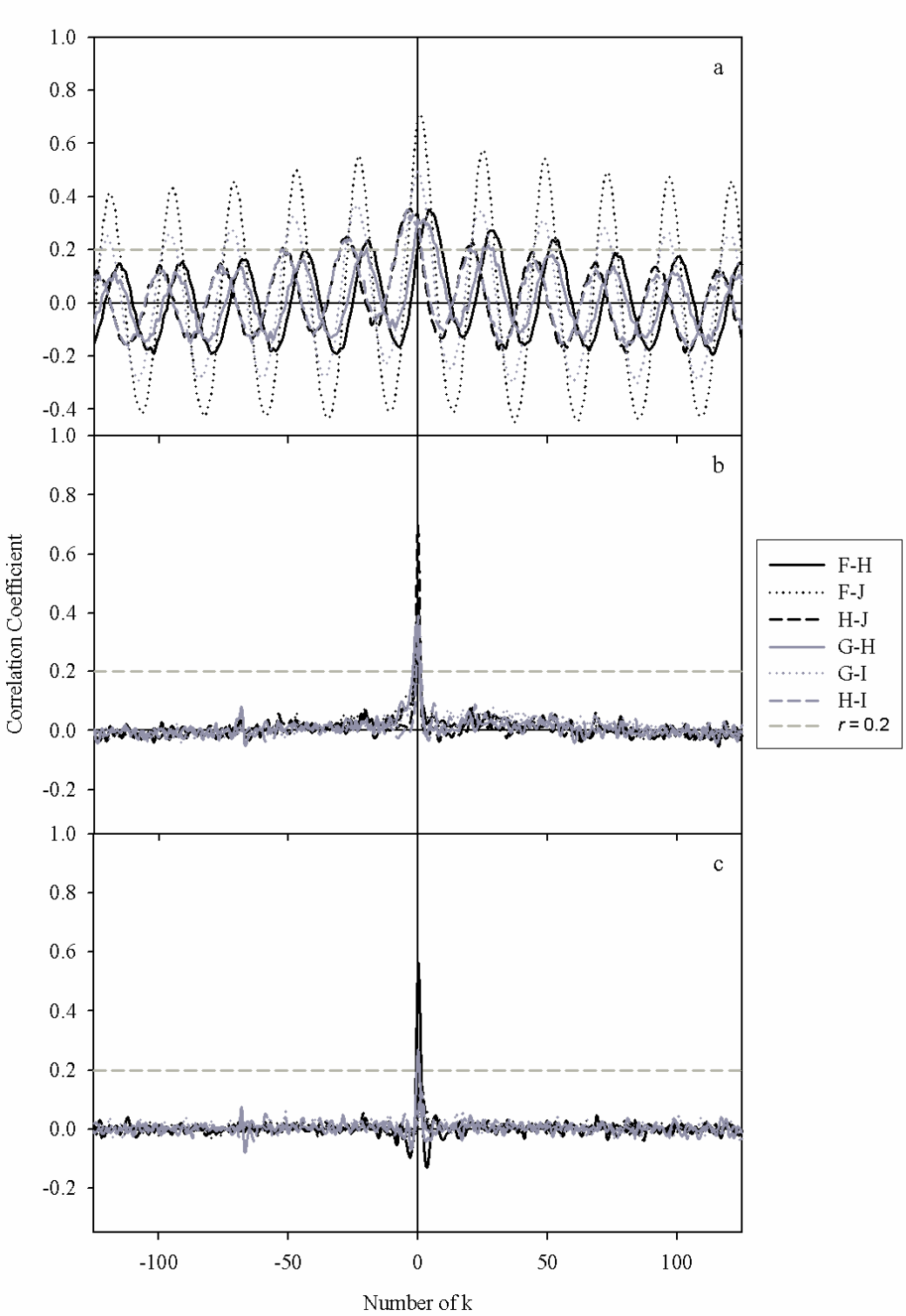

Figure IV-19: Site 2 cross-correlograms at 30 cm (a), 60 cm (b) and 140 cm (c), showing correlation between hourly transformed (first order differencing) time series between wells along longitudinal (black lines) and lateral (gray lines) profiles.

A second between-site comparison was conducted by computing cross-correlation between diurnal temperature gradients at each site. The hypothesis being tested is that despite local differences, dominating thermal transport mechanisms are similar at both sites.

The diurnal site comparison correlation shows very similar results (Figure IV-20) as the seasonal site comparison. A high degree of correlation exists among all temperature gradients of stream and 140 cm depth temperatures, with r ranging from 0.4920 to 0.4970 and peaking universally at $k = 0$. Despite local temperature differences and physical and thermal heterogeneities, there is little difference in the gradient of diurnal temperature transmission from the stream to 140 cm depth between Sites 1 and 2.

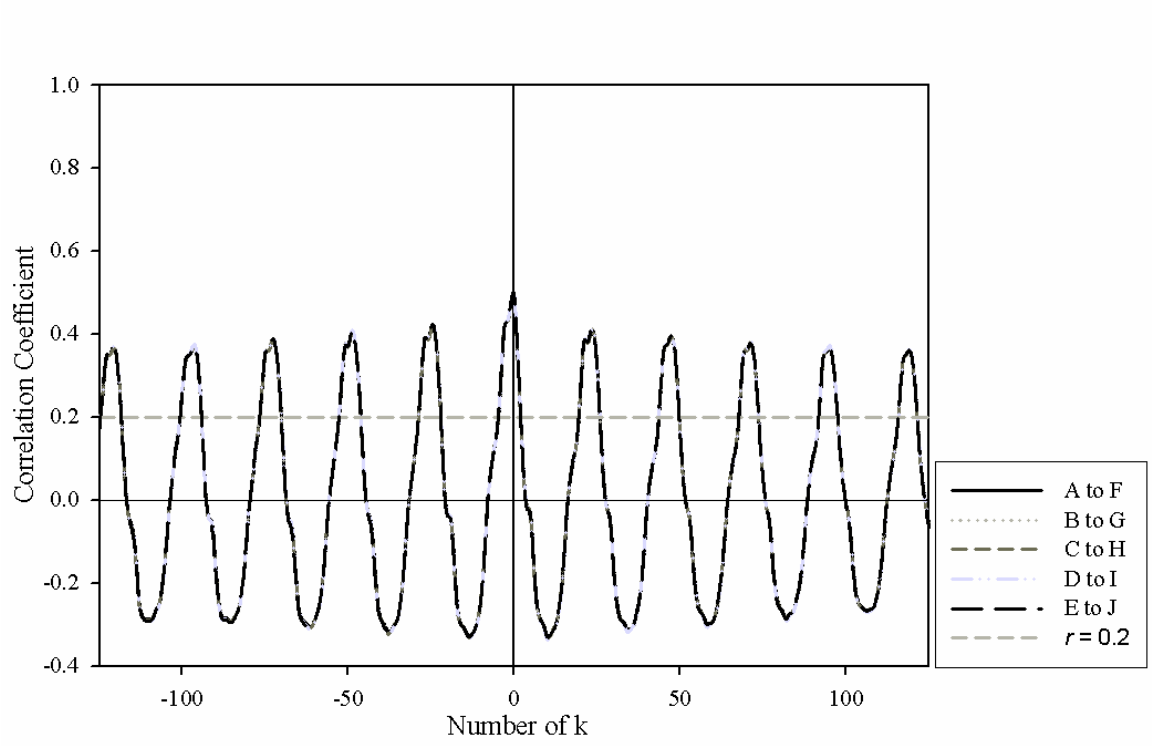

Figure IV-20: Site comparison cross-correlogram, showing correlation between hourly transformed (first order differencing) time series gradients (the difference between respective stream and 140 cm depth temperatures) of Site 1 wells to Site 2 wells at corresponding positions within LKC. All lines overlay each other exactly.

Discussion

It is likely that stream connectivity and HZ sediment physical and thermal properties are the major determining factors for temperature patterns within the HZ, simultaneously defining HZ flow paths of surface and groundwater, and the effectiveness of temperature transmission into the subsurface. Consequently, differences in one or both these properties must exist between Sites 1 and 2 to explain the differences in temperature behavior, for although both site comparisons (Figures IV-15 and IV-20) show little difference between thermal gradients, local differences were observed in all other statistical results.

It has been established by numerous authors, including Brunke and Gonser, (1997), that surface waters are the source of increased temperature ranges and variability within the HZ, as both diurnal and seasonal temperature patterns are transmitted. In contrast to this, groundwater, when mixed with surface water, has a dampening effect on diurnal temperature patterns within the HZ, as it imparts only seasonal temperature trends (Stonestrom and Constantz, 2003). It is presumed that the decreasing temperature ranges and mean temperatures, as seen in box plots (Figures IV-6 to IV-9), can be attributed to the mixing of surface and groundwater and the increasing influence of groundwater with depth.

Box plots revealed that while the stream water at Site 2 experienced greater temperature extremes than at Site 1, these were not witnessed in the Site 2 streambed temperatures. This suggests that stream connectivity is lower at Site 2 than at Site 1. Possible explanations include the allowance of less surface water infiltration, the presence of increased groundwater discharge, or perhaps the retardation of infiltration

velocities as suggested by Ringler and Hall (1975). The hypothesis of less surface water infiltration is tied to the discharge of a greater groundwater component, dampening diurnal surface water signals. This possible explanation is aligned with the establishment of Site 2 as a gaining reach. The second possibility of retarded infiltration velocities is supported by Ringer and Hall (1975), who found larger temperature gradients between stream and hyporheic waters at heavily silted sites, due to slower inter-gravel flows. Based on grain size analyses (Figure IV-2), it is believed that while silt size particles are not prevalent at Site 2, there is an increased amount of smaller size particles present, which may exert a similar effect. Though dampened in amplitude, diurnal surface water signals are still transmitted down to a 30 cm depth almost universally across Site 2 (Figure IV-17).

In addition to increased dampening of surface thermal trends, greater uniformity in thermal trends is seen in box plot and cross-correlation results at Site 2. This suggests that the site has more uniform HZ flow path patterns associated with more homogeneous sediment distribution. Vaux (1968) and Cooper (1965) observed that larger objects in or on the streambed surface respectively, cause significant disruptions to HZ flow paths and thereby thermal patterns as well, which does not appear to be the case at Site 2. Site 1 however, displays distinct thermal heterogeneity when comparing thermal trends in wells A, B, and D, to those in wells C and E, making the presence of sediment variations a possibility.

The results from Van der Hoven et al. (2008) suggest that Site 1 is a downwelling zone, while Site 2 is an upwelling zone. While the site-specific details are not addressed,

these flow dynamics potentially explain many of the trends witnessed in the statistical results of this study, as outlined below.

Advection, as involved in a losing reach or downwelling zone, is commonly considered the most effective means of thermal transport, as fluid movement is typically faster and more efficient at heat transmission than the process of conduction. Therefore, the effective transmission of diurnal temperature signals into the substrate is likely due to advection of stream water into the HZ. This goes hand in hand with the established temperature-based method of defining losing and gaining reaches of a stream, where the presence of increased diurnal signal transmission into the HZ is an indication of a losing reach (Stonestrom and Constantz, 2003).

Lags between unfiltered hourly temperatures of the stream and at 30 cm depth (showing diurnal temperature variations) ranged from 3 to 9 hours. The smallest lag of 3 hours was experienced at Site 1, where sediments are coarser and likely feature a higher hydraulic conductivity. Site 2, projected to have a slightly lower hydraulic conductivity based on sediment size, experienced lags of 6 to 8 hours.

The persistent penetrations of diurnal surface water temperature patterns to depths of 30 cm in wells C and E, and to a depth of 60 cm (Figure IV-16) in well E, as well as the shortest seasonal surface to 140 cm depth temperature pattern lags in well C and E, suggest the influence of a strong vertical advective component at Site 1. Additionally, these trends reinforce the identification of Site 1 as a downwelling zone, and pinpoint wells C and E as the point of most focused downwelling of surface water to a minimum depth of 30 cm in both wells, and to a minimum depth of 60 cm in well E. This is further reinforced by seasonal correlation coefficients of surface water to 140 cm depth

remaining above 0.6 at both wells C and E, suggesting that surface water seasonal variations are responsible for 60% of the seasonal variability witnessed at this depth. It is therefore likely that advection penetrates deeper than the minimum values stated above, yet based on the available data no conclusive statement can be made.

Though both wells C and E appear to be the location of deepest surface water penetration, well E is the location of fastest surface water penetration to a depth of 30 cm, as shown by correlation results between 30 cm temperatures in wells C and E. It appears as though thermal transport is in opposite direction to stream flow at 30 cm depth. Flow paths within the HZ and streambed can be controlled by a large number of factors. However, from what is known of Site 1 regarding sediment size and thermal heterogeneity, it is very likely that both flow paths and thermal regimes are impacted by sediment heterogeneities in the HZ and streambed. Buyck (2005) conducted a nitrate-focused study near the location of Site 1, finding gray clay in the streambed, originating possibly from collapsed cut banks, or from underlying till layers. Such clay in the HZ would act as barriers to advection, and increase the chance of preferential flow path development, which could in turn lead to uncharacteristic flow patterns, as supported by research conducted by Vaux (1968) and Becker et al. (2004).

Site 2 flow path delineation is somewhat less concise than at Site 1. The comparison of lateral and longitudinal profiles at 30 cm depth reveals that the strongest correlation exists in the longitudinal direction, this time continuously following the direction of stream flow. However, correlation between lateral temperature patterns at 30 cm depth exists also. This correlation reflects similar degrees of surface diurnal signal penetration to 30 cm depth. At depths greater than 30 cm, correlation of diurnal patterns

is only significant at $k = 0$, suggesting lateral homogeneity of temperatures across the site, but no thermal transport in the lateral or longitudinal direction fast enough to convey diurnal temperature trends. Based on statistical results, flow paths at Site 2 are mostly in the longitudinal direction, at low velocities, and active surface water infiltration is limited to the upper 30 cm of the streambed.

The process of conduction, while in part dependent on the thermal properties of a medium, is driven by temperature gradients, where steeper temperature gradients increase the effectiveness of conduction. Steepest temperature gradients appear to exist laterally at Site 1, between vertically down-welling warmer temperatures in well C and E, and cooler temperatures in wells A, B, and D. This suggests that conduction may be an important mode of heat transport in the lateral direction at Site 1. At Site 2 thermal gradients appear more gradual, suggesting conduction will be kept to a minimum. However, during the dry period at Site 2, the heating of streambed sediments by direct exposure to solar radiation may have provided a steep thermal gradient, allowing conduction an active role in the transport of heat into the HZ. A similar proposition was put forward by Shepherd et al. (1986).

Quantitative delineation of the HZ based on thermal trends has not been possible. Though statements can be made as to where the HZ definitely persists, such as at 30 cm depth in the locations of wells C, E, F, G, I, and J, where significant correlation to surface stream diurnal temperature patterns was found, the exact cut-off point between the HZ and groundwater environments is difficult to pinpoint quantitatively without a locally specific thermal groundwater signature.

It is also possible that the maximum logger installation depth managed for this study was not deep enough to penetrate the groundwater environment. Even at 140 cm depth, seasonal temperature trends vary more than by the accepted ± 3 ºC range from the annual mean air temperature of 11.2 ºC. A likely alternative explanation to lacking penetration depth is the impact of conduction on temperatures at depth. While the presence of advecting surface water defines the extent of the HZ, the presence of conduction may alter temperatures beyond the extent of the HZ, effectively masking the true groundwater thermal signature. Cross-correlation results between surface water and 140 cm depth at both sites (Figures IV-11 and IV-12) suggest at least 20% of the variability witnessed can still be explained by surface water variability. This may be coincident, based on the large number of observations used in the correlation, as well as the small degree of change in the temperatures and the fact that groundwater also has a seasonal signal. However, if not coincident, it seems possible that conduction could transmit 20% of the surface thermal signature to a depth of 140 cm below the streambed, especially considering that the seasonal trends are transmitted into the upper 30 cm by advection, leaving approximately 90 cm distance to be spanned by conduction.

Conclusion

The goal of this study was to explore the impacts of sediment size on the temperature profiles of a low gradient stream's HZ using statistical methods. Various aspects have been addressed, including variations of diurnal and seasonal temperature signal transmission, a comparison of lateral and longitudinal temperature profiles, as well as possible delineation of the HZ.

Overall, distinct differences were identified in the thermal profiles of Sites 1 and 2. Site 1 was identified as a downwelling zone with surface water penetrating deepest into the HZ at the location of wells C and E. Site 2 was characterized as a gaining reach, where the balancing between down-welling surface water and upwelling groundwater temperatures resulted in a more homogenized thermal environment. Additionally, a dampening of diurnal surface stream temperature ranges was noticed in upper HZ temperatures at Site 2. This dampening was attributed to a variety of possible causes, including a significant discharging groundwater component which would produce a dampening effect on diurnal temperatures as previously outlined. This explanation is in line with Site 2 being recognized as a gaining reach. Additionally the possibility of an increased percentage of finer sediments at the site was considered, resulting in slightly retarded inter-gravel flows causing dampening associated with the longer thermal transmission times.

A correlation between increased sediment homogeneity and more homogeneous thermal profiles was noted, though the lack of multiple sites makes definitive interpretation difficult. However, it has been well established in the literature that larger sediments as well as possible low permeability zones can disrupt HZ flow paths and thermal regimes (Vaux, 1968; and Becker et al., 2004).

It is postulated that the transmission of diurnal signals is limited by the efficiency of advection, requiring higher transmission speeds than seasonal temperature signals. Supporting this, the deepest penetration depth of diurnal temperature patterns was 60 cm in well E, while seasonal surface temperature patterns were detected universally to a depth of 140 cm.

Thermal differences in lateral and longitudinal profiles were detected, and were attributed to variations in factors affecting thermal transport, such as the presence of preferential flow paths. The longitudinal profile exhibited a greater tendency for progressive transmission of thermal signals in the downstream direction, though a thermal transmission against the direction of stream flow was detected at Site 1.

Finally, only qualitative delineation of the HZ was possible in this study. The main limitation was the lack of a locally specific thermal groundwater signature. The persistence of surface seasonal temperature trends beyond the extent of surface diurnal temperature trends was initially attributed to the possibility of insufficient logger installation depths, but is in reality more likely due to the incalculable influence of conduction on temperatures below the reach of advection.

References

Anderson MP. 2005. Heat as a Ground Water Tracer. *Ground Water* **43**: 951-968. DOI: 10.1111/j.1745-6584.2005.00052.x.

Becker MW, Georgian T, Ambrose H, Siniscalchi J, Fredrick K. 2004. Estimating flow and flux of ground water discharge using water temperature and velocity. *Journal of Hydrology* **296**: 221-233. DOI: 10.1016/j.jhydrol.2004.03.025.

Bencala KE. 1993. A perspective on stream-catchment connections. *Journal of the North American Benthological Society* **12**: 44-47.

Bencala KE. 2000. Hyporheic zone hydrologic processes. *Hydrological Processes* **14**: 2797-2798.

Bencala KE. 2005. Hyporheic Exchange Flows. In *Encyclopedia of Hydrologic Sciences*, Anderson MG. (ed) **3**: 1733-1740.

Brunke M, Gonser T. 1997. The ecological significance of exchange processes between rivers and groundwater. *Freshwater Biology* **37**: 1-33.

Buyck MS. 2005. Tracking nitrate loss and modeling flow through the hyporheic zone of a low gradient stream through the use of conservative tracers. *Thesis*.

Cardenas MB, Wilson JL, Zlotnik VA. 2004. Impact of heterogeneity, bed forms, and stream curvature on subchannel hyporheic exchange. *Water Resources Research* **40**: W08307. DOI: 10.1029/2004WR003008.

Conant B Jr. 2004. Delineating and Quantifying Ground Water Discharge Zones Using Streambed Temperatures. *Ground Water* **42**: 243-257.

Cooper AC. 1965. The effect of transported stream sediments on the survival of sockeye and pink salmon eggs and alevins. *International Pacific Salmon Fishery Commission Bulletin* **18**.

Dogwiler T, Wicks C. 2006. Thermal variation in the hyporheic zone of a karst stream. *International journal of Speleology* **35**: 59-66.

Evans EC, Greenwood MT, Petts GE. 1995. Short Communication Thermal Profiles Within River Beds. *Hydrological Processes* **9**: 19-25.

Fraser BG, Williams DD. 1998. Seasonal boundary dynamics of a groundwater/surface-water ecotone. *Ecology* **79**: 2019-2031.

Hayashi M, Rosenberry DO. 2002. Effects of ground water exchange on the hydrology and ecology of surface water. *Ground Water* **40**: 309-316.

Jenkins GM, Watts DG. 1968. *Spectral analysis and its applications*. Holden-Day: San Francisco.

Malard F, Mangin A, Uehlinger U, Ward JV. 2001. Thermal heterogeneity in the hyporheic zone of a glacial floodplain. *Canadian Journal of Fisheries and Aquatic Sciences* **58**: 1319-1335. DOI: 10.1139/cjfas-58-7-1319.

Mangin A. 1984. Pour une meilleure connaissance des systémes hydrologiques à partir des analyses corrélatoire et spectrale. *Journal of Hydrology* **67**: 25-43.

Peterson EW, Sickbert TB. 2006. Stream water bypass through a meander neck, laterally extending the hyporheic zone. *Hydrogeology Journal* **14**: 1443-1451. DOI: 10.1007/s10040-006-0050-3.

Peterson EW. 2008. Associate Professor. Department of Geography-Geology: Illinois State University. Normal, IL. Personal communication of unpublished data.

Ringler NH, Hall JD. 1975. Effects of logging on temperature, and dissolved oxygen in spawning beds. *Transactions of the American Fisheries Society* **104**: 111-121.

Shepherd BG, Hartman GF, Wilson WJ. 1986. Relationships between stream and intragravel temperatures in coastal drainages and some implications for fisheries workers. *Canadian Journal of Fisheries and Aquatic Sciences* **43**: 1818–1822.

Silliman SE, Booth DF. 1993. Analysis of time-series measurements of sediment temperature for identification of gaining vs. losing portions of Juday Creek, Indiana. *Journal of Hydrogeology* **146**: 131-148.

SPSS for Windows. Rel. 16.0.1. 2007. SPSS Inc.: Chicago.

Stonestrom DA, Constantz J (ed). 2003. Heat as a tool for studying the movement of ground water near streams. *U.S. Geological Survey Circular 1260*. U.S. Geological Survey: Denver, CO. 1-96.

Van der Hoven SJ, Fromm NJ, Peterson EW. 2008. Quantifying nitrogen cycling beneath a meander of a low gradient N-impacted agricultural stream using tracers and numerical modeling. *Hydrological Processes*: in press. DOI: 10.1002/hyp.6691.

Vaux WG. 1968. Intergravel flow and interchange of water in a streambed. *Fishery Bulletin* **66**: 479-489.

White DS, Elzinga CH, Hendricks SP. 1987. Temperature patterns within the hyporheic zone of a northern Michigan river. *Journal of North American Benthological Society* **12**: 48-60.

CHAPTER V

THE IMPACT OF STREAMBED SEDIMENT SIZE ON HYPORHEIC TEMPERATURE PROFILES IN A LOW GRADIENT THIRD-ORDER AGRICULTURAL STREAM– A MODELING APPROACH

Abstract

To develop an understanding of the impact of sediment size on temperature profiles within the hyporheic zone of a third order agricultural stream, a 2-dimensional thermal modeling approach was used. Field data were collected by two temperature probe grids along two riffles, one featuring predominantly gravel (d_{50} = 3.9 mm) and the other predominantly sand (d_{50} = 0.94 mm). Temperature loggers were positioned upon installation uniformly at 30, 60, 90, and 140 cm below the streambed surface, recording at 15-minute intervals over a 6 month period. Surface water and air temperature were recorded also.

Numerical modeling was completed using the 2-D heat transport model VS2DH. Both lateral and longitudinal profiles were modeled, though only longitudinal models were successful in reproducing observed conditions.

Movement of stream water through meanders along extended HZ flow paths had a significant impact on stream and streambed temperatures, discharging into both study sites along the stream's edges. However, while such lateral in and outflows were significant, thermal transport following the direction of stream flow dominated both site thermal profiles.

Increased sediment size led to higher hydraulic conductivities and lower porosities, impacting advection. Additionally, the degree of sediment sorting impacted thermal transport. Site 1, featuring poorly sorted gravels, showed distinct preferential flow paths, greater variation in vertical versus horizontal specific discharge, and greater variability in the dominant thermal transport mechanism. Site 2, featuring moderately

sorted sands, showed homogenization of vertical and horizontal specific discharge, as well as a uniform dominance of advection as the dominant thermal transport mechanism.

Ultimately, the results suggest that physical heterogeneities such as a greater range in sediment size or a less even stream channel are reflected as thermal heterogeneities in the subsurface.

Key words: hyporheic zone, temperature, VS2DH, down-welling

Introduction

Water temperature has had significant impacts on the field of hydrogeology, and the development of various research methods has allowed water temperature to play an integral role in many studies. More specifically, streambed temperature profiles can be used to quantify groundwater/stream interactions (Stonestrom and Constantz, 2003), and delineate flow paths in the hyporheic zone (HZ) (Conant, 2004). Despite many established uses of water and hyporheic temperatures, the volume of literature discussing temperature as a tracer remains light (Anderson, 2005), and HZ studies are mostly performed on low order, high-gradient streams (Bencala, 2005).

The HZ is defined as a zone below the stream channel where surface and groundwater mix (Conant, 2004; Hayashi and Rosenberry, 2002). Hyporheic temperatures are controlled by this mixing process, where groundwater temperatures generally vary according to mean annual air temperatures, disregarding geothermal influences, and surface water temperatures show both diel and seasonal fluctuations (Brunke and Gonser, 1997). With increasing depth and/or distance from infiltration sites the diel and seasonal fluctuations become attenuated and lagged, while the annual air

temperature cycle persists (Dogwiler and Wicks, 2006), facilitating the use of temperature as a tracer. These patterns can be a valuable tool in defining HZ depth and extent (White et al., 1987), though findings by Fraser and Williams (1998) suggest that delineations vary both seasonally as well as with event-based fluctuations.

In addition to possible HZ delineation, thermal profiles may be used to identify losing and gaining portions of a stream, as successfully done by Silliman and Booth (1993). Areas with relatively constant HZ temperatures through time were identified as gaining reaches, while reaches where HZ temperatures varied with diurnal surface stream temperature variations were identified as losing reaches.

Both advective and conductive processes can impact HZ temperatures, though advection is typically the dominant process (Evans et al., 1995). The influence of both advective and conductive processes on hyporheic water temperatures suggests that sediment size can influence the effectiveness of both by 1) partially characterizing the hydraulic conductivity of the stratum, effectively limiting advection, and 2) controlling the connectivity of the sediment, there by limiting conduction. Vaux (1968) and Cooper (1965) suggest that larger objects in or on the streambed surface respectively, alter the flow paths of hyporheic and stream waters. With respect to finer sediments, Ringler and Hall (1975) showed that the largest gradients between stream and hyporheic water temperatures occur at heavily silted sites, where slow inter-gravel flows persist. Additionally, variations in hydraulic conductivity of the streambed may result in uneven discharge and flow geometry (Becker et al., 2004).

Ultimately this study focuses on determining the effect of streambed sediment grain size on temperature profiles of the HZ, with the hope of furthering existing

knowledge of water temperature in the environment. The primary hypothesis to be addressed is that streambed sediment size affects HZ temperatures. More specifically, lateral and longitudinal temperature profiles of the HZ will be compared for likeness, and if present, sediment size impacts on HZ temperature profiles will be identified with the aid of 2-D models.

Study Site

Field investigations focused on two sites along a stretch of the Little Kickapoo Creek (LKC) running through the Illinois State University Randolph Well Field located in McLean County, central Illinois, USA (Figure V-1). Central Illinois has a temperate climate, with cold, snowy winters and hot, wet summers. Mean annual air temperature for the period from 1950 to 2002 was 11.2 ºC (Peterson and Sickbert, 2006).

LKC is a low gradient third-order perennial stream, which meanders (sinuosity of 1.8) through Wisconsinan glacial plains and originates in an urban area approximately 11 km north of the study site (Peterson and Sickbert, 2006). Regionally LKC is a gaining stream, with a gradient of 0.002. Locally, by the meander along which the 2 study sites are located, a gradient of 0.003 exists (Peterson and Sickbert, 2006). The stretch under investigation is unmodified and meanders through an approximately 300m wide alluvial valley. Terrain bordering the stream is used predominantly as agricultural farm land, alternating corn and soy bean production.

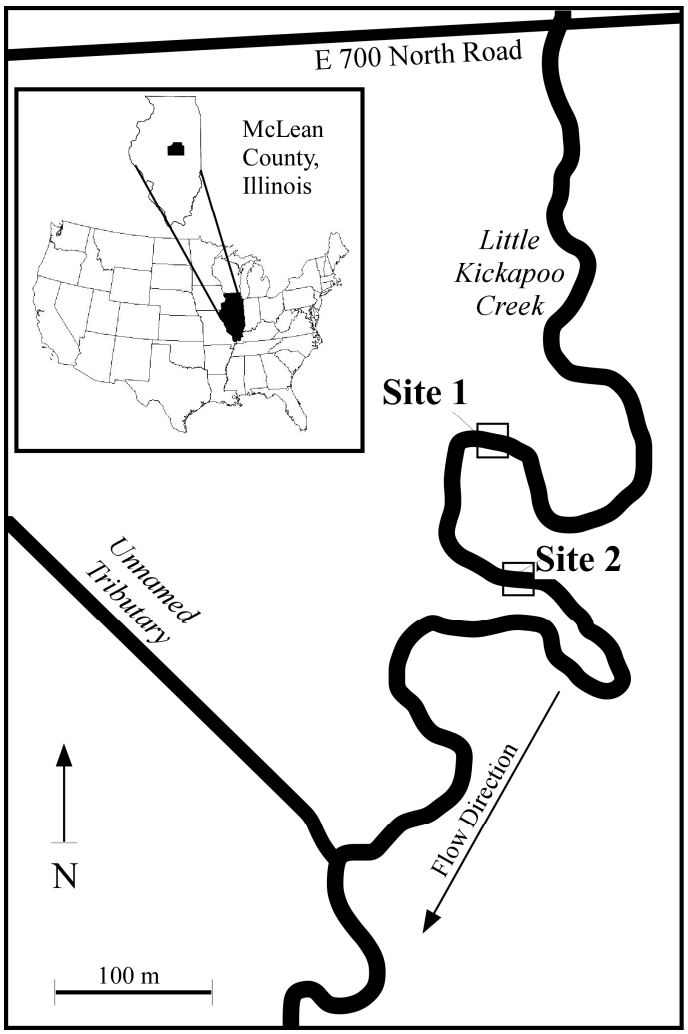

Figure V-1: Site map and site location within the US and Illinois. Site 1 is upstream and represents a gravel dominated streambed. Site 2 is downstream, representing a sand dominated streambed.

Three geologic units comprise the alluvial valley through which LKC meanders: the Wedron Formation (WF), the Henry Formation (HF), and the Cahokia Formation (CF) (listed from oldest to youngest). The WF acts as a lower confining unit to the HF, being a clay-rich low-permeability till. The HF functions as an aquifer due to its poorly sorted gravels and sands, and has an average hydraulic conductivity of 10 m/day (Peterson and Sickbert, 2006), and an average thickness of 5-7 m in the outwash valley.

Above the HF lies the CF, consisting of fine-grained sand and mud, with a thickness of up to 2 m. The LKC channel is inset into the CF, cutting into the top of the HF. LKC streambed sediments are composed of mainly HF materials, consisting primarily of gravel and coarse sand with interstitial silt. Surface sediments vary with distance along the channel.

Both sites are located in riffle sections of the stream channel. Site 1 is the further upstream site, featuring predominantly gravel (d_{50} = 3.9 mm) while Site 2 lies further downstream with predominantly sand size sediments (d_{50} = 0.94 mm) (Peterson, 2008) (Figure V-2). Sediment samples represent a composite of the top 30 cm of the streambed.

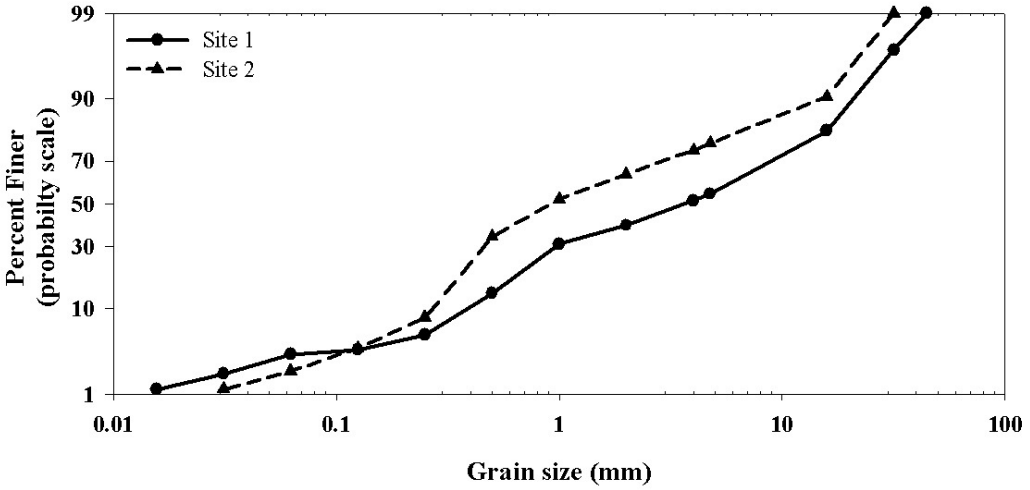

Figure V-2: Grain size analysis for Site 1 and Site 2 sections of LKC.

A conceptual model was developed based on previous research at the Randolph well field by Peterson and Sickbert (2006), Fromm (2005), and Van der Hoven et al. (2008) (Figure V-3). Stream water/groundwater flow paths through meanders have been

established by Peterson and Sickbert (2006). Theoretically, both Sites 1 and 2 should receive some meander discharge waters based on their relative locations along the stream channel, which may impact temperature regimes. Additionally, stream water may migrate into meanders, again adding complexity to model scenarios.

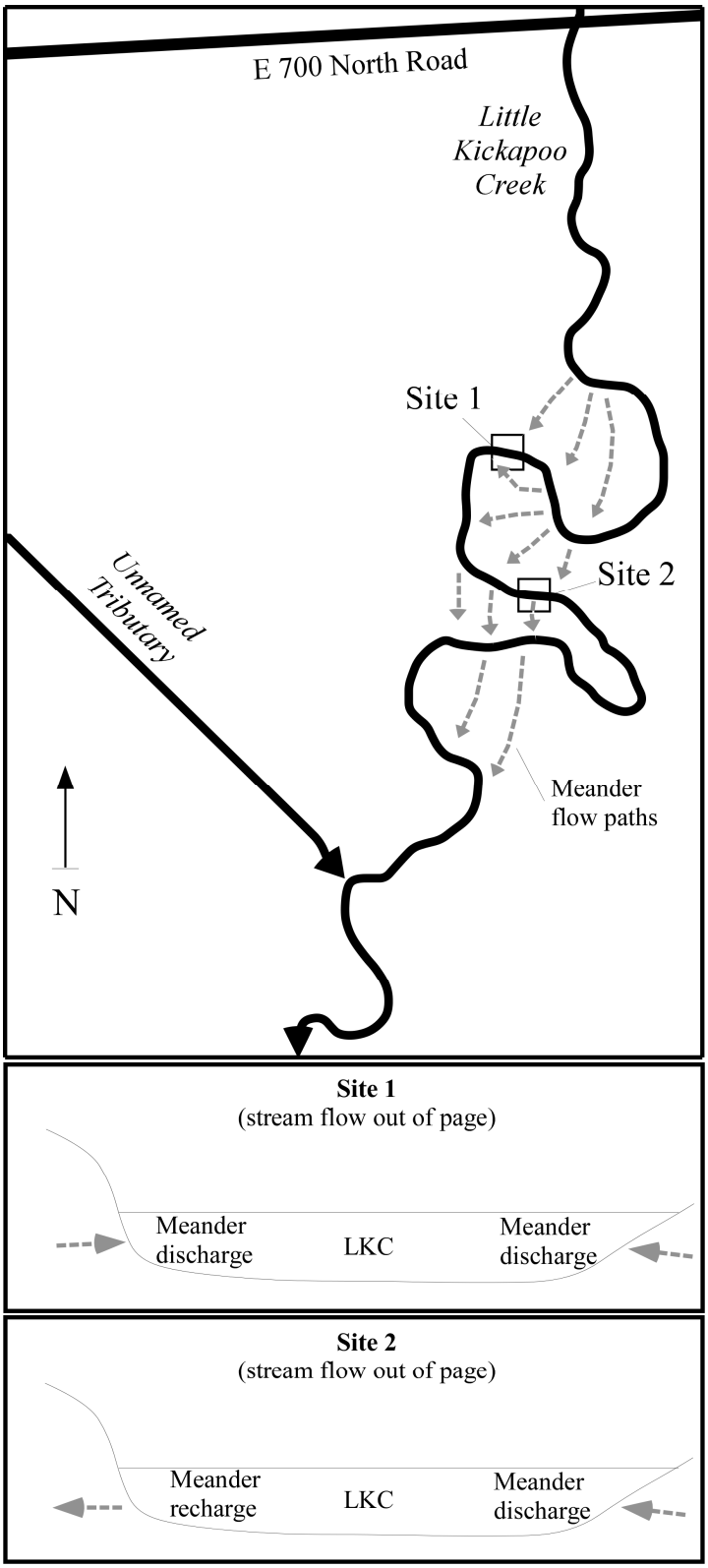

Figure V-3: Conceptual model of Randolph well field and Sites 1 and 2 with respect to meander flow-through paths.

Methodology

Temperature Measurements

Two identical temperature probe grids were set up along riffles within LKC sites. Each grid consisted of five vertical logger nests (referred to as wells) creating both lateral and longitudinal profile lines across the channel. The two profile lines intersected roughly in the stream's thalweg, where one nest provided data for both profiles (Figure V-4). Within each 6.35 cm PVC well temperature loggers were positioned at depths of 30 cm, 60 cm, 90 cm, and 140 cm (Figure V-5). Foam sealant was used to partition off different depths to reduce vertical mixing, while holes drilled into the walls at each depth provided connection to the matrix. Two different styles of temperature loggers were used, composed of 10 HOBO® Temperature/Light Data Loggers (at 25 °C, accuracy: ±0.47 °C; resolution: 0.1 °C) and 32 HOBO® Stowaway Tidbit Data Loggers (at 25 °C, accuracy: ±0.4 °C; resolution: 0.3°C). Two additional temperature loggers recorded surface water temperatures. All loggers were programmed to record temperatures at 15-minute intervals. Data collection started on the June 30, 2007 and ended on the January 16, 2008, when all loggers were removed from the substrate. Grid appearance and outer condition was monitored throughout the data collection period.

Additional data collection included stream stage and air temperature. The stream stage was recorded at a permanent stilling well located 20 m upstream of Site 1. Air temperature was obtained from a weather station 220 m away. Both stream stage and air temperature were recorded on a 15-minute interval.

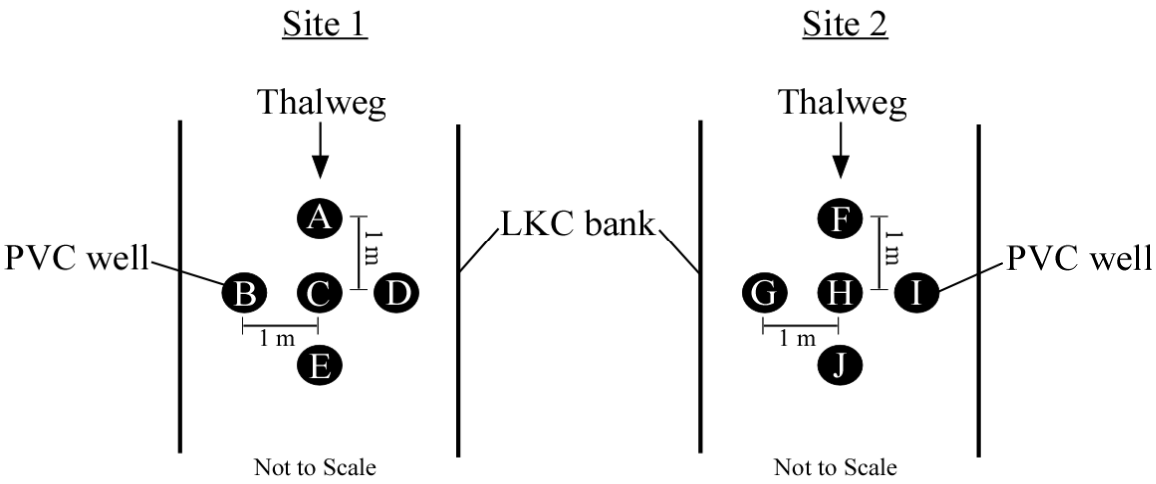

Figure V-4: Plan view of well setup in the stream channel.

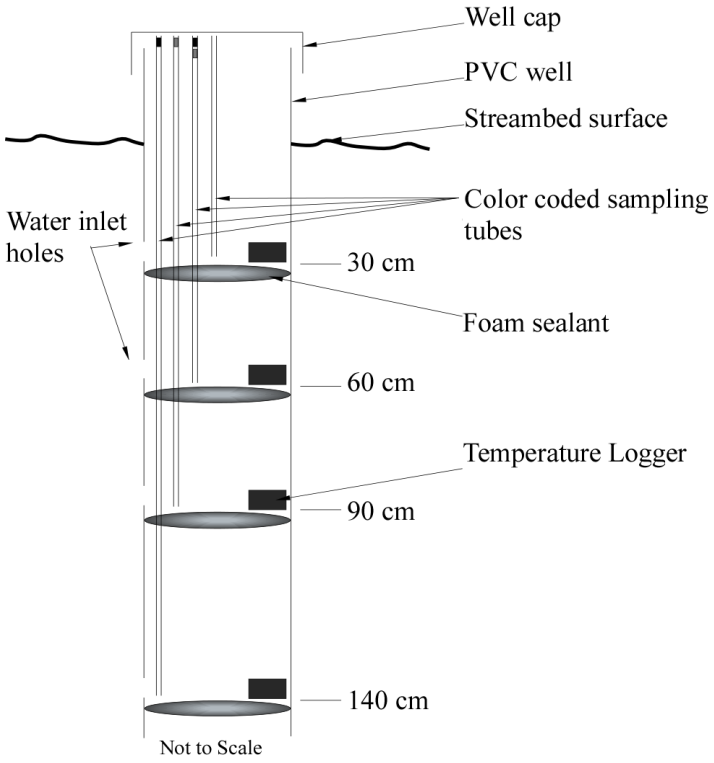

Figure V-5: Detailed view of individual well design.

Model Setup

The USGS model software VS2DH (Healy and Ronan, 1996) was used to create two models per site, one parallel to stream flow and one perpendicular to stream flow. Model domains were limited to within the well setups at each site, resulting in 2-D models with dimensions of 2 m by 1.4 m, and cell dimensions of 0.05 m by 0.04 m. The temperatures recorded in the outer wells were used as input variables for boundary conditions where applicable, while the temperatures recorded in the central well were used to evaluate the models capabilities of simulating observed conditions (Figure V-6).

Final boundary conditions were a result of calibration, and provide the best fit between modeled and observed temperatures. To recreate the observed thermal environment as accurately as possible, boundaries with an influx of water were segmented to reflect the resolution of the thermal data acquired in the field. Boundaries showing an outflux of water were represented at a lower resolution in the models, as less control was needed since temperatures do not have an impact on these boundaries in VS2DH.

Thermal and physical model properties were assumed homogeneous throughout each model domain. Initial thermal property values for the models were chosen based on findings by Lapham (1989). Initial physical parameters and boundary conditions were chosen based on interpretation of the thermal profiles, as well as the conceptual model. All parameters, except porosity, were varied within plausible ranges to create a best fit of simulated versus observed temperature values, and evaluated using the absolute mean error.

Porosity values, defined as the volume of pore space per bulk volume of the porous medium, were chosen based on literature reported values for sand/silt mixtures, with Sites 1 and 2 being assigned porosities of 0.35 and 0.4 respectively. The values were adjusted during the calibration process, and the sensitivity of the model to the porosity values was evaluated.

Select model parameters required limiting to maintain theoretical bounds. It is projected that this tendency to stray from accepted values may be due to the simplification from a 3-D system into a 2-D model. Though by using a 2-D model the assumption of a negligible third dimension must be made, the third dimension (in this case lateral input to a longitudinal model) at both sites is conceptually thought to contribute to temperature control in the HZ (Figure V-3). However, due to the nature and monetary limitations of this study a 2-D model was deemed adequate in reproducing observed conditions.

Using a bulk density range from 1.5 to 2.25 g/cm^3, theoretical ranges for both heat capacity of dry solids (C_s) and thermal conductivity of water-sediment at full saturation (K_{ts}) were based on work by Lapham (1989). C_s can be identical for both fine and coarse grained sediments, ranging from 2196600 to 2719600 J/m^3 ºC. For fine sediments, K_{ts} ranged from 4820 to 6326 J/hr m ºC. For coarse sediments, K_{ts} ranged from 6025 to 13556 J/hr m ºC. Additionally, the ratio of saturated hydraulic conductivity in the vertical direction to that in the horizontal direction (K_{zz}/K_{hh}) was limited at 1, based on the assumption that a ratio greater than 1 would be very unlikely in natural sediments.

A sensitivity analysis was conducted to assess the impact of the various parameters on model outputs, as well as provide a means of comparison between sites.

The following physical and thermal properties were varied up to ±50%: saturated hydraulic conductivity in the horizontal direction (K_{hh}); porosity; K_{zz}/K_{hh}; longitudinal dispersivity (Long. Disp.); transverse dispersivity (Transv. Disp.); K_{ts}; and C_s.

The models were run as transient, over the period of four days where stream discharge remained constant, and surface water temperatures featured a strong diurnal component (July 13 to July 16, 2007). All of the calibrated models were verified using temperatures from a second four-day period (July 23 to July 26, 2007).

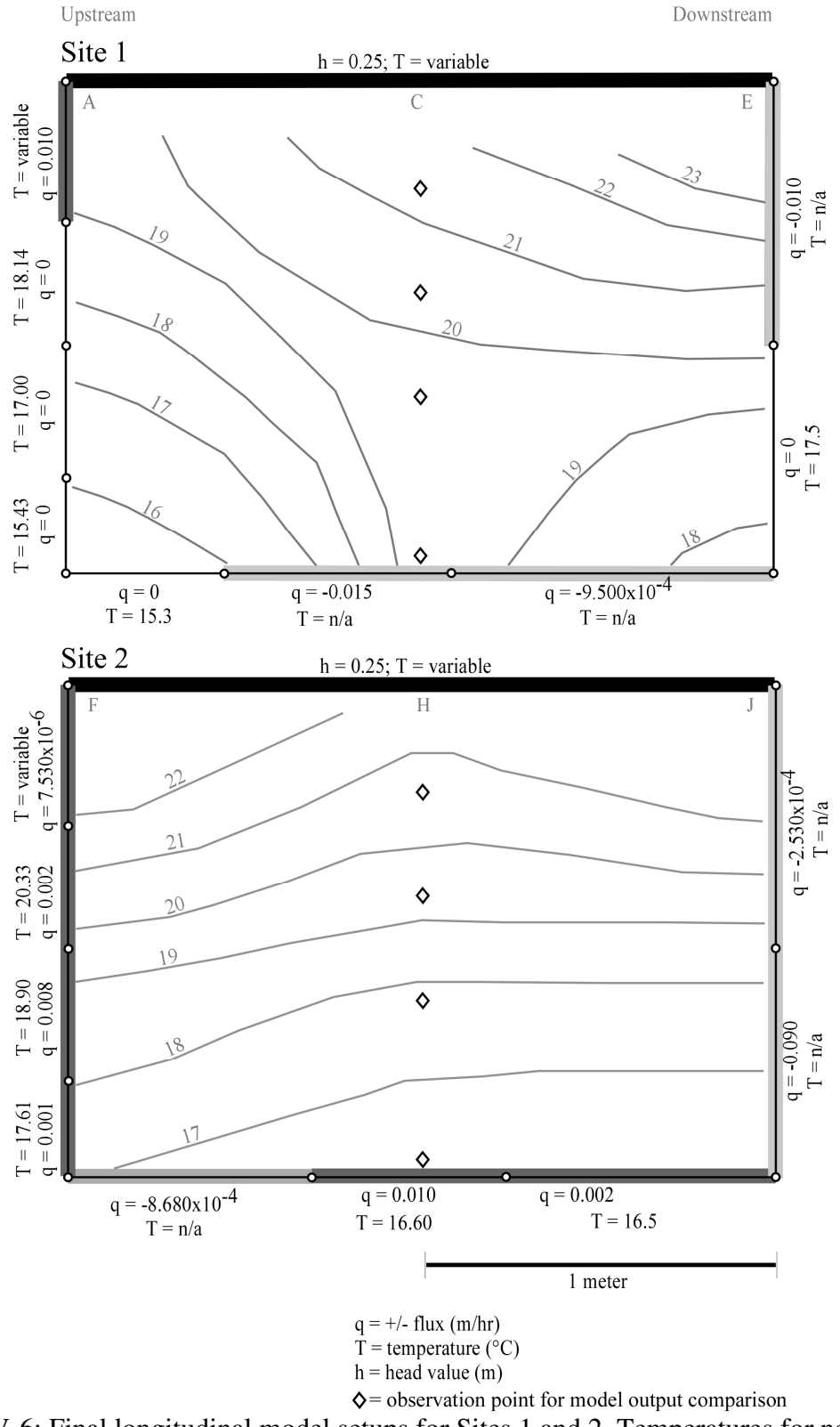

Figure V-6: Final longitudinal model setups for Sites 1 and 2. Temperatures for negative fluxes were not required and are represented by n/a.

Results and Discussion

Time Series Data

During the data collection period, several unforeseen problems were encountered. Temperature loggers located at A-90 cm, E-90 cm, G-90 cm, and I-90 cm failed completely. Additionally, the Site 1 stream logger recorded temperatures only until December 20, 2007. Furthermore, due to extensive beaver dam construction upstream of both sites, stream flow became a trickle for an intermittent period spanning from August 1, 2007 to October 15, 2007, resulting in periodic low flow conditions at Site 1, and periods of no visible surface flow at Site 2. The temperature effects of this can be seen in Figure V-7. Initially, Site 2 surface stream temperatures closely mimic Site 1 surface stream temperatures. However, near the beginning of August, Site 2 surface stream temperatures show a large increase in diurnal amplitude, approximating the variability of daily air temperatures. Additionally, surface stream temperatures at Site 2 remain warmer than at Site 1 following the end of the low flow conditions, until the failure of the Site 1 stream logger. This temperature difference is likely due to a greater short-wave radiation exposure at Site 2 once trees begin to lose their foliage.

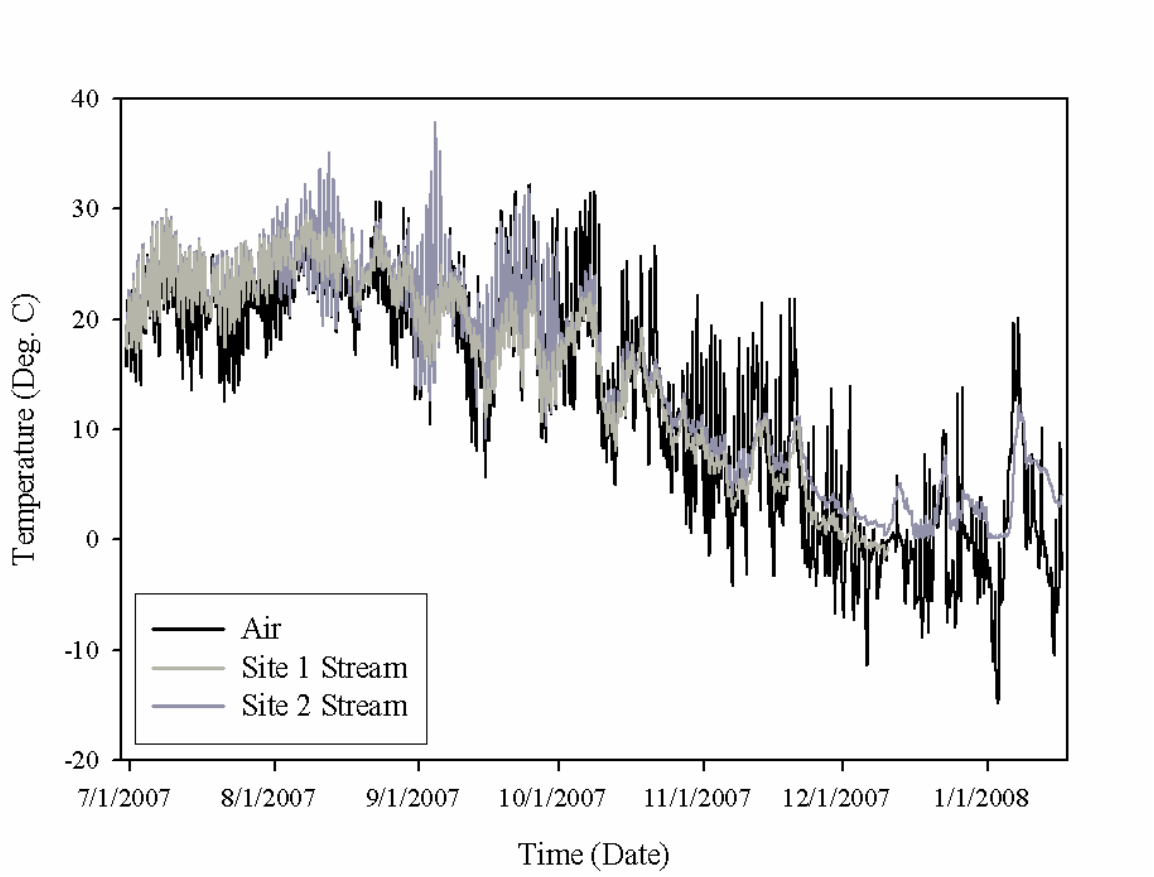

Figure V-7: Air and stream (Site 1 and Site 2) temperature 15-minute incrementing time series for entire data collection period.

When using temperature as an indicator, the degree of connectivity between a stream and its hyporheic zone can be estimated by how closely hyporheic temperatures mimic those of the associated stream. When examining summary graphs of the time series at each site per depth (Figures V-8 and V-9) several observations were made.

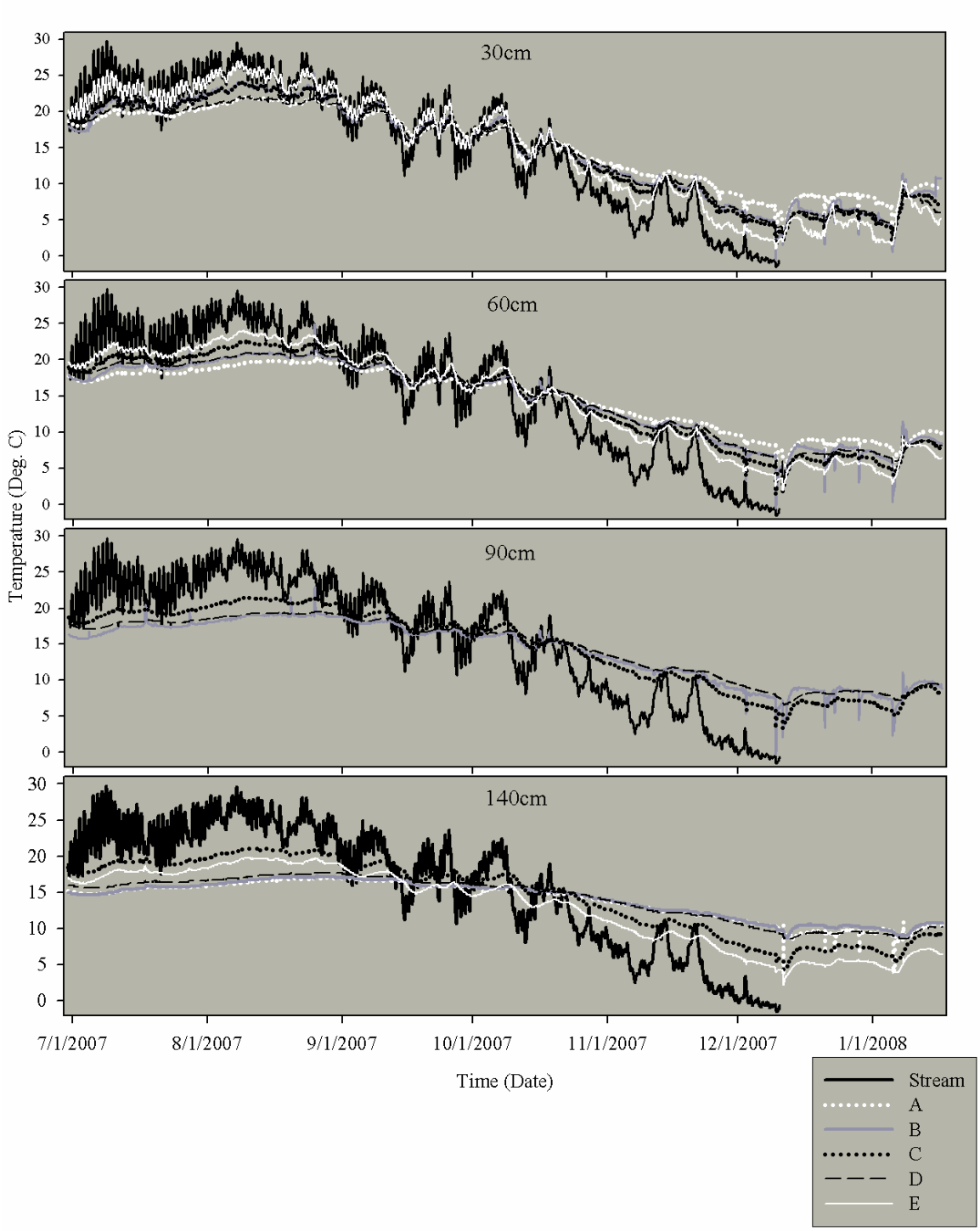

Figure V-8: Site 1 surface stream temperature and well temperatures at depths 30, 60, 90, and 140 cm within the streambed.

At Site 1, across all four depths examined, wells C and E consistently exhibit temperatures most similar to those of the stream, including strong diurnal signals at shallow depths, and mimicry of major surface stream temperature peaks and troughs at greater depths. Even at a depth of 140 cm, the presence of the main surface stream temperature peaks and troughs remains detectable, although a slight phase shift is apparent. These findings are supported by cross-correlation results from a parallel study (Chapter IV), where cross-correlation was computed between 24 hr averaged stream and streambed temperature time series, as well as between raw hourly stream and streambed temperature time series. Wells C and E consistently maintain the highest correlation coefficients (r) between stream and streambed temperatures at Site 1, even at streambed depths of 140 cm. A lag in the diurnal temperature signals at a depth of 30 cm in wells C and E was determined as 3 hrs ($r = 0.3110$) and 9 hrs ($r = 0.3650$) respectively. Cross-correlation results between 24 hr averaged stream and 140 cm depth temperatures for wells C and E indicate a uniform lag time of 32 hrs ($r = 0.617$ and 0.312 respectively), which is the shortest lag time calculated at 140 cm depth for either site.

The least connected wells at Site 1 are wells A, B, and D. In contrast to wells C and E, no definite diurnal variation is visible at 30 cm depth, and at a depth of 140 cm mainly the seasonal temperature signal remains, suggesting the presence of a large groundwater component (Brunke and Gonser, 1997). Correlations of diurnal temperature signals in wells A, B, and D yielded results below the significant r-value of 0.2, confirming that their connectivity to the stream is limited. As suggested in the conceptual model (Figure V-3), large groundwater components even at 30 cm depth within the

streambed along the sides of the stream, such as at well locations B and D, are likely derived from meander flow-through discharge.

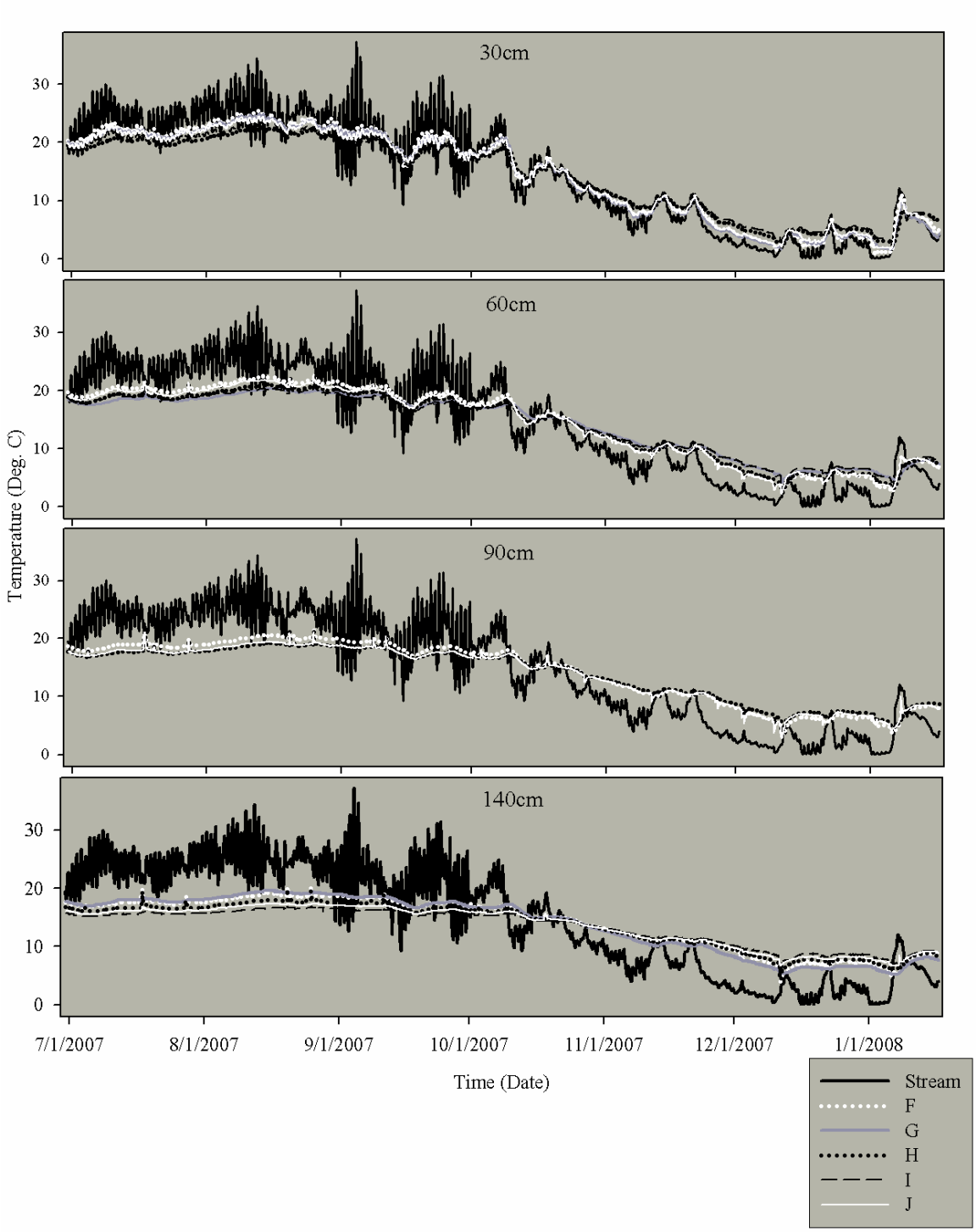

Figure V-9: Site 2 surface stream temperature and well temperatures at depths 30, 60, 90, and 140 cm below streambed.

At Site 2, all wells feature slightly varying but similar degrees of connectivity with the stream. The amplitude of diurnal temperature patterns witnessed at 30 cm depth seems decreased at this site, though in contrast to Site 1 most wells exhibit some diurnal temperature variations. These observations are again reflected by cross-correlation results. All wells except well H exhibit significant correlation between diurnal stream and 30 cm temperature patterns, with lag times ranging from 6 hrs (r = 0.5030) to 8 hrs (r = 0.3260).

A slight phase shift can be observed in the deeper temperature patterns, when comparing relative location of stream and hyporheic temperature peaks. Cross-correlation results indicate lag times of 56 hrs (r = 0.290) to 68 hrs (r = 0.312) between 24 hr averaged stream and 140 cm depth temperatures at Site 2.

The extent of the HZ within the streambed at this site is not known. However, using the presence of diurnal temperature fluctuations as an approximate indicator, the data suggests a HZ of variable depth at Site 1, where deepest surface water infiltration occurs at wells C and E. The HZ at Site 2 appears to be restricted to a universally shallower depth of 30 cm across the site. Based on these interpretations the model domains used in this study show both the HZ as well as the continuing groundwater environment beneath. Therefore the use of the term streambed throughout this study includes both the HZ as well as the groundwater environment.

Time series were plotted for all depths per well, revealing additional trends (Figure V-10; two wells are displayed, with general patterns representative of all wells). Generally, hyporheic temperatures decrease with depth in summer, as infiltrating surface water acts as a heat source to shallow hyporheic depths, and upwelling groundwater is

cooler than surface water. In the fall, these patterns change. In response to the autumn reversal, air temperatures as well as surface water temperatures begin to decrease, approaching the regional mean annual air temperature of 11.2 ºC. Groundwater also approaches the mean annual air temperature during the autumn reversal. As both surface water and groundwater approach the same temperature, their mixing within the streambed results in vertical homogenization. In winter, the reversal is complete, and streambed temperatures increase with depth, as groundwater serves as a heat source, and surface waters are cooler.

Additionally, streambed temperature spikes and plunges become apparent at several times throughout the data collection period, where streambed temperatures approach those of the stream often up to depths of 140 cm. These can be explained when stream stage is examined (Figure V-10). Streambed temperature spikes and plunges occur when stream stage spikes. Dogwiler and Wicks (2006) made similar observations in a karst system, where they found vertical and longitudinal homogenization of HZ temperatures in response to storm-induced discharge events. They postulate that this homogenization is likely due to discharge volumes overwhelming the systems thermal equilibration capabilities.

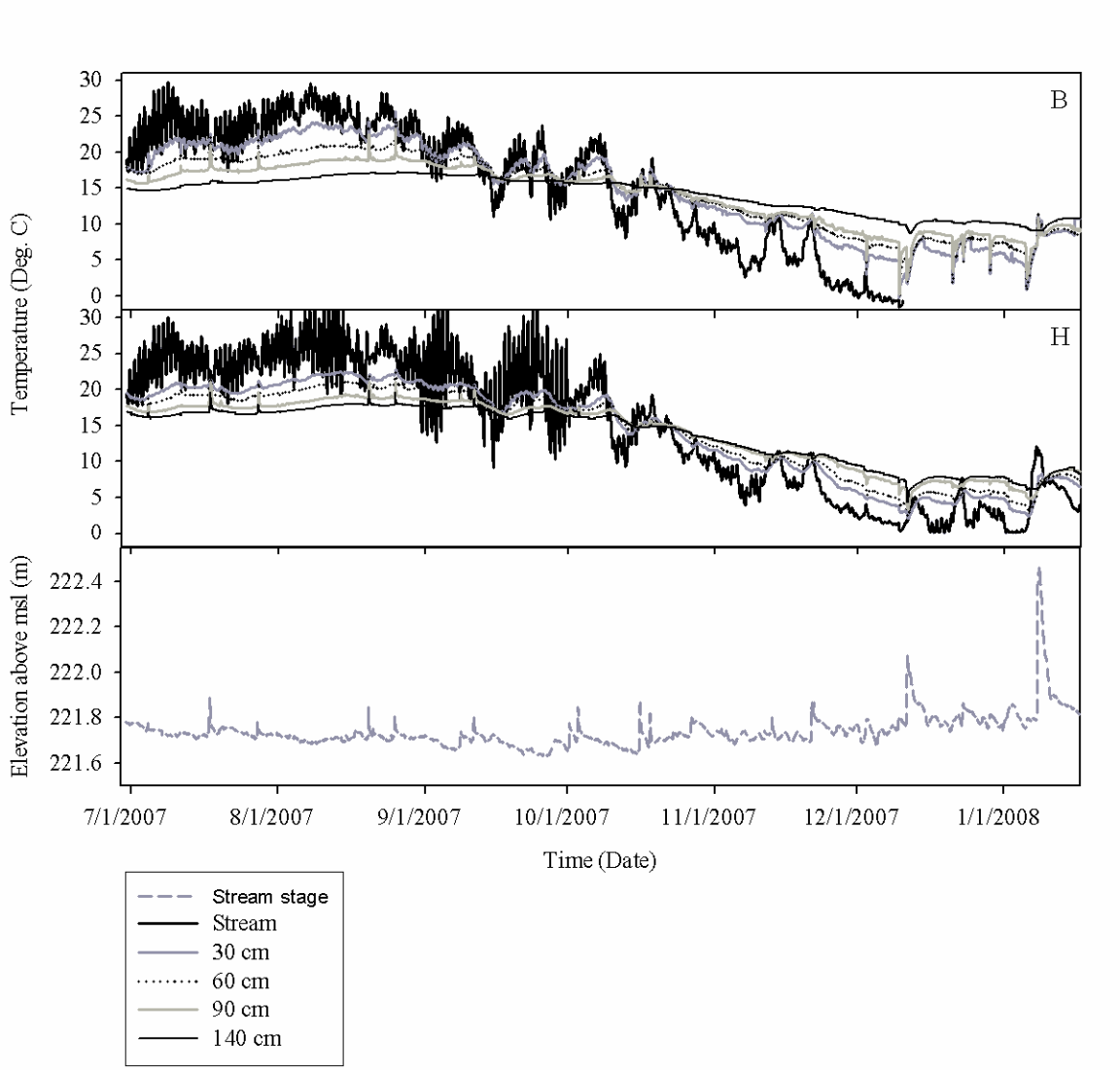

Figure V-10: Temperatures recorded in wells B and H at 4 depths, surface stream temperature, and stream stage.

Model

Both lateral and longitudinal temperature models were created for each site. In the end, only longitudinal models were able to reproduce observed temperatures with any accuracy. Numerical modeling attempts in the lateral extent appeared severely restricted by the use of a 2-D model, by low data resolution across each site, and by the likely

presence of a high degree of subsurface heterogeneity of both flow paths and materials. The 2-D modeling approach forces the assumption of 2-D inputs to the model domain, which for a lateral domain results in an assumption that inputs (water and energy) in the longitudinal direction are minimal and can effectively be considered zero. It became apparent while developing the longitudinal models that flow paths within and into the hyporheic zone, and thus temperatures also, are dominated by the direction of stream flow at this locality. In spite of the conceptual model suggesting significant lateral inputs and/or outputs at both sites, they appear negligible when compared to longitudinal inputs and outputs. This can also be seen in a comparison of lateral and longitudinal temperature profiles, based entirely on observed temperatures, at the start of the modeling period (July 13, 2007) (Figure V-11).

The hypothesis of flow paths within each contoured domain is based on a qualitative interpretation of contour patterns, which are the result of assumed mixing between warmer stream water originating at the upper surface of each domain, and cooler groundwater originating near the base of each domain, per definition of a HZ. At Site 1 the lateral profile shows only a deep flow path, where warm surface water enters mostly from the left and central stretch of the stream channel and seeps down centrally within the model domain. The longitudinal profile however, reveals a shallow flow path in addition to the deep, while also showing more clearly the area of infiltrating stream water. Despite the fact that the longitudinal model of Site 1 can not account for the infiltrating stream water from the left bank area, this exclusion is minimal in its impact on final model performance. However, lateral model performance is critically impacted by the exclusion of the shallow flow paths into the HZ revealed in the longitudinal profile,

suggesting that this component is integral to the temperatures of the HZ and streambed at Site 1. Cooler temperatures in both left and right bottom corners of the Site 1 longitudinal and lateral profiles appear to reflect the common temperature gradient of nearby sediments. An alternative interpretation could be discharging groundwater at each corner. This explanation however, would require a circular pattern of groundwater discharge surrounding an area of distinct downward flow, which seems highly unlikely.

At Site 2 the lateral profile identifies the bottom right bank area as a possible source of discharging groundwater, as suggested by the location of coolest temperatures and the protruding contour shape produced. The upper dips in temperature to either side of the center could be explained by infiltrating surface water, or by flow paths present in the longitudinal direction. The longitudinal profile indicates discharging groundwater toward the downstream section of the domain, with minimal surface infiltration occurring at both the upstream and downstream ends, and flow paths moving mainly horizontally through the streambed in the direction of stream flow. Again, although a lateral component is present, its exclusion from a longitudinal model is manageable, while the exclusion of the longitudinal component from a lateral model eliminates a major portion of what determines temperatures at this site.

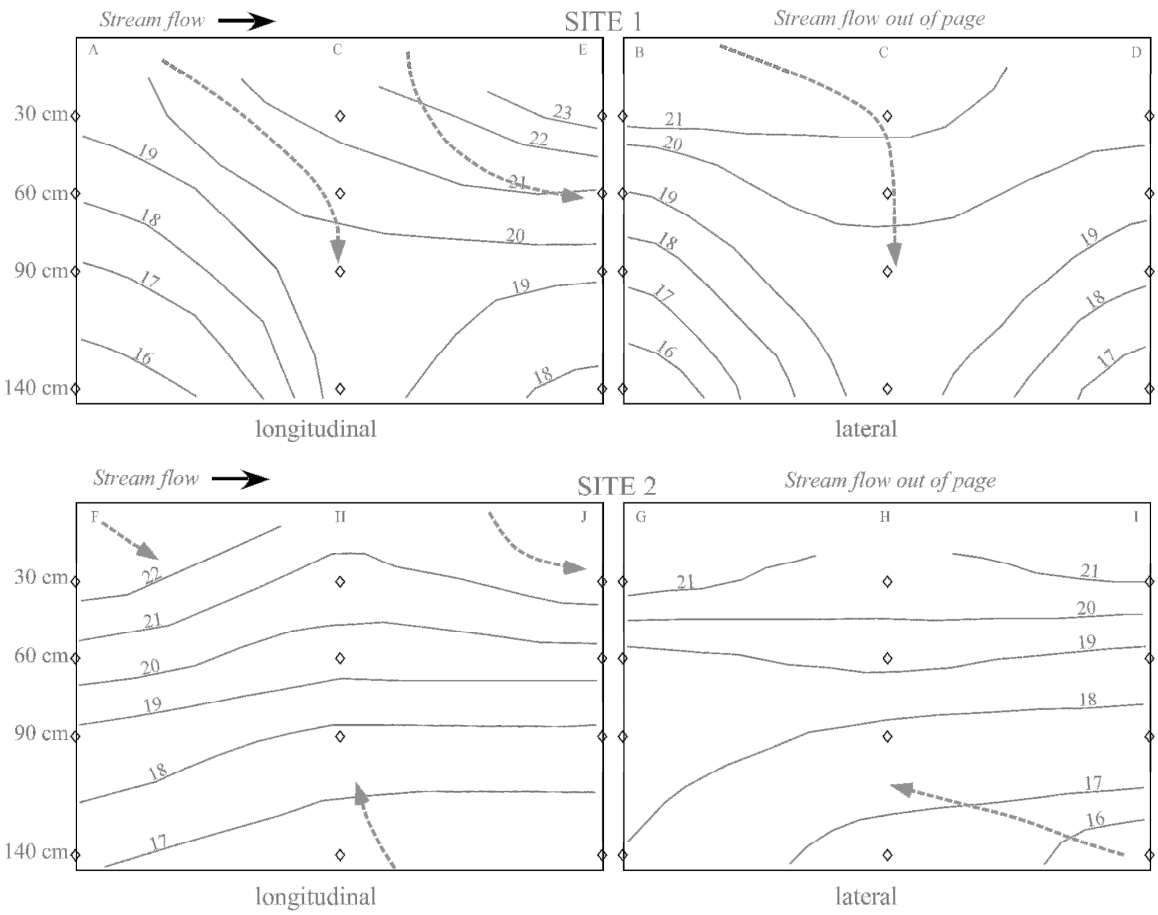

Figure V-11: Temperature profiles created based exclusively on observed temperatures, at the start of the modeling period (June 13, 2007). Contours show temperature in ºC. Diamonds represent logger locations, while gray dashed lines represent hypothesized streambed flow paths.

The temperature profile for the longitudinal model at Site 1 was a challenge to reproduce. Comparing observed temperatures with simulated temperatures, some problems with the model become apparent (Figure V-12). At depths 30 cm and 60 cm, the model is drastically overheated during the first 20-30 hours, while at depths 90 cm and 140 cm the model is under heated during this time. This initial adjustment period is thought to be the limiting factor of the minimum error magnitude achieved. Eventually

temperatures adjust across the various depths to reflect observed temperatures very closely.

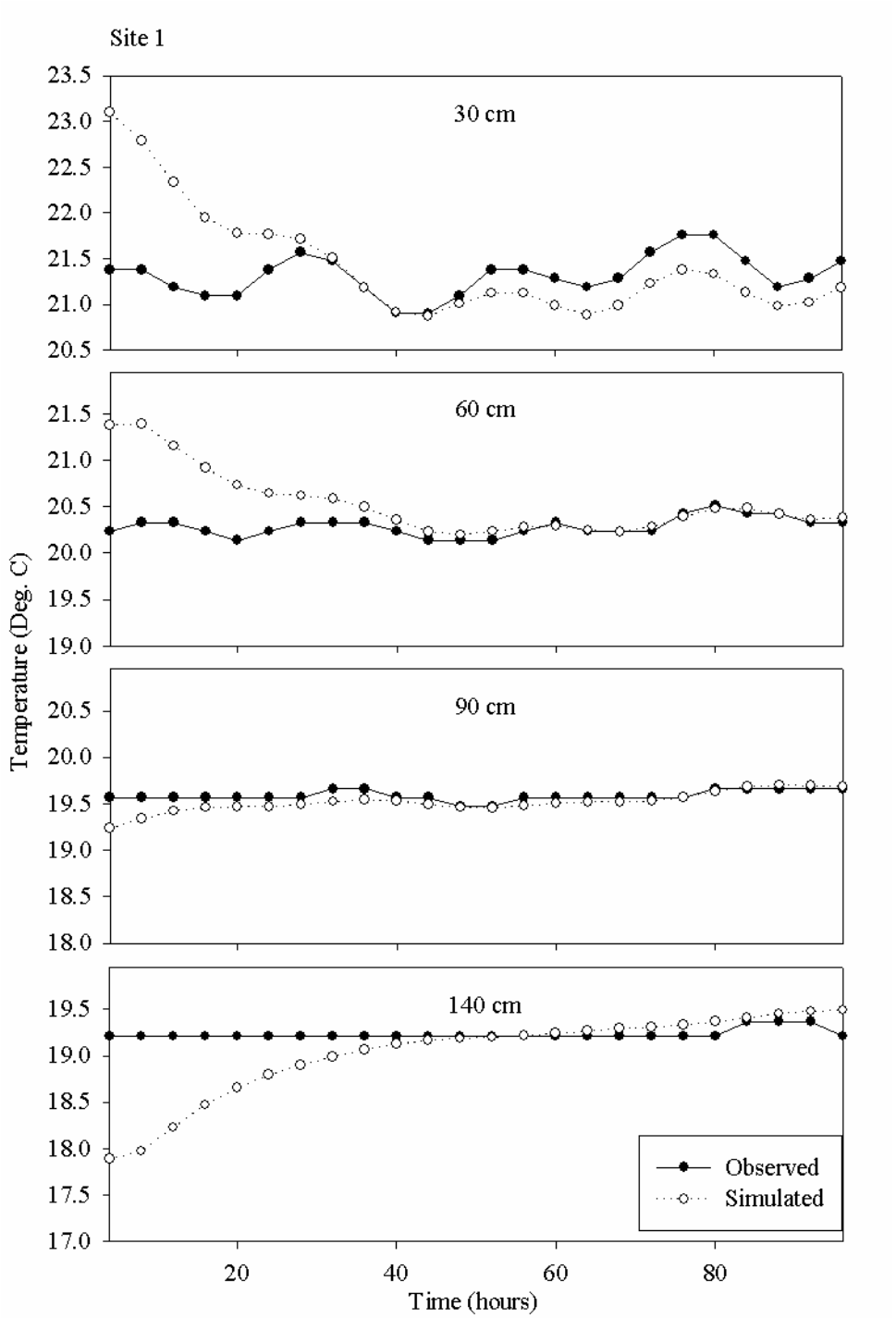

Figure V-12: Comparison of observed versus simulated temperatures per depth at Site 1.

A time series of model temperature output patterns created by the final calibrated model for Site 1 clearly shows both the downwelling to deeper flow paths, as well as to shallow flow paths (Figure V-13). The deep flow path is indicated by the 20 ºC contours, and their progressive downward movement over the 2 day time span displayed. The shallow flow path can be seen by the diurnal cycle of warmer temperatures entering and dissipating in the upper right corner and along the upper boundary of the model domain. A mean absolute error of 0.26 ºC was achieved, while the verification run produced a mean absolute error of 0.27 ºC, both of which are at the resolution of the temperature loggers.

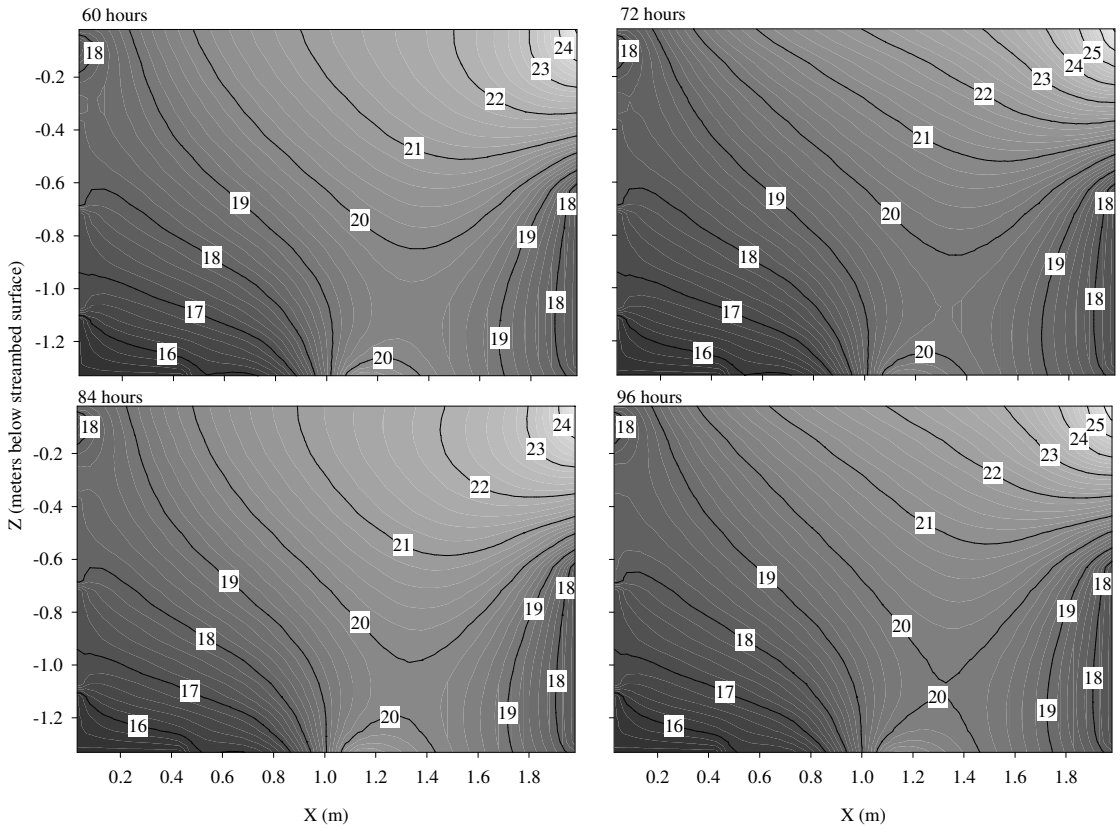

Figure V-13: Site 1 final calibrated model output temperature contour patterns at 60, 72, 84, and 96 hours since time 0. All temperatures are given in ºC. Left sides of model domains are upstream, while right model domain sides are downstream.

The temperature profile at Site 2 is more typical of a mid-riffle location within a gaining stream; surface water infiltration at shallower depths is apparent, but upwelling groundwater is also present (Figure V-14). Temperatures seem to be balanced between upwelling groundwater and infiltrating surface water, resulting in very little change in HZ temperatures through time. Silliman and Booth (1993) defined gaining reaches by a similar description as stated in the introduction. Flow paths appear to be mainly longitudinal, flowing from upstream (model domain left) to downstream (model domain right), following the direction of stream flow.

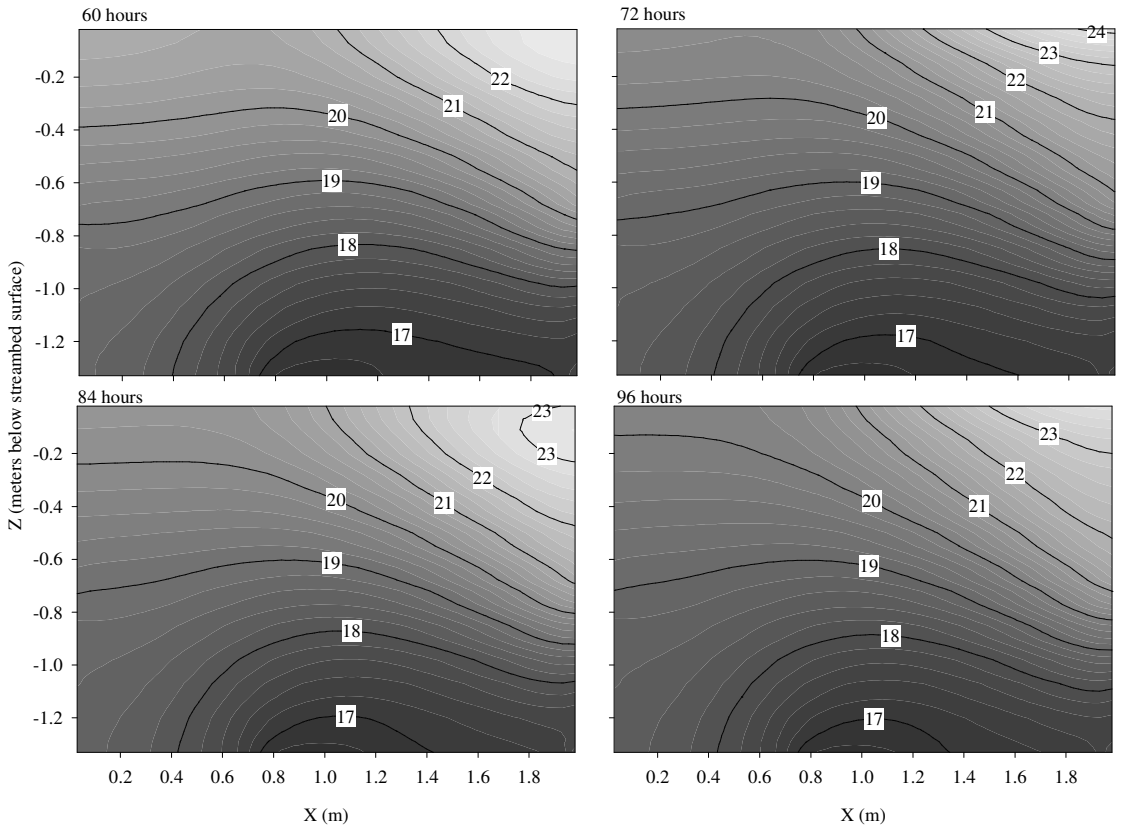

Figure V-14: Site 2 final calibrated model output temperature contour patterns at 60, 72, 84, and 96 hours since time 0. All temperatures are given in ºC. Left sides of model domains are upstream, while right model domain sides are downstream.

The time series of model temperature output patterns created by the final calibrated model for Site 2 shows the location of upwelling groundwater along the bottom domain boundary (Figure V-14), though it does not seem effective enough to prevent warming at 90 cm and 140 cm depth as witnessed in Figure V-15. Also visible are the sites of infiltrating surface water. Although limited to depths above 90 cm, they appear slightly exaggerated when compared with the initial model setup temperatures only four days earlier. A mean absolute error of 0.09 ºC was achieved, while the verification run produced a mean absolute error of 0.17 ºC, of which the original error is one order of magnitude below the resolution of the temperature loggers while the verification error is at the resolution of the loggers.

Comparing observed to simulated temperatures at Site 2, a slight drop in all temperatures can be seen within the first 10 to 20 hours (Figure V-15). It is projected that this occurrence, as witnessed similarly as either a drop or rise in the Site 1 model results, may be due to the model adjusting to boundary and flow conditions from the initial set up. Though adjustment of the initial temperature contours yields some improvement and decrease in this error, no means of removing it completely were encountered.

No defined diurnal signal is visible at any depth in observed or simulated temperatures within well H, suggesting very little surface water infiltration at this specific location, as previously shown by cross-correlation results. A constant variation in temperatures of up to 0.1 ºC is present at 60 cm and 90 cm depth, which is at or below the resolution of the temperature loggers, and not the expression of a diurnal signal.

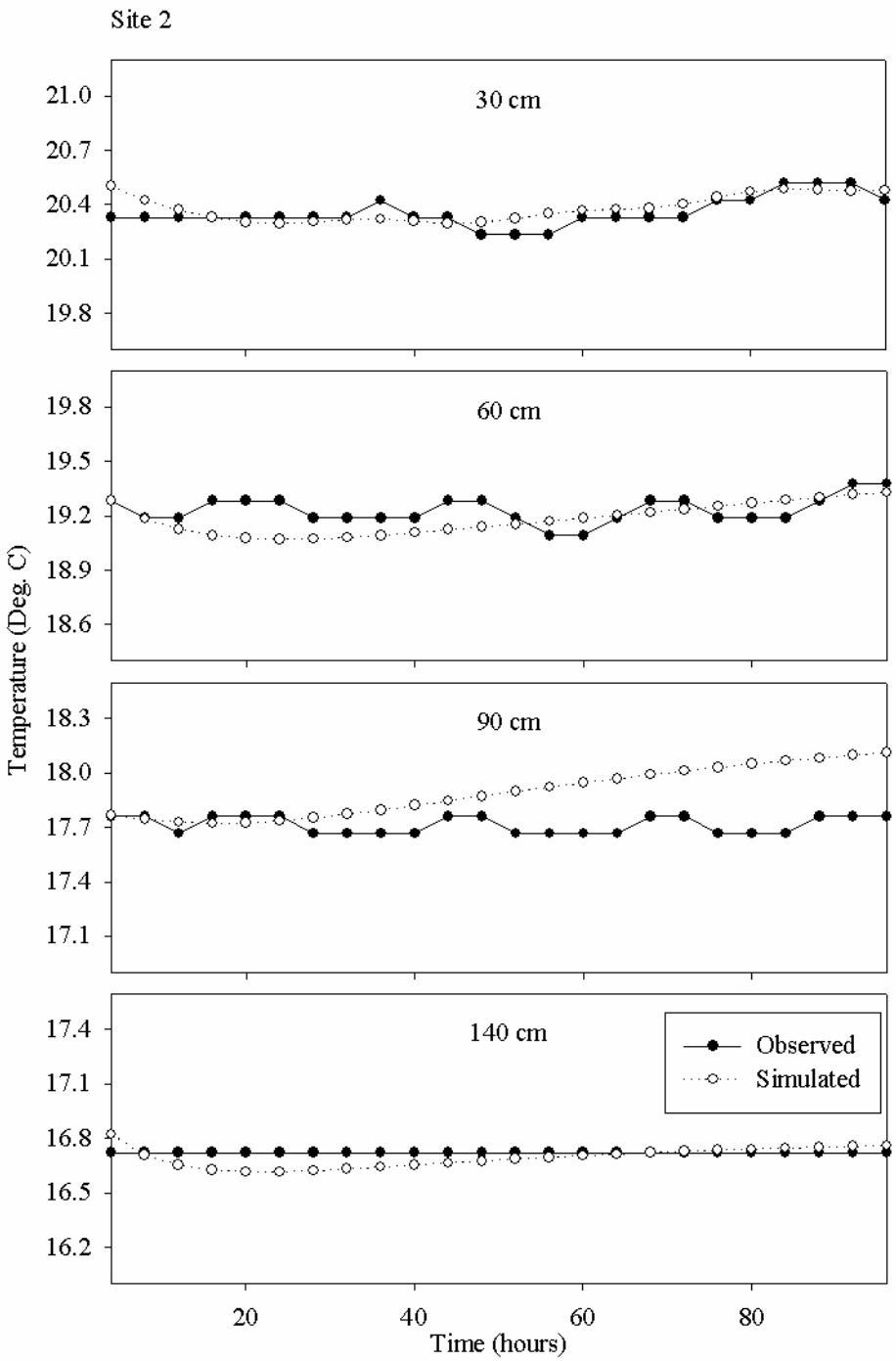

Figure V-15: Comparison of observed versus simulated temperatures per depth at Site 2.

Temperatures are most poorly reproduced by the model at 90 cm depth, where simulated temperatures exhibit a continual warming trend. It is proposed that a lateral component of cooler groundwater input, which cannot be adequately accounted for in this model, may be the explanation. When referring back to Figure V-11, a groundwater component was hypothesized as originating from the base of well I, which the conceptual model supports as being possible meander flow-through waters.

Total-head output data from both models were contoured, allowing the identification of model flow paths (Figure V-16). Despite reflecting the general patterns of hypothesized flow paths, slight differences are present.

At Site 1, while both shallow and deep flow paths are distinguishable, the hypothesized localized downwelling shown in Figure V-11 appears more site-wide in the model. Since LKC is typically considered a gaining stream, localized downwelling as hypothesized seems more appropriate. The initial hypothesis of localized downwelling is based heavily on observations presented by Stonestrom and Constantz (2003) as well as by Silliman and Booth (1993), stating firstly that HZ's in losing reaches (where downwelling is prominent) feature greater diurnal ranges even at depth (as illustrated in Figure V-8 especially for well C and E of Site 1 time series). Secondly, temperature contour patterns of a losing reach are characterized in both Stonestrom and Constantz (2003) and Silliman and Booth (1993) by surface temperatures penetrating deeply and in almost vertical fashion into the HZ, as witnessed at wells C and E. While the definition of Site 1 as a losing reach seems unrealistic given the surrounding hydrological conditions, the presence of local downwelling at wells C and E remains plausible and explains observed temperature patterns.

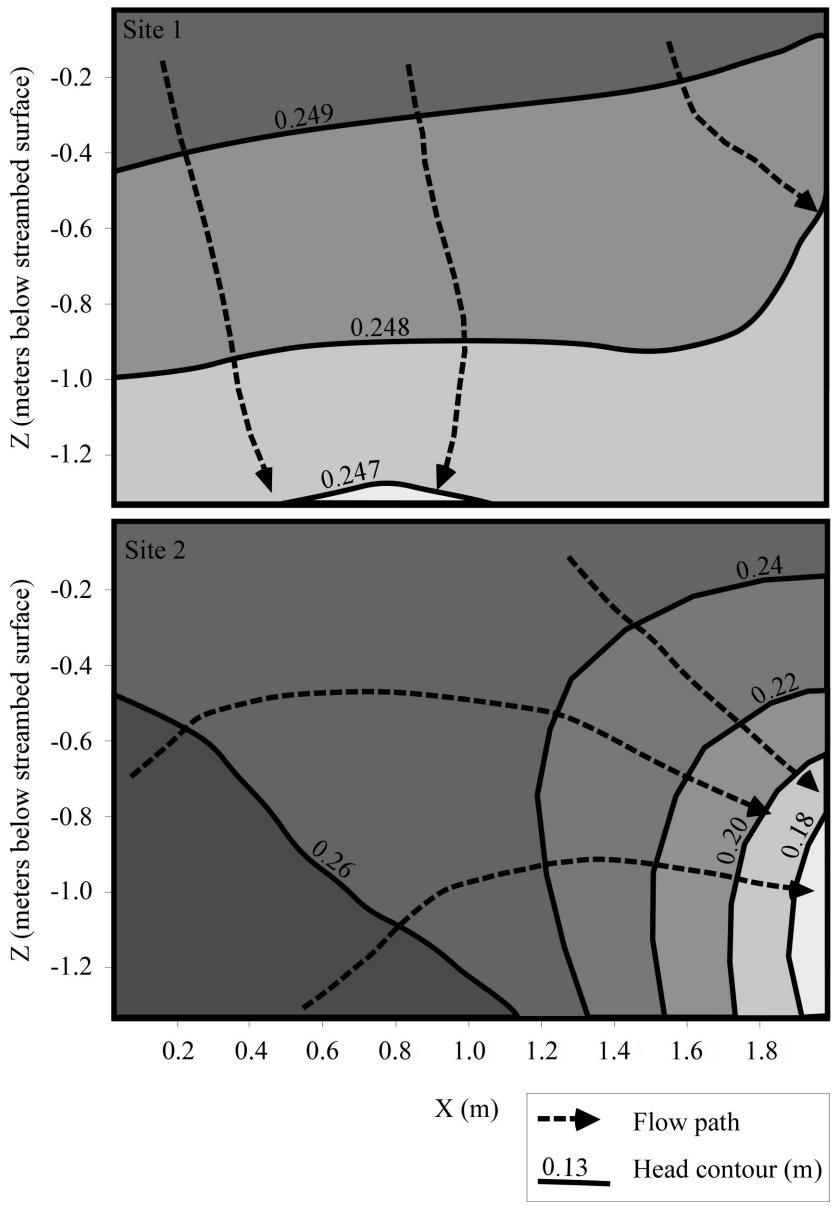

Figure V-16: Contours of model output values for total head, and dashed lines indicating flow directions.

Despite differences in hypothesized and simulated flow paths, the overlying flow path dynamics at Site 1 mimic expected patterns for the head and center of a riffle. Evans and Petts (1997) identified typical temperature profiles at varying locations within riffles.

Their findings support the flume-experiment based assumption that surface waters typically down-well at the heads of riffles, resulting in HZ temperatures closely mimicking those of stream water. This is the case at Site 1, suggesting that its location spans the head of a riffle.

Additional explanations for the flow path dynamics at Site 1 include heterogeneities in (Vaux, 1968) or on (Cooper, 1965) the streambed, or changes in hydraulic conductivity within the streambed (Becker et al., 2004). During the study period, the streambed surface maintained a uniform grain, with no large object present capable of generating the conditions proposed by Cooper (1965). Thus, the flow dynamics do not appear to be associated with heterogeneities on the streambed. However, Site 1 is characterized by a higher degree of heterogeneity in sediment sizes (Figure V-2). Also, Buyck (2005) found possible gray clay deposits within the streambed and the HF along Site 1, possibly from cut bank collapses or underlying till layers, forming areas of low permeability (possibly represented as no-flow boundaries in the model), which could act as controlling factors to hyporheic flow. Unfortunately, due to the unconsolidated nature of the streambed materials, coring for verification has not been possible. Because of the lack of specific details, the subsurface was represented as being homogenous, and did not accurately represent the potential heterogeneity.

Model flow path dynamics at Site 2 exhibit the strong horizontal flow component that was expected based on observed temperatures. However, as with model temperature contours in Figure V-14, the flow paths formed by the model at Site 2 appear exaggerated on the downstream side of the model domain. Since the model was evaluated solely based on observed temperatures in well H, temperatures near the model boundaries were

not taken into consideration during calibration or error evaluation. This is a definite weakness of both models created for this study.

Sensitivity Analysis

A sensitivity analysis reveals that the Site 1 model has a much lower tolerance for parameter changes than the Site 2 model (Figure V-17). The only similarities between their responses are noticeable sensitivities to changes in K_{hh} and K_{ts}. The sensitivity to changes in K_{hh} suggests that advection is important to thermal transport within the streambed. A decrease in K_{hh} at Site 2 results in a dramatic change in the models performance, as advection is slowed to a point where severe overheating occurs. Site 1 features more gradually increasing errors to changes in K_{hh}. The noticeable sensitivity of both models to K_{ts} suggests that while advection is important, as suggested by higher sensitivities to changes in K_{hh}, conduction also impacts streambed temperatures significantly at both sites.

Both models produced slightly smaller mean absolute errors with ever increasing porosity and C_s values, while the Site 2 model also produced smaller errors for K_{zz}/K_{hh} values greater than 1. As mentioned previously these were limited to literature based accepted ranges to prevent implausible scenarios from developing. Since neither model exhibited a high degree of sensitivity to changes in either of the respective parameters, the use of values within theoretical ranges has had little impact on final model performance, and is therefore acceptable and appropriate.

Sensitivity to changes in both longitudinal and transverse dispersivity is relatively low in the Site 1 model and negligible in the Site 2 model. This suggests that there is

greater heterogeneity of flow paths present at Site 1, where there is also a greater heterogeneity of grain sizes as seen in Figure V-2.

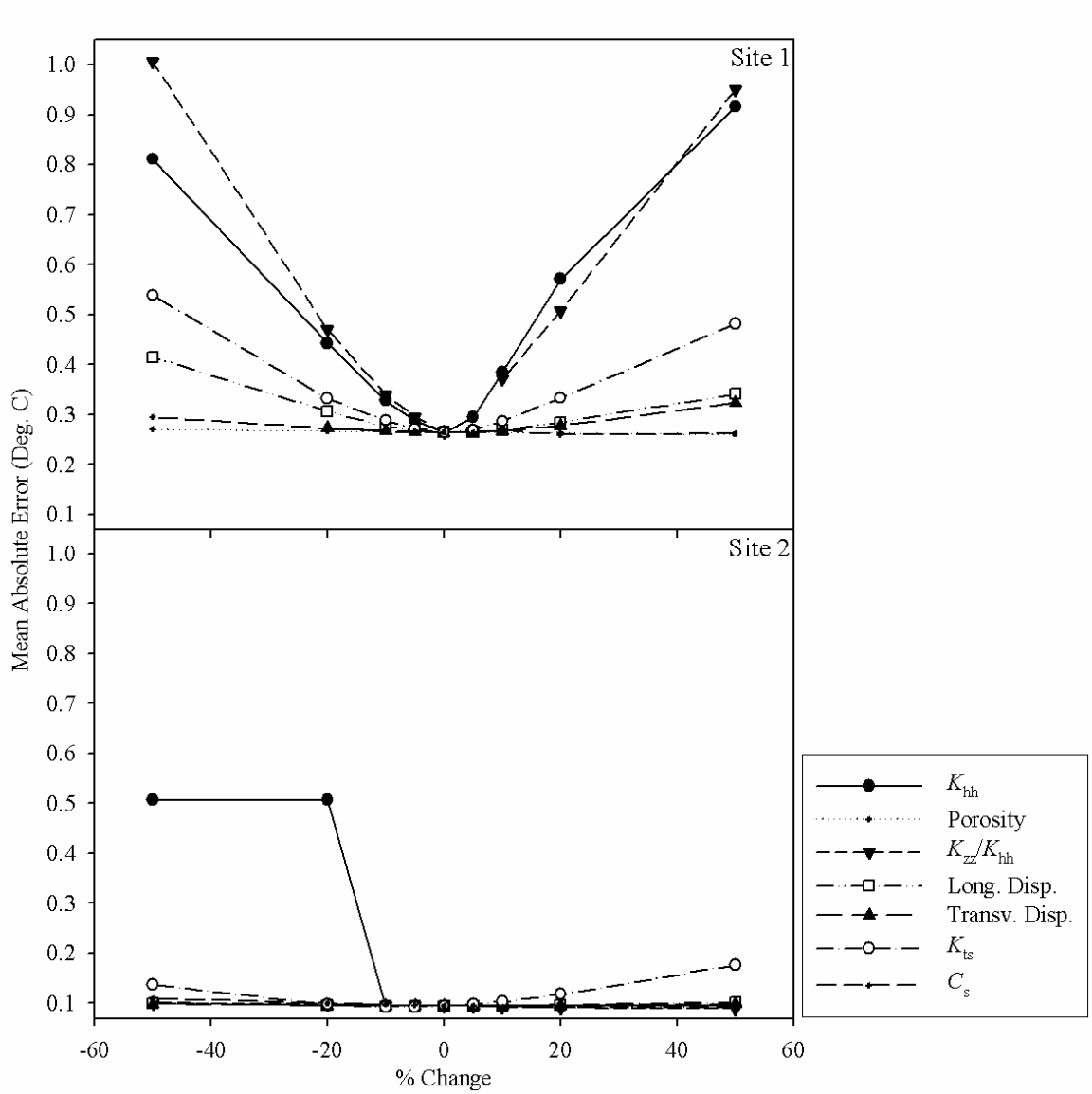

Figure V-17: Sensitivity analysis results, showing percent change versus mean absolute error for all adjustable physical and thermal model properties.

Final calibrated model parameters are outlined in Table V-1. However, before site-wide interpretations based on these values are made, it should be noted that Site 1

and 2 models were calibrated to match observed temperatures only in wells C and H respectively. Wells C and E are the only two wells at Site 1 to show significant correlation between diurnal surface and 30 cm temperatures, while well H is the only well at Site 2 to show no significant correlation between diurnal surface and 30 cm temperatures. Since models were calibrated to reproduce these specific conditions, it must be assumed that model parameters are a reflection of conditions observed in and around these wells, which may not necessarily form accurate site wide representations. However, for ease of reference, properties will be evaluated in terms of site-wide impact.

K_{hh} at the two sites differs by one order of magnitude, with a value of 5.10 m/hr (5.90×10^{-3} cm/sec) at Site 1 and 0.132 m/hr (1.5310^{-4} cm/sec) at Site 2. This difference comfortably reflects the change in grain sizes between the sites, as do porosity values which were chosen based on literature reported values (Peterson, 2008).

K_{zz}/K_{hh} at both sites is relatively high, indicating that fluid movement is not severely restricted by sediments in either the x or z directions. Site 1 features more poorly sorted sediments than Site 2, as seen in the grain size analysis (Figure V-2), explaining the slightly lower K_{zz}/K_{hh} value.

Thermal dispersivity values in VS2DH (Healy and Ronan, 1996) are assumed analogous to solute dispersivities (Stonestrom and Constantz, 2003), and as such may be evaluated by comparison to published ranges as given for example by Fetter (1993). Consequently, dispersivity values for both sites are small, and fall well within the commonly published range for observation scales between 1 and 10 m.

The coarser sediments at Site 1 feature a much higher heat conduction capacity than at Site 2, as indicated by the larger K_{ts} value. This indicates that any conduction occurring at Site 2 is less effective than at Site 1.

C_s values are identical for both sites, as both were limited at the maximum accepted value. As mentioned previously, this suggests that the simplification into a 2-D model was an oversimplification. Larger C_s values increase the models thermal buffering capabilities, which might in reality be accomplished by the constant temperatures of laterally inflowing groundwater as suggested by the conceptual model.

Table V-1: Physical and thermal properties for the calibrated models.

Model parameter	**Site 1**	**Site 2**
K_{hh} (m/hr)	5.10	0.132
Porosity	0.35	0.4
K_{zz}/K_{hh}	0.8085	1.0
Long. Disp. (m)	0.652	0.027
Transv. Disp. (m)	0.17	0.014
K_{ts} (J/hr m ^{o}C)	12350	6024
C_s (J/m^3 ^{o}C)	2719600	2719600

Thermal Transport

When site and direction specific Peclet numbers (Pe) are calculated, an interesting difference between the sites is highlighted. Using the equation $\mathrm{Pe} = \frac{qLp_w C_w}{K_{ts}}$ (Domenico and Schwartz, 1990), specific discharge (q) in the x and z directions for Site 1 of $1.67\text{x}10^{-3}$ m/hr and $6.4\text{x}10^{-3}$ m/hr respectively, and in the x and z directions for Site 2 of $4.00\text{x}10^{-3}$ m/hr and $3.9\text{x}10^{-3}$ m/hr respectively (derived from average velocities in the x

and z direction of the last time step of each model), a characteristic length (*L*) of 2 m (length of hyporheic flow path through model domain) for the x-direction and *L* of 1.4 m for the z-direction, a water density (ρ_w) of 1,000 kg/m^3, the specific heat of water (C_w) of 4186 J/kg °C, and a thermal conductivity (*K*ts) of 12350 J/hr m ^oC for Site 1, and 6024 J/hr m ^oC for Site 2 (best-fit data from model), x and z Pe's for Site 1 equaled 1.13 and 3.07 respectively, while x and z Pe's for Site 2 equaled 5.56 and 3.82 respectively.

At Site 1, the vector analysis of the model (indicating flow direction) confirms that the main direction of water movement is in the vertical direction, while at Site 2 water movement is almost equal in the x and z directions across the domain. Site 1 Pe's indicate that conduction is almost as important as advection in x-directional temperature changes, which is supported by steep temperature gradients across the domain in the x direction (Figure V-13). Advection is the dominant thermal transport mechanism in the z direction at Site 1. This appears logical as both deep and shallow flow paths trend mainly in the z direction, driving advection similarly.

At Site 2 advection is the dominant thermal transport mechanism in both x and z directions, where advection is slightly more dominant in the x direction. This is supported by thermal gradients, where horizontal thermal gradients are almost undetectable, while vertical thermal gradients are gentle.

The above observations support and confirm conceptual understandings of both sites. Site 1, featuring poorly sorted coarser sediments, has been labeled a locally downwelling zone based on observed temperature patterns, which is now supported by both model flow vectors, and advection dominating in the z direction. At Site 2, featuring moderately sorted finer sediments, flow paths carry water and temperatures both

horizontally and vertically through the domain, though the vertical is somewhat more restricted than the horizontal. This again is supported by model flow vectors, as well as by advection dominating in both x and z directions.

Conclusion

The goal of this study was to identify the impacts of streambed sediment size on temperature profiles within a low gradient stream. To accomplish this, 2-D numerical heat transport models were developed for two sites along LKC featuring different sediment sizes.

A comparison of lateral and longitudinal temperature profiles showed they differ mainly based on the location of inflows and outflows of both groundwater and surface water. It was noted that regardless of magnitude or direction, movement of stream water through meanders played a role in controlling surface stream temperatures, the presence of which is supported by the findings of both Peterson and Sickbert (2006) and Van der Hoven et al. (2008). At Sites 1 and 2 of this study these meander inflows and outflows mostly impacted lateral temperature profiles. While these lateral inflows and outflows did have significant impacts on temperatures, and their absence from longitudinal models had noticeable effects (Figure V-15; see 90 cm depth), longitudinal temperature transport controls the HZ and streambed thermal systems and overwhelms lateral thermal signals.

The impacts of sediment size were many. Fundamentally, increasing sediment size resulted in higher hydraulic conductivities and lower porosities. Additionally, the degree of sediment sorting or heterogeneity had many impacts on temperature transport. Site 1, featuring more sediment size heterogeneity, had distinct preferential flow paths

within the model domain. At Site 1, advection and conduction were almost equally as important as heat transport mechanisms in the horizontal direction, while advection dominated in the vertical, and advection velocities were greater in the vertical.

In contrast to this, Site 2 was composed of better sorted, finer sediments, had no dominant preferential flow paths. Sediment size homogeneity was also noticeable in K_{zz}/K_{hh} values, attaining a value of 1 at Site 2. Temperatures at Site 2 were predominantly controlled by advection, as revealed by the calculation of direction specific Pe numbers, where advection velocities appeared similar in magnitude regardless of x or z dimension.

Ultimately these data suggest that sediment size and heterogeneity impacts are magnified within thermal profiles of the HZ, enhancing the differences between vertical and horizontal properties. This may include but not be limited to enhancing the possibility for major preferential flow paths, introducing substantial differences in x and z dimensional velocities, and altering the dominant thermal transport processes.

References

Anderson MP. 2005. Heat as a Ground Water Tracer. *Ground Water* **43**: 951-968. DOI: 10.1111/j.1745-6584.2005.00052.x.

Becker MW, Georgian T, Ambrose H, Siniscalchi J, Fredrick K. 2004. Estimating flow and flux of ground water discharge using water temperature and velocity. *Journal of Hydrology* **296**: 221-233. DOI: 10.1016/j.jhydrol.2004.03.025.

Bencala KE. 2005. Hyporheic Exchange Flows. In *Encyclopedia of Hydrologic Sciences*, Anderson MG. (ed) **3**: 1733-1740.

Brunke M, Gonser T. 1997. The ecological significance of exchange processes between rivers and groundwater. *Freshwater Biology* **37**: 1-33.

Buyck MS. 2005. Tracking nitrate loss and modeling flow through the hyporheic zone of a low gradient stream through the use of conservative tracers. *Thesis*.

Conant B Jr. 2004. Delineating and Quantifying Ground Water Discharge Zones Using Streambed Temperatures. *Ground Water* **42**: 243-257.

Cooper AC. 1965. The effect of transported stream sediments on the survival of sockeye and pink salmon eggs and alevins. *International Pacific Salmon Fishery Commission Bulletin* **18**.

Dogwiler T, Wicks C. 2006. Thermal variation in the hyporheic zone of a karst stream. *International journal of Speleology* **35**: 59-66.

Domenico PA, Schwartz FW. 1990. *Physical and chemical hydrogeology*. Wiley: New York.

Evans EC, Greenwood MT, Petts GE. 1995. Short Communication Thermal Profiles Within River Beds. *Hydrological Processes* **9**: 19-25.

Evans EC, Petts GE. 1997. Hyporheic temperature patterns within riffles. *Hydrological Sciences* **42**: 199-213.

Fetter CW. 1993. *Contaminant hydrogeology*. Macmillan Publishing Company: New York; 458.

Fraser BG, Williams DD. 1998. Seasonal boundary dynamics of a groundwater/surface-water ecotone. *Ecology* **79**: 2019-2031.

Fromm NJ. 2005. Quantifying the flux of water and loss of nitrate as stream water flows beneath a meander of a central Illinois stream. *Thesis*.

Hayashi M, Rosenberry DO. 2002. Effects of ground water exchange on the hydrology and ecology of surface water. *Ground Water* **40**: 309-316.

Healy RW, Ronan AD. 1996. Documentation of computer program VS2DH for simulation of energy transport in variably saturated porous media: Modification of the U.S. Geological Survey's computer program VS2DT. *United States Geological Survey*: Denver, CO.

Lapham WW. 1989. In: US Geological Survey (ed) Use of temperature profiles beneath streams to determine rates of vertical ground-water flow and vertical hydraulic conductivity. US Geological Survey: Reston, VA, p 35.

Peterson EW, Sickbert TB. 2006. Stream water bypass through a meander neck, laterally extending the hyporheic zone. *Hydrogeology Journal* **14**: 1443-1451. DOI: 10.1007/s10040-006-0050-3.

Peterson EW. 2008. Associate Professor. Department of Geography-Geology: Illinois State University. Normal, IL. Personal communication of unpublished data.

Ringler NH, Hall JD. 1975. Effects of logging on temperature, and dissolved oxygen in spawning beds. *Transactions of the American Fisheries Society* **104**: 111-121.

Silliman SE, Booth DF. 1993. Analysis of time-series measurements of sediment temperature for identification of gaining vs. losing portions of Juday Creek, Indiana. *Journal of Hydrogeology* **146**: 131-148.

Stonestrom DA, Constantz J (ed). 2003. Heat as a tool for studying the movement of ground water near streams. *U.S. Geological Survey Circular 1260*. U.S. Geological Survey: Denver, CO. 1-96.

Van der Hoven SJ, Fromm NJ, Peterson EW. 2008. Quantifying nitrogen cycling beneath a meander of a low gradient N-impacted agricultural stream using tracers and numerical modeling. *Hydrological Processes*: in press. DOI: 10.1002/hyp.6691.

Vaux WG. 1968. Intergravel flow and interchange of water in a streambed. *Fishery Bulletin* **66**: 479-489.

White DS, Elzinga CH, Hendricks SP. 1987. Temperature patterns within the hyporheic zone of a northern Michigan river. *Journal of North American Benthological Society* **12**: 48-60.

CHAPTER VI

SUMMARY OF CONCLUSIONS

- Overall, HZ chloride concentrations vary little temporally and spatially, and when they do vary they do not appear to follow stream chloride concentration patterns. This suggests the influence of a more constant groundwater source (at locations where data was available) rather than a varying stream source, and is supported by the general identification of LKC as a gaining stream.
- Distinct differences in thermal profiles were identified and attributed to differences in both sediment size and the degree of sediment sorting. Site 1, featuring poorly sorted gravels, showed a high degree of thermal heterogeneity in the form of a localized downwelling zone within a gaining environment. This downwelling zone was expressed in the thermal profile through distinct preferential flow paths, the propagation of diurnal surface water temperatures to at least 60 cm at well E, and greater variability in the dominant thermal transport mechanism.
- Site 2, characterized by moderately sorted sand, showed a more vertically and horizontally homogenized thermal environment regulated by the constant mixing of upwelling groundwater and downwelling surface water. This was expressed in the thermal profile by a lack of defined preferential flow paths, propagation of diurnal surface temperatures to 30 cm only, and a uniform dominance of advection as the main thermal transport mechanism in both x and z directions. Additionally, either significant groundwater discharge, or an increased amount of finer sediments at Site 2 was deemed accountable for a noticeable temperature disparity between surface water and shallow hyporheic zone temperatures.

- Advection was projected as a major controlling factor to diurnal temperature signal penetration depth, where diurnal trends were generally limited to the upper 30 cm of the hyporheic zone. Surface seasonal trends were detected at much greater depths, leading to the conclusion that they are transmitted initially by advection into the HZ, and by conduction to areas beyond the extent of the HZ.
- Movement of stream water through meanders along extended HZ flow paths had a significant impact on stream and streambed temperatures, discharging into both study sites along the stream's edges. However, while such lateral in and outflows were significant, thermal transport following the direction of stream flow dominated both site thermal profiles.
- Lateral and longitudinal temperature profiles were compared, and found to differ based on factors influencing thermal transport, such as the presence of preferential flow paths. In general, progressive transmission of temperature signals was more apparent in longitudinal profiles, following the direction of stream flow, with minor local abnormalities detected at Site 1.
- Ultimately, these results suggest that physical heterogeneities such as a greater range in sediment size or a less even stream channel are reflected as thermal heterogeneities in the subsurface.

REFERENCES

Anderson MP. 2005. Heat as a Ground Water Tracer. *Ground Water* **43**: 951-968. DOI: 10.1111/j.1745-6584.2005.00052.x.

Becker MW, Georgian T, Ambrose H, Siniscalchi J, Fredrick K. 2004. Estimating flow and flux of ground water discharge using water temperature and velocity. *Journal of Hydrology* **296**: 221-233. DOI: 10.1016/j.jhydrol.2004.03.025.

Bencala KE. 1993. A perspective on stream-catchment connections. *Journal of the North American Benthological Society* **12**: 44-47.

Bencala KE. 2000. Hyporheic zone hydrologic processes. *Hydrological Processes* **14**: 2797-2798.

Bencala KE. 2005. Hyporheic Exchange Flows. In *Encyclopedia of Hydrologic Sciences*, Anderson MG. (ed) **3**: 1733-1740.

Boulton AJ, Scarsbrook MR, Quinn JM, Burrell GP. 1997. Land-use effects on the hyporheic ecology of five small streams near Hamilton, New Zealand. *New Zealand Journal of Marine and Freshwater Research* **31**: 3609-622.

Brunke M, Gonser T. 1997. The ecological significance of exchange processes between rivers and groundwater. *Freshwater Biology* **37**: 1-33.

Buyck MS. 2005. Tracking nitrate loss and modeling flow through the hyporheic zone of a low gradient stream through the use of conservative tracers. *Thesis*.

Cardenas MB, Wilson JL, Zlotnik VA. 2004. Impact of heterogeneity, bed forms, and stream curvature on subchannel hyporheic exchange. *Water Resources Research* **40**: W08307. DOI: 10.1029/2004WR003008.

Conant B Jr. 2004. Delineating and Quantifying Ground Water Discharge Zones Using Streambed Temperatures. *Ground Water* **42**: 243-257.

Constantz J, Cox MH, Su GW. 2003. Comparison of heat and bromide as ground water tracers near streams. *Ground Water* **41**: 647-656.

Cooper AC. 1965. The effect of transported stream sediments on the survival of sockeye and pink salmon eggs and alevins. *International Pacific Salmon Fishery Commission Bulletin* **18**.

Dogwiler T, Wicks C. 2006. Thermal variation in the hyporheic zone of a karst stream. *International journal of Speleology* **35**: 59-66.

Domenico PA, Schwartz FW. 1990. *Physical and chemical hydrogeology*. Wiley: New York.

Evans EC, Greenwood MT, Petts GE. 1995. Short Communication Thermal Profiles Within River Beds. *Hydrological Processes* **9**: 19-25.

Evans EC, Petts GE. 1997. Hyporheic temperature patterns within riffles. *Hydrological Sciences* **42**: 199-213.

Fetter CW. 1993. *Contaminant hydrogeology*. Macmillan Publishing Company: New York; 458.

Fraser BG, Williams DD. 1998. Seasonal boundary dynamics of a groundwater/surface-water ecotone. *Ecology* **79**: 2019-2031.

Fromm NJ. 2005. Quantifying the flux of water and loss of nitrate as stream water flows beneath a meander of a central Illinois stream. *Thesis*.

Hayashi M, Rosenberry DO. 2002. Effects of ground water exchange on the hydrology and ecology of surface water. *Ground Water* **40**: 309-316.

Healy RW, Ronan AD. 1996. Documentation of computer program VS2DH for simulation of energy transport in variably saturated porous media: Modification of the U.S. Geological Survey's computer program VS2DT. *United States Geological Survey*: Denver, CO.

Jenkins GM, Watts DG. 1968. *Spectral analysis and its applications*. Holden-Day: San Francisco.

Jones JB, Holmes RM. 1996. Surface-subsurface interactions in stream ecosystems. *TREE* **11**: 239-242.

Keery J, Binley A, Crook N, Smith JWN. 2007. Temporal and spatial variability of groundwater-surface water fluxes: Development and application of an analytical method using temperature time series. *Journal of Hydrology* **336**: 1-16. DOI: 10.1016/j.jhydrol.2006.12.003.

Lapham WW. 1989. In: US Geological Survey (ed) Use of temperature profiles beneath streams to determine rates of vertical ground-water flow and vertical hydraulic conductivity. US Geological Survey: Reston, VA, p 35.

Lax S, Peterson EW. (*in review*). Characterization of chloride transport in the unsaturated zone near salted roads. *Environmental Geology*.

Malard F, Mangin A, Uehlinger U, Ward JV. 2001. Thermal heterogeneity in the hyporheic zone of a glacial floodplain. *Canadian Journal of Fisheries and Aquatic Sciences* **58**: 1319-1335. DOI: 10.1139/cjfas-58-7-1319.

Mangin A. 1984. Pour une meilleure connaissance des systémes hydrologiques à partir des analyses corrélatoire et spectrale. *Journal of Hydrology* **67**: 25-43.

Peterson EW, Sickbert TB. 2006. Stream water bypass through a meander neck, laterally extending the hyporheic zone. *Hydrogeology Journal* **14**: 1443-1451. DOI: 10.1007/s10040-006-0050-3.

Peterson EW. 2008. Associate Professor. Department of Geography-Geology: Illinois State University. Normal, IL. Personal communication of unpublished data.

Ringler NH, Hall JD. 1975. Effects of logging on temperature, and dissolved oxygen in spawning beds. *Transactions of the American Fisheries Society* **104**: 111-121.

Shepherd BG, Hartman GF, Wilson WJ. 1986. Relationships between stream and intragravel temperatures in coastal drainages and some implications for fisheries workers. *Canadian Journal of Fisheries and Aquatic Sciences* **43**: 1818–1822.

Silliman SE, Booth DF. 1993. Analysis of time-series measurements of sediment temperature for identification of gaining vs. losing portions of Juday Creek, Indiana. *Journal of Hydrogeology* **146**: 131-148.

Sinokrot BA, Stefan HG. 1993. Stream Temperature Dynamics - Measurement and Modeling. *Water Resources Research* **29**: 2299-2312.

SPSS for Windows. Rel. 16.0.1. 2007. SPSS Inc.: Chicago.

Stonestrom DA, Constantz J (ed). 2003. Heat as a tool for studying the movement of ground water near streams. *U.S. Geological Survey Circular 1260*. U.S. Geological Survey: Denver, CO. 1-96.

Van der Hoven SJ, Fromm NJ, Peterson EW. 2008. Quantifying nitrogen cycling beneath a meander of a low gradient N-impacted agricultural stream using tracers and numerical modeling. *Hydrological Processes*: in press. DOI: 10.1002/hyp.6691.

Van der Hoven SJ. 2008. Associate Professor. Department of Geography-Geology: Illinois State University. Normal, IL. Personal communication of unpublished data.

Vaux WG. 1968. Intergravel flow and interchange of water in a streambed. *Fishery Bulletin* **66**: 479-489.

White DS, Elzinga CH, Hendricks SP. 1987. Temperature patterns within the hyporheic zone of a northern Michigan river. *Journal of North American Benthological Society* **12**: 48-60.